Doctoral (Ph.D.) Dissertation

DEVELOPMENT OF A PHOTOACOUSTIC SYSTEM FOR THE SELECTIVE DETECTION AND ANALYSIS OF AMMONIA GAS ISOTOPES

OUMA EMILY AWUOR

Supervisor:

Prof. Dr. Zoltán Bozóki

Doctoral School of Environmental Sciences

Department of Optics and Quantum Electronics

Faculty of Science and Informatics

University of Szeged

Szeged, 2022

Table of contents

List of Figures

List of Tables

1. Introduction

Global urgency to cut down on carbon dioxide emissions which has been documented to reach its highest level in history [1] has led to the need to reduce the use of fossil fuels in our everyday lives. In most industrial processes, the so-called clean or green energy sources and processes are rapidly being developed and tested in the hope of substantially decarbonising the energy sector, and reducing the ecological footprints of the world's population. One such green energy process is the electrochemical synthesis of ammonia which has been identified to be environmentally sustainable, less polluting and a preferable alternative to the currently used energy-intensive Haber-Bosch process. This process combines nitrogen from the air with hydrogen derived mainly from natural gas (methane) for ammonia production and is thereby deemed unfriendly to the environment because of its huge energy requirements and CO_2 emissions. Although the electrochemical synthesis of ammonia is mostly in the research stage, the ammonia detection methods employed so far have been documented to be insufficient due to various reasons. The more pronounced one is their inability to reliably measure the low ammonia gas produced (in sub-ppm levels), without the interference of common contaminants. This is partly due to its polarity and large abundance in the atmosphere to an extent that the detected amounts could easily originate from different contamination sources (air, human breath, the N_2 gas source, unstable N-containing compounds, etc.). To counter this particular problem, the use of isotopically labelled nitrogen gas has been introduced to distinguish between the ammonia gas produced from the electrochemical synthesis process and the probable contaminants. The greatest disadvantage of the analytical methods employed so far, for the NH_3 isotopic measurements is their inability to suppress water signals in order to quantitatively determine the $^{15}NH_3$ signal owing to the small mass difference of 0.008 amu between H_2O and $^{15}NH_3$, which causes uncertainties in the detection of $^{15}NH_3$ at low ammonia concentrations [2]. One spectrometry method i.e. photoacoustic spectroscopy has shown an ability to detect NH_3 at very low concentrations ($\approx$ 50 ppb) [3]. My thesis, therefore, focuses on the use of the photoacoustic detection method in the making of a near-infrared ammonia gas detection system that can selectively and sensitively detect and differentiate between the ammonia isotopes at relatively low concentrations. The developed system is expected to contribute to the research and advancement of the current technologies for ammonia production and detection in addition to improving the quantitative results where the determination of isotopically labelled ammonia is required.

The immediate planned application for the developed near infra-red photoacoustic (NIR-PA) system is in the detection and quantification of the discharged ammonia gas during the electro-

reduction process of nitrogen gas and water or steam. Another planned project is in the agricultural sector where the system can be used to investigate both soil and plant physiological processes. This would involve the isotopic tracing of the denitrification process in the soil/vegetation by application of ^{15}N labelled fertilizer to estimate the nitrogen loss in form of ammonia. The transformation of soil N, like denitrification or the N fixation by plants, could also be traced by this technique. The developed system is also expected to find an application in the source apportionment of atmospheric ammonia concentrations. The change in abundance ($\delta^{15}NH_3$, ‰) i.e., the source signature is representative of the given physical and chemical process. Identifying the ammonia source (e.g., agricultural or fossil fuel combustion process, industry, heating, traffic) by nitrogen isotope helps in designing a mitigation strategy for policymakers.

The overview of my thesis is as follows, in chapter two I will give the general literature review on the analyte (ammonia), its isotopes, current measuring instruments (together with their limitations), target application and a working theory of the proposed photoacoustic method to be used in my constructed system. In chapter three, I will then outline my objectives and the specific problems to be tackled. Chapter four will give a theoretical description of the resources and methods used while explaining their working modes and mechanisms. Chapter five will then cover the results and discussions of the optimization and the calibration of the developed near-infrared photoacoustic system, giving an insight into its operation and attempts to improve it. Lastly, I will give the conclusions together with the new scientific results and a summary of the whole work.

2. Literature review

Ammonia (NH_3) gas is colourless and lighter than air with a pungent characteristic smell. The boiling point of liquid anhydrous NH_3 is –33.34 $^{\circ}$C at atmospheric pressure. Generally, above 9-10 bar pressures at ambient temperature, NH_3 retains its liquid state, enabling it to be stored in low-pressure vessels [4]. Atmospheric NH_3 is the third most abundant gas containing nitrogen in the atmosphere after N_2 and N_2O and the only alkaline gas. It plays a primary role in the formation of secondary particulate matter on reaction with atmospheric acidic species, notably, sulphuric and nitric acid to form $PM_{2.5}$ aerosols in the atmosphere. In general, this ammonia-containing aerosol causes air quality, visibility and atmospheric radiation balance degradation [5]. This makes NH_3 an air pollutant that contributes to the eutrophication and acidification of ecosystems. As a result, NH_3 emissions and deposition have generated much interest and concern among environmentalists, epidemiologists and ecosystem scientists [6]. Major sources of NH_3 have been documented to be from agricultural sources, i.e., fertilizers used on farms and waste from domesticated animals. The non-agricultural sources which are problematic in terms of quantification owing to their diffuse spatial distribution are natural soils, vegetation, human waste (sewage sludge), human respiration, wild animals and oceans [7]. Other notable sources include industrial and fossil fuel combustion in the traffic sector, especially in urban areas [5].

Two scientists, Fritz Haber and Carl Bosch in the years 1905 and 1910 invented and discovered an industrial process for NH_3 production, respectively, for which they both won a Nobel Prize, and the process is still widely applied today. Currently, traditional Haber-Bosch plants produce NH_3 using natural gas (50%), oil (31%) or coal (19%) as feedstock [8]. The natural gas process which presents the best available technique utilizes methane which is a fossil fuel as a raw material for hydrogen in its NH_3 synthesis as summarized in the equations below [9];

$$CH_4 + 2\,H_2O \rightarrow 4\,H_2 + CO_2 \text{ (Steam reforming reaction)} \quad (1)$$

$$N_2(g) + 3\,H_2(g) \rightarrow 2\,NH_3(g) \text{ (Ammonia hydrogenation reaction)} \quad (2)$$

The steam reforming reaction that generates the hydrogen is separate from the ammonia hydrogenation reaction which is kinetically disfavoured at ambient temperature and pressure. To bypass the kinetic limitation, the Haber-Bosch process is carried out at high temperatures and pressure making it energy-intensive.

The most common applications of NH_3 either in its pure form or as the feedstock of other chemicals include;

- The chemical industry: This incorporates the production of pure NH_3 for various purposes. Examples are, fertilizers in the agricultural sector, refrigerant gas in the food processing industries, alkaline cleansers (window and floor), dyes, fibres and plastics, explosives [ammonium nitrate and trinitrotoluene (TNT)], in the manufacture of synthetic polymers (acrylics and nylons) [10], and lastly for $DeNO_x$ processes applicable in power plants for NO_x emission reduction [11].

These applications and others are summarised in Figure 1.

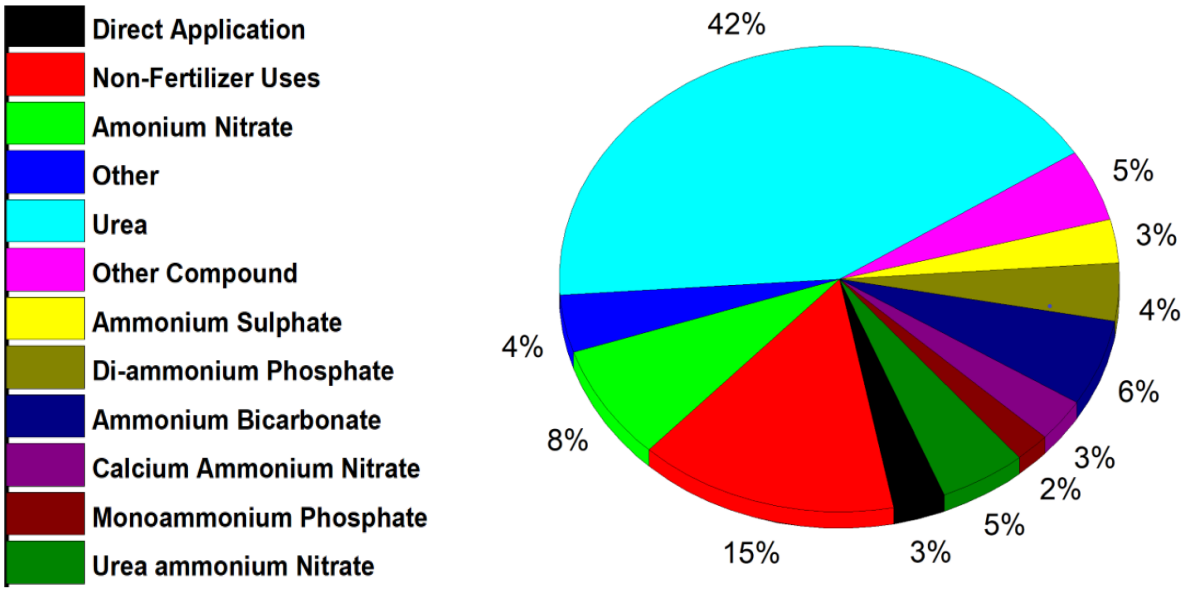

Figure 1: Ammonia applications as a percentage of total manufactured ammonia [12].

Furthermore, the determination of ammonia concentration is important in the following areas:

- Environmental analysis monitoring [13,14]
- Diagnostic tool in medicine where breath ammonia has been used in the assessment of *Helicobacter pylori* infection, and also when measured as a correlation against blood samples, in the determination of blood urea nitrogen and creatinine that serves as indicators of nitrogenous waste loading in a haemodialysis patient [15–17]
- Automotive industry. Here NH_3 sensing is important for three major reasons. First for quality monitoring of exhaust gas to be able to track and reduce gaseous pollution in the environment [18,19]. Secondly to monitor and determine the air quality in the passenger compartment to control the ventilation by filtering the incoming air for any pollution [20] and lastly for the NO_x reduction specifically in the diesel engines [21,22].

Table 1 summarizes the requirements for NH_3 gas analysis in the above-mentioned application areas.

Table 1: Summary of the requirements for common NH_3 gas analysis in different application areas [23].

Application	***Temperature range***	***Detection limit***	***Response time required***
1. Automotive industry			
- Quantifying NH_3 gas emissions from vehicles	Up to 300 ˚C	4 -> 2000 g/min [18]	Seconds
- Passenger cabin air quality	0-40 ˚C	50 ppm	≈ 1s
- Detect NH_3 slip	Up to 600 ˚C	1-100 ppm [19]	Seconds
2. Chemical industry			
- As a leakage alarm	Up to 500 ˚C	20 - >1000 ppm [24]	Minutes
3. Environmental monitoring			
- Dairy and livestock rearing industry	0-40 ˚C	0.1ppb to >200 ppm[25]	Minutes
- Monitoring ambient conditions	10-40 ˚C	0.1 to 10 ppb [26]	≈ 1min
4. Medical diagnostic field			
- Breath analysis	20-40 ˚C	50-200 ppb [15,16]	≈ 1min

2.1 Ammonia isotopes

Isotopes are two or more types of atoms that have the same atomic number and position in the periodic table and that differ in nucleon numbers due to different numbers of neutrons in their nuclei. This isotope number is always written as a left superscript. The isotopic abundance of an atom relative to a given standard can be expressed as in equation 3;

$$\delta_{\text{standard}} = \left(\frac{R_{\text{sample}}}{R_{\text{standard}}} - 1\right) \times 1000 \quad (3)$$

$$\text{where } R = \frac{\text{abundance of the heavy isotope}}{\text{abundance of the light isotope}} \quad (4)$$

The term δ_{standard} denotes the isotope ratio of the sample expressed in delta units (‰, per mil) relative to the standard material. R_{sample} and R_{standard} are the absolute isotope ratios of the sample and reference material, respectively [27]. Most atoms have both major and minor isotopes dictated by either the majority or rarity of their atoms in nature. For most applications, the determination and quantification in terms of concentration of a target gas are often enough, but for more in-depth understanding, the study of the target gas isotope ratios which tends to give more information about the gas source identification has been carried out [6,28,29].

NH_3 has two stable isotopes 99.636% of $^{14}NH_3$ and 0.364% of $^{15}NH_3$ [30]. The nitrogen atomic isotopic ratio $R = {}^{15}\mathrm{N} / {}^{14}\mathrm{N}$ expressed as parts per thousand ‰ is

$$\delta^{15}\mathrm{N}(‰) = \left[\frac{R_{\mathrm{sample}}}{R_{\mathrm{standard}}} - 1\right] \times 1000 \quad (5)$$

where R_{standard} = 0.00364 and corresponds to 0.364 weight % of ^{15}N. Major sources of $^{15}NH_3$ include fossil fuel combustion [31,32] whose emissions are generated from coal-fired plants, urban traffic, and agricultural farm machinery. Higher abundance of $^{15}NH_3$ from fossil fuel sources as compared to lower $^{15}NH_3$ values observed from agricultural sources have also been noted. This is attributed to the NH_3 formation during high-temperature combustion and the associated fractionation [33–35]. The depletion or enrichment of the $^{15}NH_3$ produced during combustion-related factors is largely dependent on catalytic converter efficiency and the temperature of the catalysts of every vehicle [36,37]. Another notable source is the agricultural sector whose emissions are from livestock waste [6,30,34,38,39] and fertilizer use [40–42] where $^{15}NH_3$ measured ranges are widely variable due to the difference in urea, fertilizer type, application rates, potential equilibrium and kinetic fractionation during volatilization process.

2.2 Electrochemical synthesis of ammonia

Ammonia production through the Haber-Bosch process occurs by feeding molecular nitrogen and hydrogen reactants over an iron catalyst at high pressure and temperature. This is an energy-intensive and methane-based method whose steam reformation process (equation 1) consumes 3~5% of the world's total natural gas [43], to produce approximately 146 million metric tons of NH_3 and 2.16 tonne CO_2/tonne NH_3 which amounts to more than 300 million metric tons of CO_2 annually [44,45]. This makes it a major contributor to greenhouse gas emissions and has tremendously increased the atmospheric CO_2 to ≈ 400 ppm [46]. Research has also noted that at the current rate of consumption, fossil fuel reserves formed over millions of years may be depleted in about 100 years.

Although the reported Haber-Bosch process energy efficiency is above average (≈ 55%), the capital costs involved are exorbitant because of the very high temperatures (~450 °C) and pressures (20-40 MPa) required. The process is therefore viewed as environmentally unsustainable because of the pressure and demands it exerts on the already scarce resources. Also, due to the above process's significant contribution to climate change i.e.

high CO_2 emission which roughly accounts for 7% of the total (666 Gt/y) and 0.5% of the anthropogenic (12 Gt/y) global annual emission, it has become imperative in the scientific community to develop alternative methods for NH_3 synthesis. Although electrochemical synthesis of NH_3 is a field that is still largely in the research and development stage, preliminary results leading to NH_3 production through the electro-reduction of nitrogen gas and water or steam have been well documented [47–50].

For electrochemical nitrogen (N_2) conversion to NH_3 process the following equation applies:

$$\frac{1}{2}\,N_2 + 3\,H^+ + 3\,e^- \rightarrow NH_3 \qquad (6)$$

Nitrogen gas is supplied at the cathode which leads to hydrogen atoms being generated at the cathode and the production of NH_3 according to equation 6. Generally, unlike the Haber-Bosch process, electrochemical synthesis of NH_3 under mild conditions is an environmentally friendly process since it has a provision for direct conversion of renewable energy (electricity) into chemical energy (in form of NH_3) with zero CO_2 emission [51]. Different types of electrolytes have been tested including but not limited to liquid electrolytes, e.g. organic solvents [52], ionic liquids [53], molten salts [9,54], solid-state electrolytes [55] and aqueous electrolytes [56–58]. Each has its advantages and disadvantages in terms of costs, efficiency, reaction rate and simplicity (design and implementation). Some disadvantages that cut across these electrochemical methods are the low efficiency (0.1-8%) that has so far been achieved [54], inaccurate determination of low NH_3 levels because it is the most abundant alkaline gas in the atmosphere and as such exists almost everywhere including but not limited to human expired breath (0.3-3.0 ppm ammonia), ambient atmosphere (0.0001-0.01 ppm ammonia) and unstable N-containing compounds incorporated in the experimental set-up [59]. For the electrochemical synthesis of the NH_3 process, the suitability and operation of the electrochemical cell chosen are determined by two major parameters: its Faradaic efficiency and NH_3 formation rate. Estimation of both parameters which are independent of the NH_3 concentration is determined by the accurate measurement of the NH_3 produced electrochemically. This is not always easily achievable due to its solubility in water, polarity and small molecular size which makes it dissolve in water and adsorb on the experimental handling surfaces, for example, the tubing and other laboratory materials. Therefore, in most catalytic experiments, quantitative measurement of NH_3 is carried out in aqueous solutions [60].

2.3 Ammonia measurement methods

Currently, several field and analytical methods have been employed for NH_3 measurements largely depending on their main emission sources i.e. fossil fuel combustion or agricultural sources. Common methods documented so far are flux measurements, chemical sampling and a wide sort of spectroscopic methods (spanning through the whole electromagnetic spectrum). Flux measurement which is based partly on both concentration and micrometeorological measurements includes Tracer Gas Ratio Technique (TGRT), enclosure and micrometeorological methods and Passive Flux Samples (PFS). The main disadvantages of this method are high costs, replicability issues and difficulties in correctly duplicating surface and environmental aspects in closed spaces thereby leading to large approximations and empiricism [61]. Out of the four techniques, only two, namely, TGRT and PFS which operates on the principle of diffusion have been confirmed to be applicable in NH_3 isotope measurements. A study by Bhattarai et al. showed that collecting samples that were representative of emission sources presented a big challenge when it came to fingerprinting $\delta^{15}N(NH_3)$ values of the NH_3 emission sources [62]. Also, the isotopic fractionation during NH_3 gas-to-particle conversion remained unclear, especially under varying ambient field conditions and therefore, required further field and laboratory research to validate theoretical isotopic fractionation predictions. Bhattarai's study investigated the validity of formerly reported NH_3 emission sources as a representative for tracer studies and made a review of the recent isotope-related progress done in the collection of $NH_x(NH_3 + NH_4^+)$ for $\delta^{15}N$ (NH_3) isotope source signature of major NH_3 emission sources.

The second method is the chemical sampling method which comprises of Saraz method for the determination of NH_3 emissions (SMDAE) [63], gas washing [61], continuous annular denuder systems (AMANDA) [61], wet efficient diffusion denuder (WEDD) [64], and Long Path Absorption Photometer (LOPAP). SMDAE has good accuracy, and is easy to construct and transport but is based on diffusion to a reaction surface hence requiring a longer sampling time (hours) [63]. Gas washing has high sensitivity but is labour-intensive and prone to sample contamination hence is mostly applicable where fast sampling is not required. AMANDA is most suitable for micrometeorological gradient measurement of NH_3 but has a low precision [61]. Apart from AMANDA and WEDD, the other wet chemical sampling method's suitability for NH_3 isotope measurements has not been reported in the literature.

The most widely used NH_3 measurement method is spectrometry. Here several instruments/techniques have been applied. They include; Fourier Transform Infrared Spectrometry (FTIR) which is capable of simultaneous measurement of different targeted gas

species although in most instances it may have limited sensitivity due to spectral overlap [65]. Chemical Ionization Mass Spectrometry (CIMS) which uses ion-molecule reactions to selectively ionise and detect trace NH_3 in ambient air, is sensitive, selective and offers reliably fast time resolution. CIMS major challenge is in its understanding and controlling its background signal [66]. Ion Mobility Spectrometry (IMS) is based on the determination of the mobility in electric fields of gas-phase ions derived from constituents in a target sample. IMS has high sensitivity and fast response during ion mobility spectra but low resolving power and very limited selectivity [67]. Tunable Diode Laser Absorption Spectrometers (TDLAS) can be tuned to specifically select a single absorption line of a given sample gas without interference or overlap from other gas species absorption lines thereby making it very selective but it is highly sensitive to noise levels [64,68]. Chemiluminescence detectors have also been applied in NH_3 measurements. They make use of quantitative optical emission measurements realised from energised chemical species to be able to calculate the analyte concentration in either solution or gas phase. Although a simple instrument with low detection limits and wide dynamic ranges, it suffers from a lack of sufficient selectivity and sensitivity to various physicochemical factors [61]. Differential Optical Absorption Spectroscopy (DOAS) has a fast response and low maintenance but high noise levels [25]. Cavity ring-down spectroscopy (CRDS), a sensitive absorption technique where the rate of absorption rather than the magnitude of the absorption of a light pulse confined in an optical cavity is measured, is simple to set-up and is also independent of pulse-to-pulse fluctuations of the laser although CRDS is very expensive as compared to other spectroscopic techniques [69,70]. Quantum Cascade Laser Absorption Spectroscopy (QCLAS) has high sensitivity, fast response time and a high spectral resolution which gives good selectivity between different targeted species [71]. Lastly and of importance to our work is Photoacoustic Spectroscopy (PAS) which has been documented to be easy to operate under field conditions, and has high precision and fast response time [14,72,73]. Further benefits are because of the minimum detection limit (MDC) which is largely independent of the laser gas interaction time length. This quality, therefore, ensures the sensitivity and miniaturisation of the PAS equipment. On top of this PAS also exhibits zero-background property while its signal tends to vary linearly as a function of the absorbed laser power. Examples of research done in this area include Huszár [3] and Pogány [74] whose detecting systems for measuring ambient ammonia concentration had MDC of 50 ppb and 0.5 ppb with a response time of 2 min and 30 min respectively. They both used wavelength modulations and distributed feedback diode lasers, but the latter installed a tungsten (VI) oxide preconcentration unit for the ammonia sampling. Others, including Bozóki (0.6 ppm, 3 min) [75],

Schilt (0.1 ppb) [14], Miller (0.15 ppb) [76], and Wang (0.86 ppb, 5 min) [77], all used different types of lasers with differing amount of powers and sampling flow rates for their measurements. Wang (16 ppb) [78] in his breath ammonia detection experiments and Besson (0.6 ppb, 10 sec) [79] both used erbium-doped fibre lasers, with the former performing multiwavelength measurements and the latter single wavelength measurement at the near infra-red range. Lastly, Bonilla-Manrique (785 ppb) [80], and Guo (3.2 ppb, 30 sec) [81] incorporated an optical microphone and fibre-optic extrinsic Fabry-Perot interferometer-based cantilever microphone respectively into their PAS experiments. Although most spectrometry methods can detect NH_3 isotopes, very few can distinguish between its isotopologues.

Currently, six types of techniques are employed in the determination of the total NH_3 concentration generated by the electrochemical synthesis process. These include spectrophotometry which is aqueous-based and uses the salicylate method and Nessler's reagent. The methods are low-cost and have been noted to show good sensitivity. In comparing the two, Nessler's method has a shorter detection time and relies on fewer reagents than the salicylate method, although the former is considered toxic and has a very limited shelf life (3 weeks) in addition to requiring extra pre-treatments for the eliminations of metallic ions and sulphides that could potentially interfere with its operation [82]. The second technique is Ion chromatography, which ensures reproducibility, quick simultaneous detection of multiple ions and a low detection limit. The major disadvantage of the method is its inability to differentiate between $^{14}NH_3$ and $^{15}NH_3$ isotopes since $^{15}NH_4^+$ and H_3O^+ share similar nominal m/z, a situation that has not been solved even by the application of Ion chromatography-mass spectrometry [83]. Other techniques are the Fluorometric method and the ^1H NMR. The former displays high sensitivity but suffers from interference by amino acids and amines which acutely affects ammonia quantification, while the latter although being a direct method and highly selective also suffers from accurate ammonia measurement due to the laborious NH_3 isolation through distillation and hence lengthy data acquisition time [84,85]. The last two techniques are ultra-high-performance liquid chromatography-mass spectrometry which is capable of quantifying and distinguishing between the two NH_3 isotopologues [86], and the ion-selective electrode (ISE) which has a large detection range and is practically suited for continuous monitoring. However, the ISE has been continually plagued by poor sensitivity of NH_3-N, especially at low concentrations, a factor that currently limits its widespread application [87]. The above-mentioned techniques and other commercial products applied in the NH_3 quantification during the electrocatalytic process are summarized in Table 2.

Table 2: A summary of different ammonia detection methods employed in electrocatalytic studies including commercial products.

Method including commercial products	MDC and response time	Detection range/ Ammonia formation rate	Challenges
- External cavity quantum cascade laser [88]	150 ppb (50 ms) 10 ppb (10s)	9.4-10.8 μm at a 20 Hz rate	- Low tuning range hindering multi-gas sensing
- NMR spectroscopy (800MHz) [89]	51 ppb		- Expensive, sensitive to contamination and needs a large sensing volume
- Ammonia ion sensing electrode. 1. ASTM D1426-15 [90] 2. APHA 4500-NH_3 D [91]	1. 0.5 ppm 2. 0.03 ppm	1. 0.5-1000 ppm NH_3-N 2. 0.03-1400 ppm NH_3-N	- Precision decreases with low NH_3 concentration. - Possible escape of gaseous ammonia
- IR Spectroscopy [92]		2.0×10^{-8} mol s^{-1} cm^{-2}	- Spectra interpretation requires expertise - Limited quantitative analysis under very high and low concentrations conditions
- Chemical ionization mass spectrometry (CIMS) [66]	0.05 ppbv (5 sec)	0.05-0.1 ppbv	- Problem controlling background signal
- Mass spectrometry [93]		4×10^{-9} mol s^{-1} cm^{-2} at 72 mA cm^{-2}	- Uncertainties at very low NH_3 concentrations.
- Cavity ringdown spectrometry (CRDS)		1. 2.9×10^{-9} mol s^{-1} cm^{-2} at 12.5 mA cm^{-2} [94] 2. 0.5×10^{-9} mol s^{-1} cm^{-2} at 2.4 V (applied potential) [95]	- Analytes are limited by the availability of tunable laser light at the appropriate wavelength. - Very expensive.
- Ion chromatography [96]	0.02 ppm	0.02-40 ppm	- Aliphatic amines and metal ions e.g. Na^+
- Phenate method [97]	0.01 ppm	0.01-2.0 ppm	- Random colour development error and Low toxicity
- Spectrophotometry 1. Salicylate method [97] 2. Nessler's reagent method [97]	 0.01 ppm 0.025 ppm	 0.01-1.0 ppm 0.025-5.0 ppm	 - Strong PH effect while exhibiting low toxicity - Time-consuming - Stability and toxicity issues
- Surface-enhanced Raman scattering [98]	sub 1ppm (1 sec)		- Poor repeatability which hinders reliable quantitative measurements

The unit conversions used are 1 ppm ≈ 1 mg L^{-1}, and 1 mol L^{-1} NH_3 or NH_4^+ ≈ 14000 ppm of NH_3-N, 17000 ppm of NH_3 or 18000 ppm of NH_4^+.

In practice, the accurate determination of the generated NH_3 using the above methods has encountered several challenges as documented in the last column of Table 2. To overcome the above problems, while also providing definite proof that the generated ammonia is from the N_2 electroreduction and not the various contaminants, it has become imperative to use isotopically labelled nitrogen for the electrocatalytic process.

2.4 Photoacoustic measurement method

Photoacoustic (PA) spectroscopy is an optical absorption spectroscopy technique that directly measures optical absorption by converting the absorbed light energy into sound energy. The PA effect was first recognized by Alexander Graham Bell in the 1880s when he discovered that thin discs of selenium emitted sound when exposed to a rapidly interrupted beam of sunlight [99]. There are five important mechanisms responsible for photoacoustic signal generation including dielectric breakdown, vaporization, thermo-elastic expansion, electrostriction, and radiation pressure. The first two mechanisms involve an irreversible change of state in materials and are rarely used for imaging. Electrostriction and radiation pressure, in general, contribute minimally to photoacoustic signal generation, especially in low optical absorption samples, and are usually neglected. Thermo-expansion is considered a major mechanism. The amount of energy material absorbs is proportional to its concentration. The absorbed light energy is released as heat and it makes the pressure rise. When the incident light is modulated or pulsed at the modulation frequency, the pressure increase is periodic at the modulation frequency, and a pressure wave is created, or sound waves, which are easily recorded with a microphone. The amplitude of the generated sound is directly proportional to the concentration of the absorbed gas component [100].

PAS is, therefore, the measurement of the effect of absorbed light on matter (gas, liquid and solid) through acoustic detection. From Figure 2, it can be seen that a PA signal which is recorded by a microphone is the amplitude of the electric output signal of the microphone at the frequency of laser modulation (generated via the PA effect). This signal can be generated not only by periodically modulated light sources but e.g. by pulsed lasers too and not only in gases but in liquids and solids too. PAS is a powerful technique to study concentration at very small levels (part per billion or even part per trillion) which makes it quite sensitive in comparison to other conventional spectroscopic techniques.

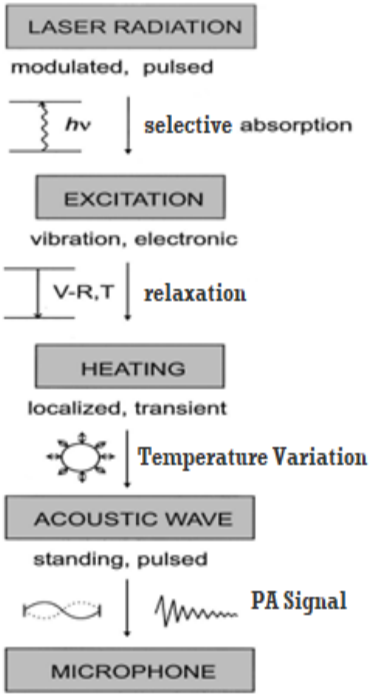

Figure 2: Schematic of the physical processes occurring after optical excitation of molecules using modulated or pulsed. The resulting expansion launches standing or pulsed acoustic waves, which are detected with a microphone [100].

The selectivity of the PA method is attributed to its high-resolution spectroscopic base. The NIR wavelength which has been applied in this work has been documented to have overtones and absorption bands of many molecules. Hence from the spectroscopic point of view, it can be termed as crowded. To overcome this, cross-sensitivities measurements were done to be able to identify all the interfering molecules in our chosen NIR wavelength measurements range.

All spectroscopic methods yield quantitative information by measuring the amount of light a substance absorbs. PAS measures this more sensitively and precisely since it is a direct method, unlike other indirect spectroscopy techniques. There is a huge need for high-sensitivity in gas detectors in research and industrial field which often deal with highly toxic gases, considered hazardous at very low levels. Our daily lives generate a large amount of polluting gases, some of which are dangerous with long-term exposure to trace amounts e.g., carbon monoxide, methane, hydrogen sulphide and nitrogen oxide. Because of its superior sensitivity to comparable techniques, PAS is therefore generally favoured.

2.4.1 Theory of photoacoustic (PA) spectroscopy

The PA signal generated and recorded by the microphone is given by the following equation [99];

$$M_{\mathrm{PA}} = S_{\mathrm{M}} \times P_{\mathrm{in}} \times \left(C_{\mathrm{cell}} \times \alpha_{\mathrm{mol}} \times c_{\mathrm{i}} + A_{\mathrm{b}}\right), \quad (7)$$

Where:

M_{PA} (mV)	Microphone signal which gives the amplitude of the Fourier component of the microphone signal at the frequency of light modulation
C_{cell} (Pa·cm/W)	Photoacoustic cell constant
S_M (mV/Pa)	Microphone sensitivity
P_{in} (W)	Incoming exciting light power
α_{mol} (1/(cm· ppm))	The specific optical absorption coefficient, of the light-absorbing components at the wavelength of the exciting light
c_i (ppm)	The concentration of the light-absorbing components
A_b (Pa/W)	Background PA signal generation efficiency

The PA signal usually has a phase lag with respect to the light intensity which depends on the time scale of the collisional relaxation processes, and a noise that increases with decreasing frequency and volume. The quantity $S_{\mathrm{M}} \times P_{\mathrm{in}} \times A_{\mathrm{b}}$ in Equation 7 is called the background signal which is also generated at the laser modulation frequency and arises due to the absorption of modulated light by the windows or the walls of the cell. The standard deviation of this background signal is called background noise and during measurements, great care should always be taken to minimize it.

The minimum detectable concentration (MDC) of a photoacoustic system is a ratio of three times the standard deviation of the background signal (σ) (background noise) divided by the sensitivity (m). σ denotes the standard deviation of the measured signal when the concentration of the measured analyte is zero in the PA chamber. This can be achieved by measuring in null-gas which does not contain the measured analyte but otherwise, its composition is the same as much as possible as that of the target analyte. In ideal cases, null- gas can be generated from the target analyte by removing the component to be measured using a scrubber material. MDC is denoted in Equation 8.

$$\mathrm{MDC} = \frac{3.3\sigma}{\mathrm{m}} \quad (8)$$

There are several ways of determining the background signal, where the most common method is by performing a background measurement at the exact target analyte absorption

wavelength but in a gas mixture devoid of the target analyte. This is mostly achieved by using synthetic zero-gas (normally pure nitrogen) in its natural form or from a cylinder, as was the case in this study.

From equation 7 it can be seen that whenever the background signal is zero or negligible then the PA signal is linearly proportional to the concentration of the light-absorbing target species [99]. This proportionality is generally valid in a wide concentration range; that is, the dynamic range of PA instruments is usually four to five orders of magnitude in concentration.

2.4.1.1 General structure of the photoacoustic system

The standard PA measurement set-up contains a light source (in most cases a laser is used), a PA cell, an electronic driver and a gas sampling unit. The sampled gas is introduced into the PA cell, the PA signal is generated there and measured by microphones attached to the cell. The generated sound signal by the PA effect is normally low, so amplifying and signal processing is needed. One of the important quantities should be the signal-per-noise ratio. The better the signal-per-noise ratio is, the higher the sensitivity of the concentration measurement. The acoustic resonator, which amplifies the generated acoustic signal, is set inside the photoacoustic cell. Optical windows through which light enters and leaves the cell are installed in the photoacoustic cell; acoustic filters (i.e., specially designed buffer volumes, low-pass-filter), gas connections to the gas sampling system and a pump can also be set depending on the target of the measurement to be done.

2.4.1.2 Photoacoustic signal calculation

A photoacoustic signal is a vector quantity that can be described by the amplitude (r) and phase of the signal (ϕ) or x and y components of the signal. One of the major factors that influence both the amplitude and the phase of the generated PA signal is the delayed molecular relaxation effects whose amplitude dependence on the photoacoustic signal can be incorporated in equation 7 using parameter η and summarised as [99] ;

$$\eta = \frac{1}{\sqrt{1+(\omega\tau)^2}} \tag{9}$$

Where $\omega = 2\pi f$ is the modulation frequency and the value η is dependent on the molecular relaxation time τ. The PA signal detected at the microphone has a phase lag with respect to the incident light power. This occurs since the PA signal generation is complex and occurs through various independent sub-processes as depicted in Figure 2. The phase of the PA signal denoted by ϕ has a dependency on the molecular relaxation time as shown by equation 10.

$$tg\phi = -\omega\tau \tag{10}$$

Generally, for the molecular relaxation effects to be considered insignificant, $\omega\tau \ll 1$ and the PA signal will be in phase with the laser modulation ($\emptyset = 0$). When the molecular relaxation process is slow, then $\omega\tau \gg 1$, and the PA signal will be shifted with respect to the laser modulation ($\emptyset \neq 0$) [101]. Phase is most important when it is variable i.e., changing for different measured components.

Figure 3 gives the amplitude value of the PA signal represented in a complex plane as $r = \sqrt{X^2 + Y^2}$.

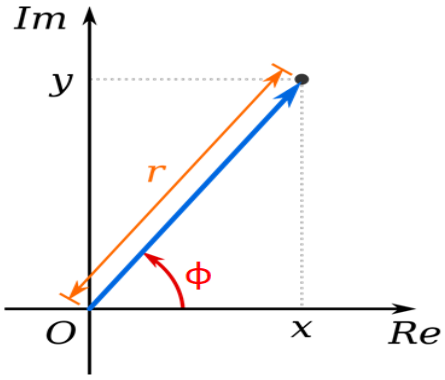

Figure 3: Graphical illustration of the photoacoustic signal depicting the phase (ϕ) and the amplitude (r) in a complex plane [102].

The absolute value of the PA signal, together with the X and Y components can be measured resulting in a differential signal between the PA signals at two wavelengths (WL_1 and WL_2) which can then be calculated as:

$$\text{PA signal}_{(WL1-WL2)} = \sqrt{(X_{WL1} - X_{WL2})^2 + (Y_{WL1} - Y_{WL2})^2} \tag{11}$$

The resulting signal in equation 11 has been noted to be almost double in size of the individual PA signal at specific wavelength values. If wavelength modulation (WM) is applied, PA signals at two specific wavelengths, have opposite phases i.e., PA(WL_1) and PA(WL_2) correspond to two peaks of the first derivative of a single absorption line. Consequently, the subtractions in equation 11 increases (almost double) these signals.

The phase difference is the consequence of the applied WM to the PA signal, and while it increases the sensitivity of the measurement system, it is also a very efficient tool for decreasing cross-sensitivities too. Whenever an interfering component generates roughly equal PA signals at the measurement wavelengths with the same phase, this subtraction diminishes its influence.

3. Objectives

The Photoacoustic Research Group of the University of Szeged has for the past two decades been working on the various applications and adaptations of its photoacoustic systems which have grown from demonstrative laboratory devices to reliable and well-engineered field instruments. One such promising application is in the detection and quantification of the discharged ammonia gas during the electro-reduction process of nitrogen gas and water or steam. As was previously shown, the accurate determination of the NH_3 generated during electrochemical synthesis has encountered several challenges and the currently available analytical techniques do not meet the requirements.
I, therefore, aim to develop an alternative method for the selective, rapid, and sensitive measurement of ammonia generated in the electrochemical synthesis by using a NIR-PA system. I will also demonstrate experimental quantitative isotopic measurements that aim to decrease the cross-sensitivity of common contaminants.

My main aim is to design and build a gas concentration measurement device for the photo-electrochemistry research group based on the PAS concept, which can be able to selectively measure and differentiate between ammonia gas isotopes.

To achieve this goal, there is a need for methodological development, construction of the measuring instruments and finally, the development of gas sampling procedures to be used. The following subtasks were therefore planned:

1. Design and construction of a NIR-PA system capable of selectively measuring and differentiating between ammonia gas isotopes ($^{14}NH_3$ and $^{15}NH_3$).
2. Optimisation of the measurement and modulation parameters (wavelength, and laser operating temperature).
3. Testing and calibration of the newly developed NIR-PA system.
4. Evaluation of the developed NIR-PA system.

4. Resources and methods

4.1 General remarks on NIR-PA system development

For the last two decades, the University of Szeged Photoacoustic research group has published articles and dedicated themselves to developing PA systems based on near-infrared (NIR) telecommunication type fibre coupled with distributed feedback (DFB) diode laser light sources. Most of these have found applications in different fields including meteorology [103,104], medical diagnosis [105], flux measurements [103], and the petrol industry [106,107]. The possibility of using the long wavelength end of the near-infrared (e.g., the wavelength range of around 2000 nm) for my system rather than the telecommunication window was considered. This was because there are considerably stronger absorption lines in this long wavelength region compared to the telecommunication window wavelength range. Although tempting, the idea was decided against for three major reasons. Firstly, the few mW light power of a typical diode laser operating in the longer wavelength range is comparable to ≈50 mW light power of a telecommunication diode laser which has the extra advantage of being able to be doubled by simply fibre coupling two of them, for increased light power. This is so because the generated PA signal depends on the product of the optical absorption coefficient and the light power, a product that is approximately equal for the two types of lasers, therefore the disadvantage of weaker absorption lines can be compensated by the much higher light power of the telecommunication diode lasers. Secondly, another advantage of the telecommunication type diode laser is their availability in a fibre coupled construction, making them very robust with an operational lifetime > 10 years. Lastly, they are more cost-effective than their long wavelength counterparts.

Apart from the choice of the wavelength range, other main components of the fabricated NIR-PA system included the PA detection cell, the light sources and integrated electronics for signal control and measurement as discussed below.

4.1.1 Photoacoustic detection cell

For laser light detection purposes, two types of photoacoustic chambers currently exist, non-resonant and resonant chambers [100]. In summary, for a resonant chamber, the modulation frequency used should coincide with one of the chamber modes (longitudinal, azimuthal or radial) unlike for the non-resonant case. Although the non-resonant has the advantage of the possibility of using a small volume chamber, its background signals caused by the absorption of the target gas by the windows and walls of the chamber severely limit the

PA systems' sensitivity. For my case, I used a resonant chamber that was identical to previously used PA detection systems in various University of Szeged PA Research Group applications. The detection unit was a longitudinal differential PA cell characterised by a cell constant of C≈20 mV×cm/W. This simply means that, on shinning the PA cell with a modulated laser light having a light power of P = 1 mW, at the wavelength of the laser, the gas within the cell will have an optical absorption coefficient of α = 1 cm^{-1} and the microphone signal (M) generated at the laser modulation frequency, set to be equal to the first longitudinal acoustic resonance frequency of the cell, will be M ≈20 mV.

The PA detection cell design used is shown in Figure 4.

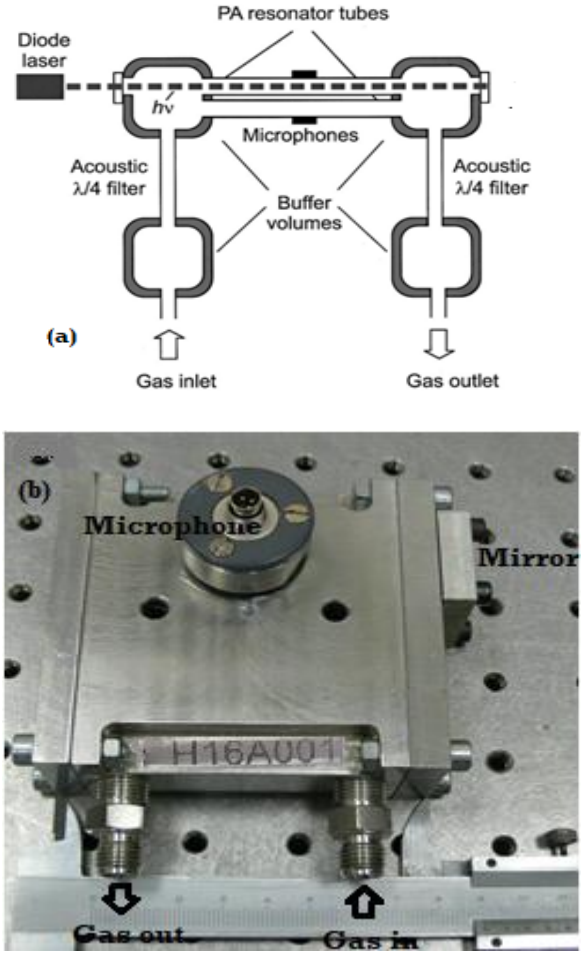

Figure 4: (a) A typical schematic of a differential PA cell made by the University of Szeged Photoacoustic Research Group [108]. **(b):** Shows the PA cell used incorporating a back-reflecting mirror at the exit window.

Two cylindrical acoustic resonator tubes of size 4 cm long and 3.5 mm inner diameter, placed between two λ/4 acoustic filters were used in the PA cell. The gas flow passed through both resonator tubes while an excited laser beam was projected through a window on one side

of the chamber, made of quartz glass and coated with an anti-reflection layer, parallel to the longitudinal axis and into only one resonator tube. The beam then excited the sample gas in the first longitudinal resonance (0, 0, 1 mode) whose Eigen-frequency was ≈ 4500 Hz with a quality factor ≈ 10, thereby generating a PA signal in only one tube. The resonance frequency of the chamber was dependent on the gas composition through the sound propagation velocity, which was a non-linear function of temperature, eliminated in our experiments by using a temperature-stabilized chamber. The resonator tubes then opened into two buffer volumes where the gas to be measured was already fed through $\lambda/4$ acoustic filters with the use of a flow rate controller which limited both the response time of the measurement system and the absorption-desorption process of NH_3 gas on the PA window, cell wall and the gas handling system. This in general helped in eliminating the acoustic losses through the PA cell openings. For my application, I aimed to increase the signal-to-noise ratio by doubling the path through which light was absorbed within the PA cell. This was achieved by mounting a back-reflecting mirror right after the exit window of the PA cell as shown in Figure 4b. (NB: this was included in the PA cell design after preliminary experiments of the NIR-PA system without the mirror showed low sensitivity and its calibration gave high values of MDC, see results section.)

Two detecting microphones (EK 3029, Knowles Inc., sensitivity 50 mV/Pa at normal pressure) were centrally placed into holes that were drilled into the resonator tubes. Although the microphones used were electrets and therefore did not require biasing (due to their diaphragms being polarized during the manufacturing process) they still needed a supply voltage for them to operate. The purpose of the acoustic filters shown in Figure 4(a), was to filter out the noise generated by the gas flow since the measurements were performed with a continuous gas flow to ensure that the composition of the gas in the chamber at any given time was the same as the gas to be measured. A differential measurement was done by the PA system since although the PA chamber had two resonators of equal size, the projected laser light only passed through one of them enabling its microphone to detect both the PA signal and noise while the other microphone that was situated in the second resonator only detected noise. The overall measurement was then found by subtracting the signals from the two microphones.

4.1.2 Light sources used for the photoacoustic detection

For my work, two types of lasers were used the tunable external cavity and distributed feedback diode lasers which are discussed in the next section.

4.1.2.1 Tunable external cavity diode laser

An external cavity diode laser (ECDL) of type Sacher TEC 520 which had a tunable wavelength range between 1470 nm and 1590 nm was used. Its output light power was ≈ 50 mW which was measured when the laser was amplitude modulated since the DC was 0, and the AC was defined as a square wave function from a threshold value to a manufacturer's maximum current of 325 mA. Generally, an ECDL uses the diffraction grating technique as its wavelength-selective element in an external resonator. The emission wavelength was therefore defined by two features, namely, the cavity mode and amplification range of the gain medium. The Sacher TEC 520 had a synchronization between its grating and cavity-defined wavelengths controlled by simple rotation of the tuning mirror cased inside the laser. By using the Littman-Metcalf configuration, the output beam tended to have a fixed direction that exhibited a smaller linewidth [109].

For this laser, a microphone amplifier was used which was powered by a 24 V DC. The input signal was from the microphone attached to the PA cell while the output signal was connected to the lock-in amplifier through its A/I connection. Figure 5 gives a block diagram of the measurement set-up.

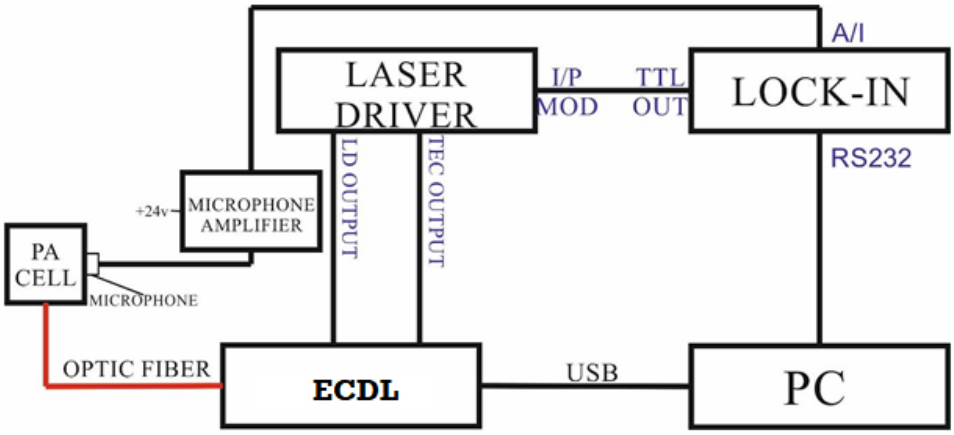

Figure 5: Block diagram of the measurement set-up using the tunable external cavity diode laser.

NB: for the preliminary testing of the NIR-PA system without the back reflecting mirror, the external cavity diode laser was not used.

4.1.2.2 Distributed feedback diode laser

A telecommunication fibre coupled DFB diode laser (type: FOL15DCWD-A82-19560-A, Furukawa Inc.) having an emitted light power of ≈ 45 mW was used. The laser had an emission wavelength continuously tunable between 1530 nm-1532 nm and a laser temperature tuned between 5 and 30 °C. The laser was operated in a wavelength-modulated mode with an

unmodulated current set to be close to 300 mA (that is the manufacturer-specified maximum allowable current), with a small amplitude rectangular modulation superimposed on it.

4.1.3 Laser light modulation

For my application, I incorporated the use of multi-wavelength measurements to first suppress the spectral interference, secondly, improve the sensitivity of the ammonia isotope measuring the NIR-PA system and lastly be able to measure different components simultaneously.

An increase in laser power increases the PA signal where the limits of the laser power are governed by the total laser-generated background fluctuations since higher power (tens of mW) increases the integration time which in turn increases the response time of the system. Also, the sensitivity of the system is directly proportional to the laser power. A trade-off between the sensitivity and response time was therefore sought by increasing the averaging time of the measurements. This had the added advantage of decreasing the noise levels which from equation 8, can be seen to considerably lower the MDC. Taking this into consideration and to increase the system's sensitivity, I, therefore, chose to add a second DFB diode laser within my NIR-PA system by use of a fibre coupler (FL-PBC-64-P-2-L-1-Q, Fiberlogix). Due to the manufacturing technology of these lasers, the two have slightly different emission wavelengths that were eliminated by operating them at different temperatures. From the integrated electronics point, the two lasers act as one with a combined emitted light power of 85 mW (due to some coupling losses). After matching their emission wavelengths, the current characteristics of the two lasers were practically identical.

For photoacoustic signals, laser light modulation is necessary. This can be achieved by either amplitude or WM. Amplitude modulation (AM) by the use of mechanical choppers with a repetition rate of a few Hz to a few kHz has been employed to modulate the light output from the gas lasers. Although simple and achieving 100% modulation depth, the process generates coherent noise mostly by the chopper which interferes with the sensitivity of the system as the noise generated adds to the unwanted background signals in the PA cell. One way of circumventing this problem is by varying the current in the discharge tube laser, although less noisy, the modulation depth achieved is much less than 100% and the modulation frequency is much smaller (<100 Hz). Other general AM methods include electro-optics and acousto-optics. In the former case polarization of the laser beam is varied by the application of a voltage to a birefringent crystal while a second polarizer filters the beam entering the sample field. In the

latter, density waves that cause diffraction are generated in a crystal in response to the application of a sound frequency vibration on the crystal. The advantages of acousto-optics modulation over the electro-optics method are its low driving power, simpler electronics and high extinction ratio; its main drawback is the lower modulation bandwidth [110].

In short, AM involves a periodic variation of the diode laser current between selected values above and below the opening current which ensures that the laser is effectively switched on and off during the modulation. I chose to use the WM method whereby the current of the laser was modulated with a reduced amplitude to tune the laser online and offline. This interaction between the modulated light and NH_3 absorption line then gives rise to signals of different harmonics of the modulation frequency which can be detected using a lock-in amplifier and reading its amplitude that is directly proportional to NH_3 gas concentration. The DFB laser in my NIR-PA system was therefore operated in a wavelength-modulated mode with the unmodulated current set to be close to 300 mA (manufacturer-specified maximum allowable current), and a small amplitude rectangular modulation superimposed on it in a manner that the amplitude of the modulated part of the current was always much lower than the unmodulated (constant) current. The major advantage of WM over AM is its ability to shift the detection to higher frequencies where laser intensity (noise) is greatly reduced [111,112].

4.1.4 Integrated electronics for the NIR-PA signal control and measurement

A highly integrated piece of electronics (manufactured by VIDEOTON Holding Ltd., Hungary) was used. Its main purpose was to amplify, provide temporal averaging and filter the microphone signal, control the temperatures of the laser and the detection cell and lastly feed the modulated driving current to the diode laser. The electronics software is built from a set of subroutines that are programmed to perform various tasks. Three important subroutines include the main one which was programmed to enhance the signal-to-noise ratio by temporal averaging of the microphone signal over a given period. It then, through the application of the digital lock-in technique, calculated the amplitude and phase of the averaged microphone signal at the frequency which was equivalent to the laser modulation frequency. The lock-in technique applicable to our PA signal measurements had two general features. First, the signal-to-noise ratio of the measurement was inversely proportional to the square root of the signal averaging time and secondly, the digital lock-in technique quantified the PA signal in the form of a complex number having a real and an imaginary part which was both proportional to the amount of light absorbed within the PA cell. This quantification helped in the calculation of the amplitude and phase from its real and imaginary parts. The other two subroutines were for

changing the laser wavelength through laser temperature or current variation (important for my case since my measurement was a multi-wavelength measurement) and calculating the actual concentration of the analyte(s) with the help of pre-determined calibration constants.

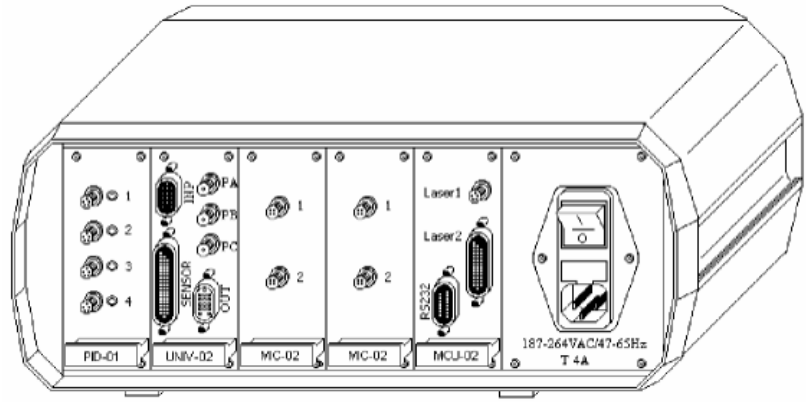

Figure 6: Schematics of integrated electronics (manufactured by VIDEOTON Holding Ltd., Hungary) used for laser control and signal processing in the NIR–PA system measurements. From right to left the electronic unit parts are as follows; on-off power switch, communication port (below), laser drivers (MCU-02), microphone amplifiers (MC-02), input and output ports for temperature sensors and mass flow controllers (UNIV-02) and lastly, the temperature controllers for the diode lasers (PID-01).

The data was then transferred to a personal computer through a communication port RS232 / RS485, 4-20 mA, with a Modbus interface in a real-time mode during measurement. Alternatively, the data could also be stored in the memory of the electronics for a maximum period of two months. The electronic was programmable in the computer basic language (PYTHON), therefore the measurement control and concentration calculation procedures were prepared on a separate program.

4.1.5 Gas handling unit

The gas handling unit defines and connects the whole NIR-PA system experimental ensemble. In my case, it contained mass flow controllers to regulate the gas flow from the cylinders to the PA cell, noise filters which were attached to the PA cell for the gas noise level control, and needle valves for regulating and changing the direction of the gas flow and finally gas tubing for conducting the gas stream. Bozóki et al. [99] have emphasized the need for a careful selection of the gas tubing materials, especially in the case of measuring highly polar molecules e.g. NH_3 gas due to the adsorption-desorption processes which mostly occur on the walls of the gas tubing system and the PA cell. These processes have a direct bearing on the overall response time of the NIR-PA system. For my case, taking into account the above, I used

PTFE plastic for the gas tubing (being careful to keep the length to a minimum) and in permissible instances used high gas flow rates. The PA cell was made of stainless steel.

4.2 Development of the NIR-PA system and measurement procedure

The experimental set-up of Figure 7 was used for the $^{14}NH_3$ and $^{15}NH_3$ spectra measurements and it consisted of two main parts: the ammonia gas generation unit that offered the possibility of generating various mixtures of $^{14}NH_3$ and $^{15}NH_3$ isotopes and the NIR-PA system, operated either by an ECDL or by a DFB diode laser. From Figure 7, two modes were operational; the mass-flow controller mixing mode, and the chemical reaction-based mode marked by a dashed rectangle. In the first mode, the dashed rectangle part in Figure 7 was bypassed and two calibrated mass flow controllers were used to mix and regulate the gas flow from the NH_3 in the N_2 cylinder (1000 ppm) and pure N_2 (both cylinders were supplied by the Messer company and have a purity of 5.0).

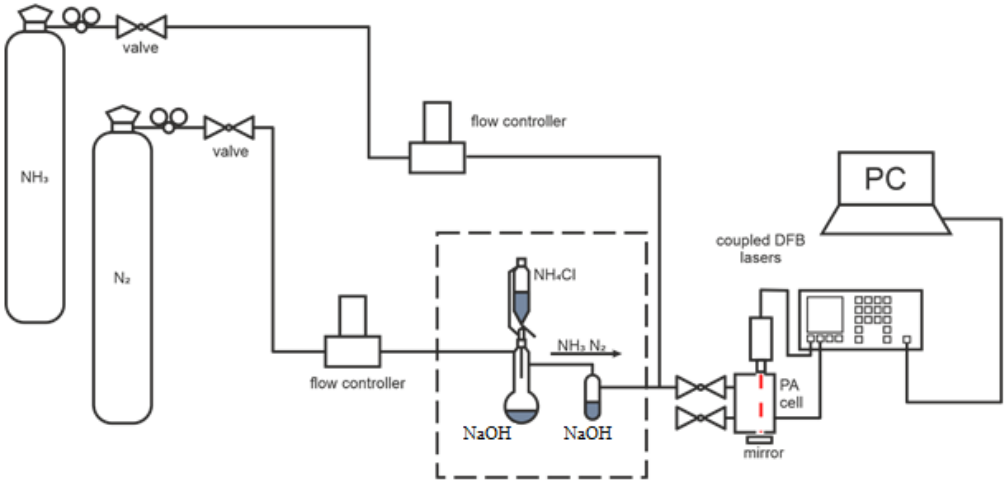

Figure 7: Schematics of the experimental measurement set-up.

For the chemical reaction-based mode, the mass flow controller attached to the NH_3 in the N_2 cylinder (1000 ppm) was closed and the pure N_2 gas was used to purge the chemical reaction part of the NIR-PA system through the PA cell. The chemical reaction in equation 12 was used in the generation of NH_3 gas for the chemical-reaction mode;

$$NaOH_{(s)} + NH_4Cl_{(aq)} \rightarrow H_2O_{(aq)} + NaCl_{(s)} + NH_{3(g)} \quad (12)$$

Granular NaOH and two types of ammonium chloride were used; ammonium-^{15}N chloride (Sigma Aldrich, atom ratio of ^{15}N between 98% - 99%) and normal ammonium chloride (Sigma Aldrich ≥ 99.5%) in powder form. Different mixtures of ammonium chloride

containing ^{14}N and ^{15}N marked isotopes intended to span a wide range were generated, these include:

Mixture 1: ammonium chloride containing 0%,^{14}N and 100%, ^{15}N marked isotope, dissolved in 10 ml of distilled water.

Mixture 2: ammonium chloride containing 25%,^{14}N and 75%, ^{15}N marked isotope, dissolved in 10 ml of distilled water.

Mixture 3: ammonium chloride containing 50%, ^{14}N and 50%, ^{15}N marked isotope, dissolved in 10 ml of distilled water.

Mixture 4: ammonium chloride containing 75%, ^{14}N and 25%, ^{15}N marked isotope, dissolved in 10 ml of distilled water.

Mixture 5: ammonium chloride containing 100%, ^{14}N and 0%, ^{15}N marked isotope, dissolved in 10 ml of distilled water.

From these mixtures, the ammonia gas was developed as per equation 12 and the generated $^{14}NH_3$ and $^{15}NH_3$ spectra were measured as mentioned below.

A side-tubed Erlenmeyer flask was fitted with gas inlet pipes on both sides and solid NaOH (0.1g) was placed inside the flask. One side tube was introduced with pure N_2 gas, which was used as a diluent and carrier gas, at a flow rate of 150 ml/min. On the other tube, the developed mixture of NH_3 and N_2 was exited. NH_4Cl (0.14 g) dissolved in 10 ml of distilled water and homogenized for 20-25 minutes was added to the flask via a dropping funnel from above as shown in the dashed rectangle of Figure 7. A stable concentration was ensured by evenly timing the drops and performing the measurements before the dripping stopped. The developed NH_3-N_2 gas mixture was then passed over granular NaOH to reduce its water vapour content and into the PA cell for a spectrum recording. According to our estimations, ≈ 5000 ppm ammonia was generated as follows;

NaOH = 0.1 g; NH_4Cl g = 0.14 g; and molar mass NH_3 = 17.03 g/mol whose gas volume is 24.5 dm^3 by Avogadro's law. The experiment was performed in a 1/400 molar mass portion therefore the amount of the NH_3 gas volume generated during the entire measurement period was $24.5L \div 400 = 0.06125L$. The total time taken to record the two spectra was 80 minutes; therefore $0.06125\ l \div 80\ min = 0.000765\ l/min$, amount of gas was generated. Since the diluted nitrogen gas flow was 0.15 l/min, then the concentration was;

$0.000765 \div 0.15 = 0.005$ i.e., $0.5\% \approx 5000\ ppm$.

Apart from the spectral measurements, resonance and calibration measurements, response time together with the cross-sensitivity determination of the NIR-PA system were also carried out.

4.3 Structure of the measurement system

4.3.1 Optimization of the modulation parameters

This was started by recording the PA spectra of water vapour, $^{14}NH_3$ and $^{15}NH_3$ isotopes using the ECDL. Given the information on the $^{15}NH_3$ rotational-vibrational absorption spectrum in the near-infrared [113], the ECDL was believed to have sufficient wavelength coverage for finding the optimal measurement wavelengths. Strong $^{14}NH_3$ absorption bands were identified in the wavelength range of 1480-1540 nm. It was then expected that due to the small molecular weight difference between the two NH_3 isotopes, $^{15}NH_3$ absorption bands would simply overlap or at least partially overlap with those of $^{14}NH_3$. Based on the recorded spectra, the strongest NH_3 absorption lines which consisted of the two-wavelength range 1520 - 1523 nm and 1530.5 - 1533.5 nm were chosen primarily since these ranges coincided with weak water vapour absorption lines. Next, spectral measurements within the 1530.5 - 1533.5 nm wavelength range were executed using the DFB lasers. This was done because with the ECDL no suitable cross-interference-free wavelengths of the isotopes were found hence the need for using the DFB diode lasers under temperature tuning mode for further optimization. The two lasers have already been described elsewhere (section 4.1.2). Several NH_3 isotopes, CO_2 and water vapour spectra were recorded in two steps. First laser temperature tuning was carried out followed by current tuning. In the former case, the amplitude of the laser current was held constant for each scan but was changed from one scan to another. An optimum laser modulation amplitude and measurement wavelength set that had none or least spectral interference were chosen from the recorded spectra. For the latter case, screening was performed whereby the laser temperatures with which all the selected wavelengths were available and provided the highest possible PA signals equivalent to the maximum sensitivity of the isotope measurements were selected.

4.3.2 Water vapour measurement

The NIR-PAS system was used to measure the water vapour spectrum in the atmosphere at the wavelength range of 1470-1590 nm. The schematic of the experimental set-up is shown in

Figure 8. The recorded water vapour spectrum was then compared to the spectra of the NH_3 isotopes to identify the overlapping spectral lines and determine their cross-sensitivity.

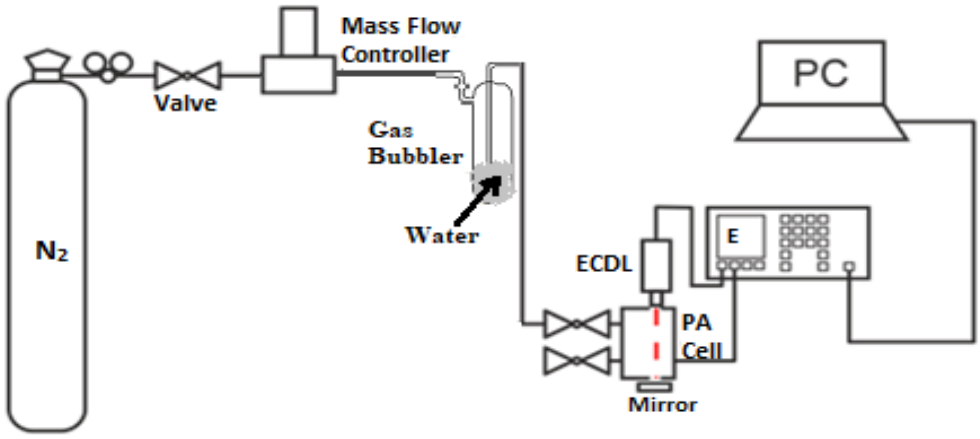

Figure 8: Schematics of the experimental set-up used for the water vapour measurement.

4.4 Calibration of the NIR-PAS system

Calibration is the comparison of measurement values delivered by a device under test with those of a calibration standard of known accuracy. In principle, PAS is a zero-background method which shows a linear relationship between the PA signal generated and the concentration of the measured target component. One major reason for non-linearity could be the difference in the phase of the photoacoustic signal and background signal, especially when dealing with low target concentrations as explained in section 2.4.1.2. Experimentally, there is always some measured signal at the target gas zero concentration. Possible reasons for this include; electrical noise of the apparatus connected to the cell, static interference of the microphone or even absorption of scattered light by the windows and walls of the PA cell. Because of this, proper calibration of the system is essential for reliable PA concentration measurements. For my developed system, calibration of $^{14}NH_3$ was done using 5 ppm, 10 ppm, and 95 ppm NH_3 gas cylinders (Figure 9) while, $^{15}NH_3$ calibration (Figure 10) was done using the provided solutions of mixtures 1-5, detailed in section 4.2. Each of the concentrations was measured for about one hour in continuous mode. After each measurement, the cell was purged with pure N_2 gas for 30 minutes before switching the solutions.

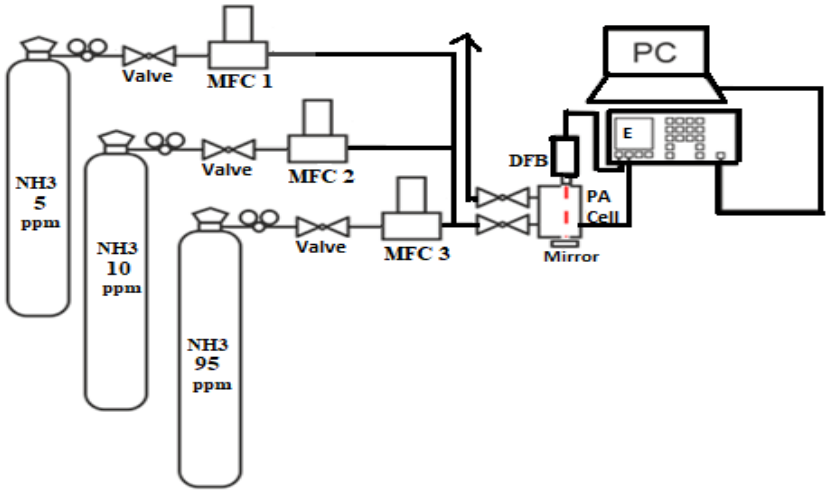

Figure 9: Schematic of the experimental set-up for $^{14}NH_3$ calibration consisting of coupled DFB lasers connected to different concentrations of NH_3 gas cylinders, mass flow controllers (MFC), gas tap (GT), a photoacoustic signal analyser (E = electronics) and a storage unit (personal computer, PC).

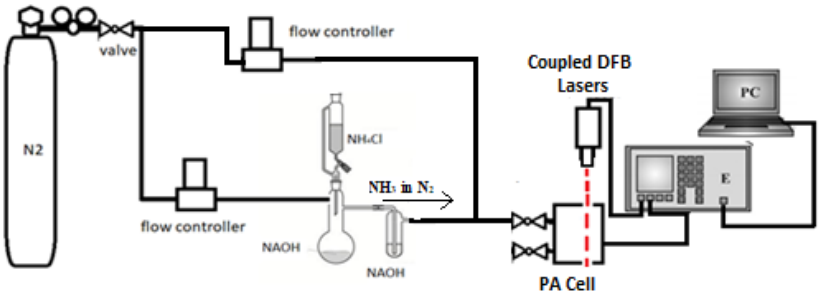

Figure 10: Schematic of the experimental set-up for the $^{15}NH_3$ calibration consisting of coupled DFB lasers connected to the NH_3 gas generating system, a photoacoustic signal analyser (E = electronics), and a storage unit (personal computer, PC).

During the calibration of the NIR-PA system, the numerical values of analytical parameters used were determined with the help of the gas generation methods described in Section 4.2. The operational software of the NIR-PA system was programmed to first measure at all of the chosen wavelengths and then convert these measured PA signals to two final quantities PA_{14} and PA_{15} having a high sensitivity against $^{14}NH_3$ and $^{15}NH_3$ gas, respectively. The slope of the calibration line fitted on the data points of PA_{14} vs. $^{14}NH_3$ concentrations in ppm directly gave the $^{14}NH_3$ sensitivity. The determination of $^{15}NH_3$ sensitivity was not as straightforward due to limited information on the concentration of $^{15}NH_3$ in the generated gas mixtures used in the calibration process. However, since the NIR-PA system was already calibrated against $^{14}NH_3$ concentration, the measured PA_{14} signal was first used to determine the actual value of $^{14}NH_3$ concentration, from which, by knowing the mixing ratio of the isotope

labelled salts, $^{15}NH_3$ concentration was calculated too. Once the $^{15}NH_3$ concentration was determined, the calculation of the $^{15}NH_3$ sensitivity parameter of the NIR-PA system by using the measured PA_{15} signals became straightforward. Next, cross-sensitivities of both $^{14}NH_3$ and $^{15}NH_3$ were determined. The above measurement sequence is summarised in Table 3.

Table 3: A summary sequence of procedures applied during the determination of the sensitivity and cross-sensitivity parameters.

	Measured parameter	**Applied gas generator**	**Supplementary data required**	**The procedure for generating the required supplementary data**
Step 1	$^{14}NH_3$ sensitivity	Mass flow controller	None	None
Step 2	$^{15}NH_3$ sensitivity	Chemical reaction	Actual value of $^{15}NH_3$ concentration	$^{15}NH_3$ concentration was determined in two steps: 1. Determination of $^{14}NH_3$ concentration from the measured value of PA_{14} with the help of the $^{14}NH_3$ sensitivity parameter determined in Step 1. 2. Calculation of $^{15}NH_3$ concentration from $^{14}NH_3$ concentration by using the mixing ratio of the isotope labelled salts.
Step 3	$^{15}NH_3$ cross-sensitivity	Mass flow controller	Actual value of $^{14}NH_3$ concentration	$^{14}NH_3$ concentration was then calculated from the measured value of PA_{14} with the help of the $^{14}NH_3$ sensitivity parameter determined in Step 1.
Step 4	$^{14}NH_3$ cross-sensitivity	Chemical reaction	Actual value of $^{15}NH_3$ concentration	$^{15}NH_3$ concentration was calculated from the measured value of PA_{15} with the help of the $^{15}NH_3$ sensitivity parameter determined in Step 2

4.5 Response time measurements

Response time is defined as the time needed for the PA signal to vary between 0% and 100% of its total variation caused by a step change in the concentration. It is dependent on the concentration of the target analyte, in that a higher concentration gives a shorter response time and vice versa. Response time of concentration measuring instruments is usually quoted as $T_{10\text{-}90\%}$ referring to the time taken for the instrument output to rise from 10% of the initial value to 90% of the final value. $T_{10\text{-}90\%}$ was calculated for NH_3 measurement presented here

accordingly. The response time dependency on the concentration was negligible, particularly in the concentration range of the presented measurements. $T_{10\text{-}90\%}$ was measured by using the mass-flow controller mixing mode which was modified by adding a four-way valve to the initial arrangement as depicted in Figure 11.

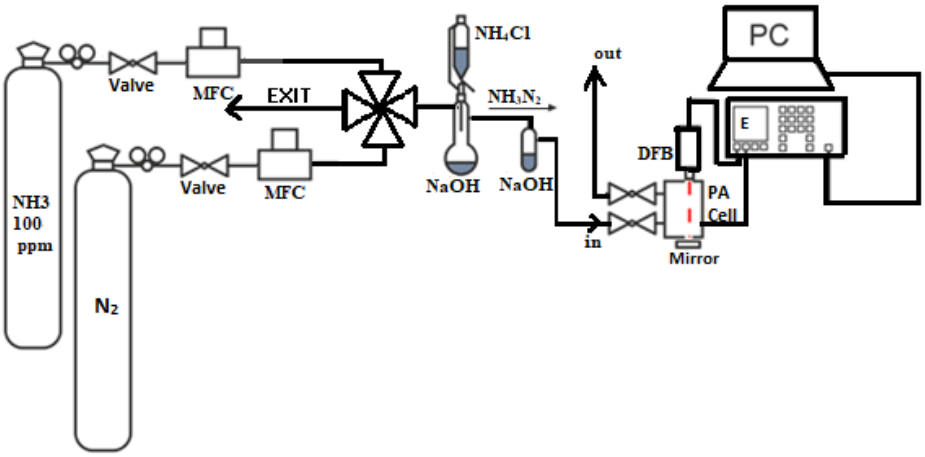

Figure 11: Schematics used for the NIR-PA system response time measurement.

The initial pure nitrogen cylinder used during calibration was retained while the 1000 ppm (in nitrogen) $^{14}NH_3$ gas cylinder was switched with a 100 ppm (in nitrogen) $^{14}NH_3$ gas cylinder from the same manufacturing company (Messer, Hungary). Through the flow controllers set to 0.4 l/min, both gas streams from the nitrogen and ammonia cylinders were set to flow continuously, one of them through the by-pass while the other through the PA cell at any given time. The use of a four-way valve enabled the steplike concentration variation required for the response time determination.

5. Results and discussion

5.1 Optimization of the modulation parameters

5.1.1 Using ECDL

From the experimental set-up shown in Figure 7 while using the ECDL, the laser power was recorded as ~50 mW. $^{14}NH_3$ gas at 1000 ppm was then confined into the PA cell by letting it flow in continuously through a mass flow controller (at a flow rate of 150 ml/min) and into the cell. A spectrum measurement was then done at a wavelength range of 1470 nm-1590 nm at steps of 0.1 nm. The modulation current DC was 0 mA, and the AC kept fluctuating and was controlled by the lock-in apparatus. A heating system was installed, and the PA cell was mounted onto it (see Figure 12) to reduce the effect of changing temperature and hold it constant. Fluctuating temperature affects the sensitivity of the system in various ways, e.g. the resonance frequency of the resonator is temperature dependent and the adsorption-desorption process of NH_3 molecules on the walls of the PA cell depends on temperature too. For my measurements, 50 $^{\circ}$C was found to be the optimum operating temperature.

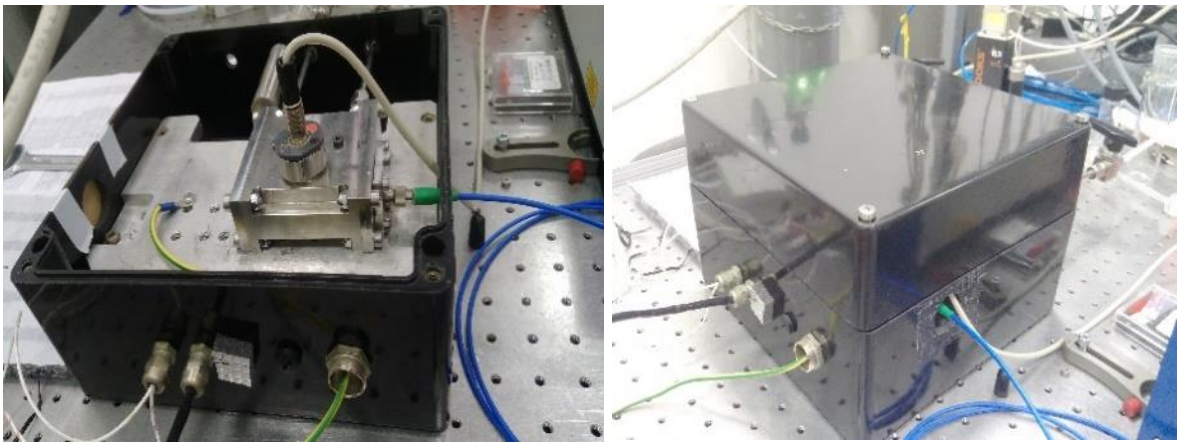

Figure 12: Photoacoustic cell heating system.

Next, using the chemical reaction-based mode marked by a dashed rectangle in Figure 7, a spectrum recording of $^{15}NH_3$ gas (using mixture 1) was also done. In most cases, spectral interference can be simply eliminated by choosing a measurement wavelength which does not overlap with the absorption bands of other molecular compounds. In my case, spectral interference was almost unavoidable since my chosen NIR spectrum range was overcrowded with several absorption bands and overtones of other molecules, notably water vapour and CO_2. The set-up in Figure 8 was therefore used to measure the water vapour spectrum not in the

ambient atmosphere at the wavelength range of 1470 nm-1590 nm. The recorded spectrum was then compared to the generated $^{14}NH_3$ and $^{15}NH_3$isotope spectrum measured previously.

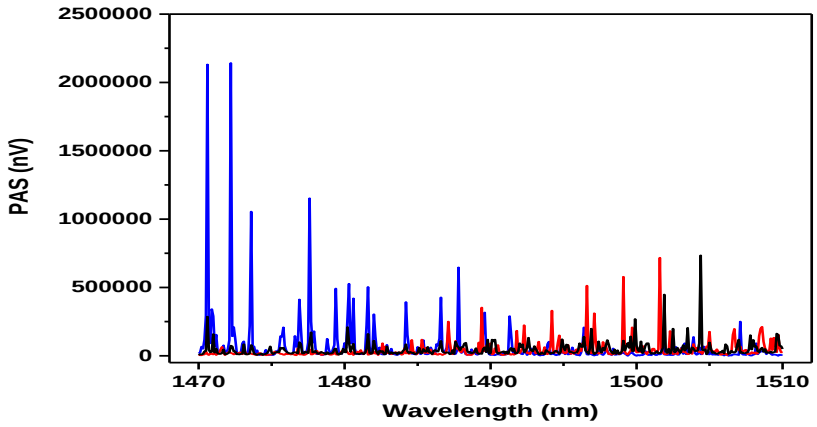

(a).

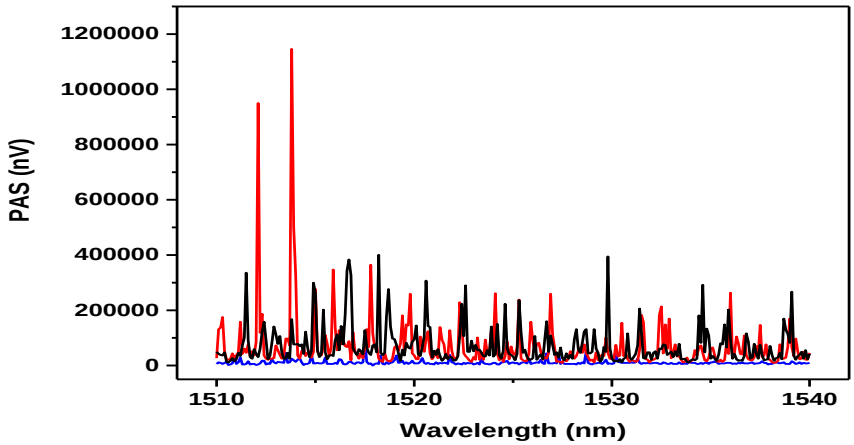

(b).

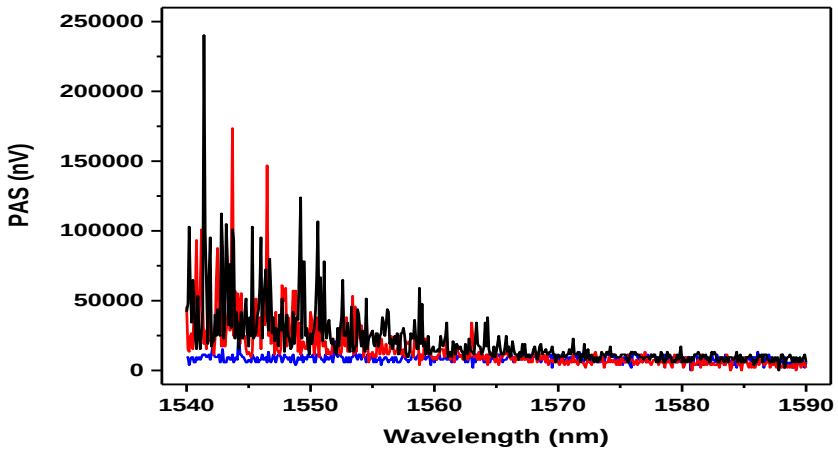

(c).

Figure 13: Comparison of NH_3 isotopes; $^{14}NH_3$ (red line), generated $^{15}NH_3$ (black line) and H_2O vapour spectra (blue line) separated into the wavelength ranges of (a); 1470 – 1510 nm, (b); 1510 – 1540 nm and lastly (c); 1540 – 1590 nm.

From figure 13, there were a lot of strong H_2O vapour lines up to the wavelength of 1490 nm. The ammonia wavelength around 1510 nm would be sufficient, but even here the H_2O vapour lines overlapped with the generated $^{15}NH_3$ absorption lines. Due to these reasons, wavelength measurements below 1510 nm were discarded. Further spectra measurements were done with the different generated mixtures of ammonium chloride containing ^{14}N and ^{15}N marked isotopes in the wavelength range of 1510-1540 nm. A comparison graph of the generated ammonia spectra from all the developed mixtures was then recorded as shown in Figure 14.

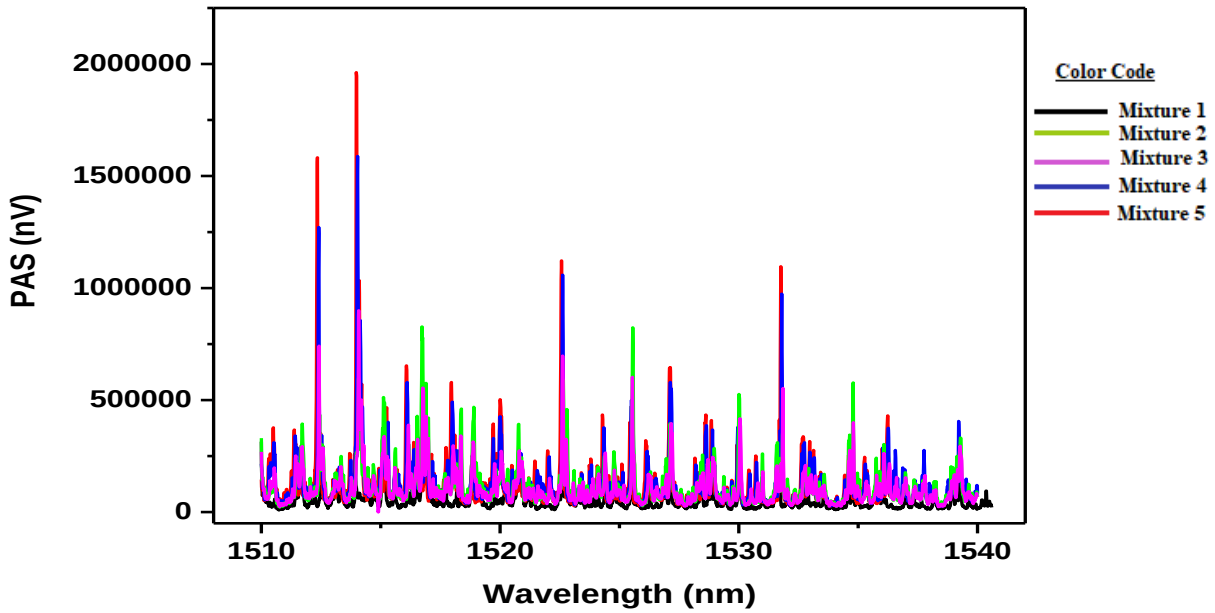

Figure 14: Comparison spectra of the generated gas mixtures containing different amounts of ammonium chloride isotopes; (a) mixture 1: (0% ^{14}N and 100% ^{15}N), (b) mixture 2: (25% ^{14}N and 75% ^{15}N) (b) mixture 3: (50% ^{14}N and 50% ^{15}N), (c) mixture 4: (75% ^{14}N and 25% ^{15}N), and lastly, (d) mixture 5: (100% ^{14}N and 0% ^{15}N).

A comparison of the NH_3 isotope mixture concentration at each given peak wavelength was then done and a summary was recorded in Table 4. The numbers in red show the mixture with the highest concentration at that particular wavelength. The peak analysed were numbered as shown in Figure 15.

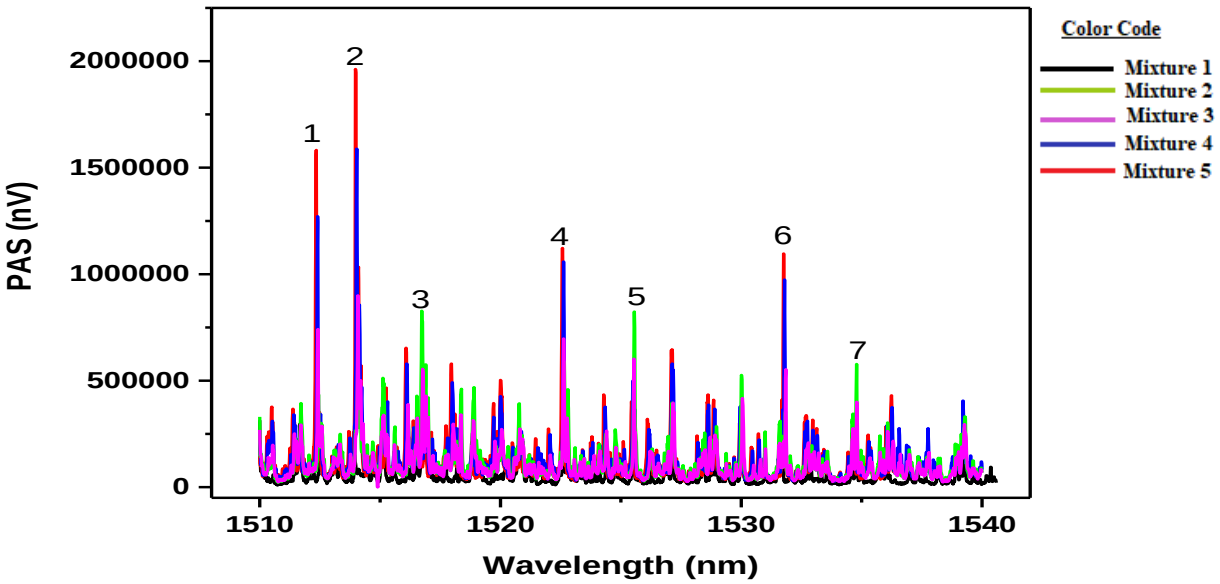

Figure 15: Numbering of the peaks that were used to analyse the mixtures containing different amounts of ammonium chloride isotopes. Mixture 1: (0% ^{14}N and 100% ^{15}N), mixture 2: 25% ^{14}N and 75% ^{15}N, mixture 3: 50% ^{14}N and 50% ^{15}N, mixture 4: 75% ^{14}N and 25% ^{15}N, and lastly, mixture 5:100% ^{14}N and 0% ^{15}N.

Table 4: Summary of the NH_3 isotope mixture concentration at given a peak wavelength. The peaks analysed are numbered as shown in Figure 15.

Peak (No.)	Isotope Mixture of $^{14}NH_3$ (%)	Wavelength (nm)	PA Signal (10^{-3}V)
1	100	1512.34	1.568
	75		0.3364
	50		0.1386
	25		0.0812
2	100	1513.98	1.9627
	75		0.4785
	50		0.2197
	25		0.2691
3	100	1516.73	0.1250
	75		0.2314
	50		0.2314
	25		0.8210
4	100	1522.56	1.116
	75		0.2484
	50		0.2076
	25		0.1295
5	100	1525.55	0.1108

	75 50 25		0.3090 0.4284 0.8148
6	100 75 50 25	1531.76	1.081 0.2519 0.1061 0.1317
7	100 75 50 25	1534.78	0.0627 0.1340 0.3568 0.5685

From the results of the peak absorption wavelength given in Table 4, I decided to carry out a multi-wavelength analysis. The ranges of the recorded wavelength measurement were 1510 nm to 1535 nm which was further analysed using the ECDL. Spectra of $^{14}NH_3$, $^{15}NH_3$ and H_2O vapour were recorded as in Figure 16, to determine the proper wavelength measurements required by my NIR-PA system.

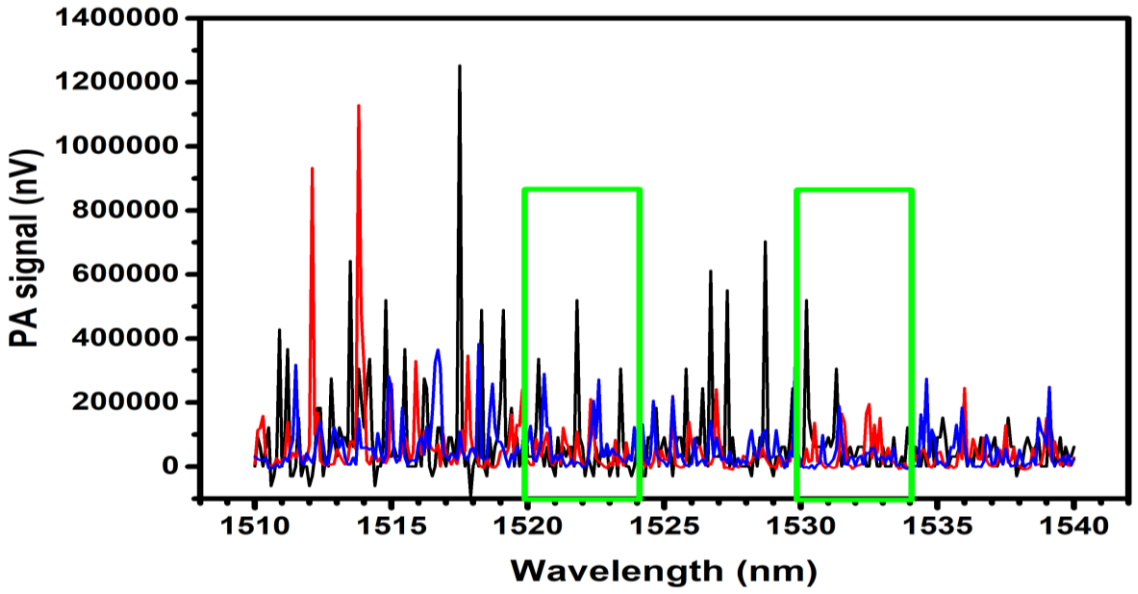

Figure 16: PA spectra of $^{15}NH_3$ (blue line), $^{14}NH_3$ (red line) and water vapour (black line) recorded by an ECDL. The two-wavelength ranges marked with green rectangles were investigated in detail by searching for optimal measurement lines.

On analysing Figure 16, there appeared to be a lot of spectral overlap between water vapour and NH_3 isotopes hence a perfect spectral separation between the absorbed lines was not a prioritised selection criterion in this phase of system optimization. As previously explained wavelengths below 1510 nm were excluded owing to the strong water vapour

absorption lines (see Figure 13 (a)). Consequently, two wavelength ranges were found to meet the primary selection criteria i.e., NH_3 lines overlapping with weak water vapour absorption lines. These were the 1520-1523 nm and the 1530-1534 nm ranges (marked with a green line box in Figure 16) where spectral measurements with wavelength-modulated DFB lasers were planned. The purpose of the wavelength-modulated DFB lasers was to help in minimizing the spectral cross-sensitivities by optimizing the laser operational parameters. The DFB diode laser also has greater power than that of the ECDL and a capacity of being wavelength modulated. However, the wavelength tuning range of a DFB laser is much less than that of an ECDL: either ≈3 nm or ≈0.5 nm depending on whether tuning is achieved by changing the temperature or the driving current of the laser, respectively. Whenever the measurement can be performed on wavelengths that are within a sufficiently narrow range (i.e., in a range of less than 0.5 nm) current tuning-based multi-wavelength measurement is preferable as its execution time is typically in the sub-second range, while, due to the thermal inertia of the diode laser, the characteristic time scale of a temperature tuning even in case of nearby wavelengths is typically several tens of seconds.

Upon further analysis, no suitable cross interference-free wavelengths in the 1520 - 1523 nm range were found, hence only the 1530-1534 nm range was selected for further optimisation.

5.1.2 Using DFB Lasers

Ammonia measurement with DFB lasers i.e., optimisation of measurement parameters by WM was carried out over several days. Two lasers were used for increased power and better sensitivity of the system as explained in section 4.1.3. In determining the optimum parameters to be used, the values of laser modulation current i.e., both modulated (I_{AC}) and unmodulated (I_{DC}), together with the laser temperature producing a maximum PA signal were varied and noted. The I_{AC} values varied between 2.3-22.9 mA such that at any given time, the total sum of I_{AC} + I_{DC} was always 300 mA (maximum applicable current). A spectrum was then recorded for each modulation setting between 10 $^{\circ}$C and 30 $^{\circ}$C with a temperature step of 0.01 $^{\circ}$C using a 1000 ppm $^{14}NH_3$ cylinder. A background signal measurement on ammonia absorption peak was also measured using 10 points (with each point taking a measuring average time of 27.5 seconds) in an N_2 gas cylinder with a 100 ml/min flow rate. For the first laser, measurements of both PA and background signals were recorded in Table 5, while for the second laser, in Table 6. Care was taken to ensure that both parameter tables had identical experimental settings during measurement.

Table 5: Modulation parameters using DFB laser1.

AC (mA)	DC (mA)	T (°C) [location of absorption line]	PA signal (nV) [at the absorption peak]	Background signal (nV) [measured using N_2 gas]
2.3	297.5	10.75	135703	994.9
4.6	295.3	10.88	244414	1242.7
6.9	293	11.02	305730	1554.5
9.1	290.1	11.08	328202	1675.5
11.4	288.4	11.19	326655	1697.2
13.7	283.8	11.55	334610	3347.5
13.7	286.1	11.25	319280	1485.8
16.0	283.8	11.25	92930	1212.8
18.3	281.5	11.33	285529	1750.8
20.6	279.2	11.29	359053	1586.0
22.9	276.9	11.25	327345	2154.6

Table 6: Modulation parameters using DFB laser 2.

AC (mA)	DC (mA)	T (^{0}C) [location of absorption line]	PA signal (nV) [at the absorption peak]	Background signal (nV) [measured using N_2 gas]
2.3	297.5	11.48	159664	650.5
4.6	295.3	11.58	287041	877.1
6.9	293	11.68	397200	1112.4
9.1	290.1	11.74	420977	1085.9
11.4	288.4	11.85	399517	938.9
13.7	283.8	12.17	334537	2496.7
13.7	286.1	11.91	414137	990.7
16.0	283.8	11.91	110742	902.6
18.3	281.5	11.94	383550	942.5
20.6	279.2	11.96	433147	1140.3

22.9	276.9	12.02	463017	1129.7

Figures 17 (a) and (b) show the results from which the magnitude of the PA signal value at the maximum determined NH_3 absorption line was measured. From each of the figures, a maximum peak was identified and labelled in red in both Tables (5 and 6) and the graph.

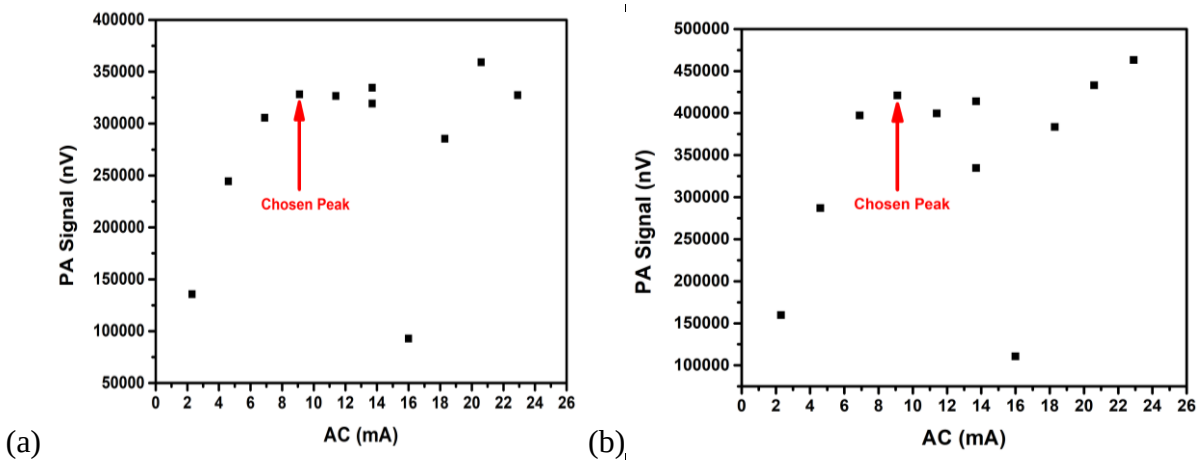

Figure 17: Plot of the PA Signal against the AC. The optimal chosen parameter for the first laser (a) is the first peak marked in red in Table 5, while for the second laser (b), it is the first peak marked in red in Table 6.

After the determination of the optimal temperature and current (I_{AC} and I_{DC}) parameters, a coupled DFB diode laser whose $\lambda \approx 1532$ nm $\pm$ 1 nm and light power $\approx$ 45 mW, was used to perform a laser WM (by changing the temperature) using the experimental set-up shown in Figure 7. Figure 18 shows a comparison measurement of ammonia isotopes, water vapour and carbon dioxide since their absorption lines overlap. In addition to the modulation parameters used, it can be seen that water vapour does not cause any cross-sensitivity since there are well-separated absorption lines of water vapour and NH_3 isotopes in the temperature range of 14 $^{\circ}$C – 20 $^{\circ}$C. The maximum CO_2 signal is 100,000 nV, whereas the background air contains ~ 400 ppm CO_2, the signal is therefore 40 nV, which causes negligible cross-sensitivity.

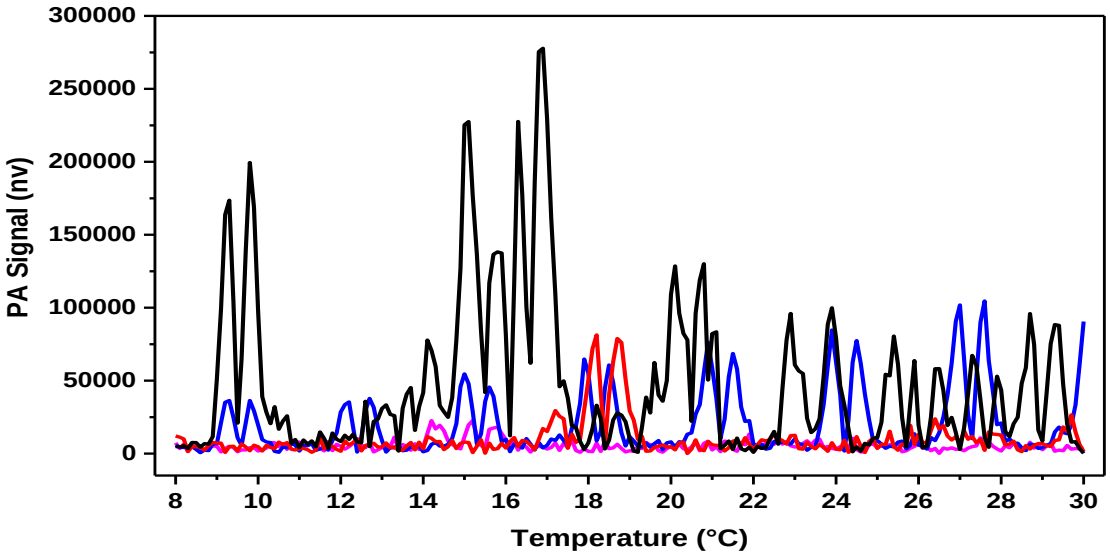

Figure 18: Comparison of cross-sensitivity spectra of different measured components, water vapour (purple line), 100 % CO_2 (blue line), 95 ppm $^{14}NH_3$ (red), 600 ppm $^{15}NH_3$ (black line).

Figure 19, shows NH_3 isotope analysis done by the preliminary NIR-PA system without the back reflecting mirror in the temperature range of 14 °C - 30 °C. The selected four wavelengths representing the peak temperatures chosen for the $^{14}NH_3$ and $^{15}NH_3$ calibration measurements are recorded in Table 7.

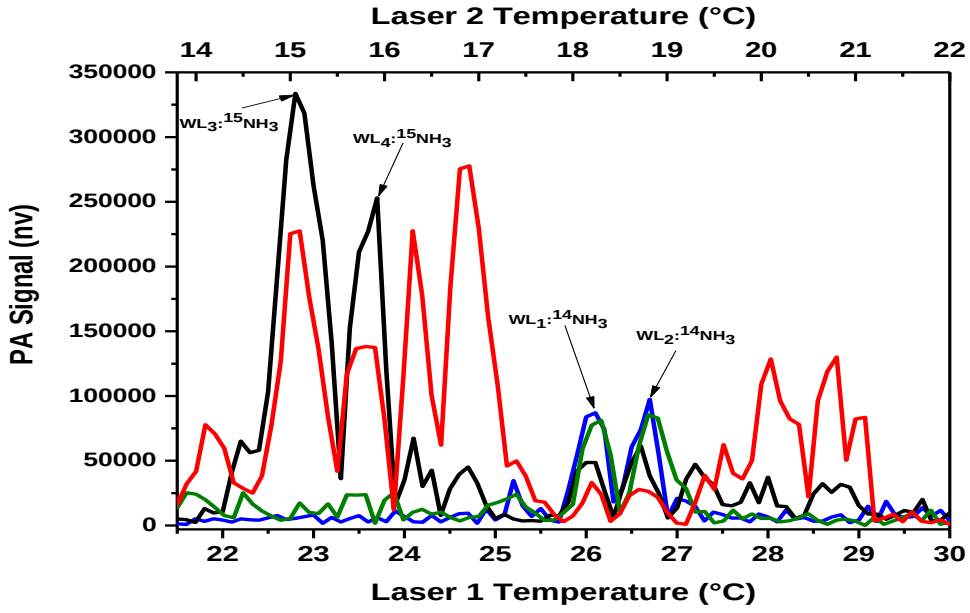

Figure 19: Selection of wavelength for measurement of $^{14}NH_3$ and $^{15}NH_3$ by preliminary NIR-PA system without the back reflecting mirror. The upper X-axis corresponds to the temperature of laser 2, depicting $^{14}NH_3$ (blue) and $^{15}NH_3$ (red) while the lower X-axis corresponds to the temperature of laser 1, depicting $^{14}NH_3$ (green) and $^{15}NH_3$ (black).

Table 7: Selection of temperatures used for the $^{14}NH_3$ and $^{15}NH_3$ calibrations (see section 5.2.1).

LASER 1	LASER 2
WL1 → 17.20 °C ; $^{14}NH_3$	**WL1** → 25.10 °C ; $^{14}NH_3$
WL2 → 18.20 °C ; $^{14}NH_3$	**WL2** → 26.00 °C ; $^{14}NH_3$
WL3 → 14.90 °C ; $^{15}NH_3$	**WL3** → 22.70 °C ; $^{15}NH_3$
WL4 → 15.80 °C ; $^{15}NH_3$	**WL4** → 23.50 °C ; $^{15}NH_3$

After the completion of a measurement cycle with all four PA wavelengths, a differential measurement was applied i.e. the difference between the PA signals measured at the chosen wavelengths, was calculated to determine the $^{14}NH_3$ and $^{15}NH_3$ concentrations, as follows:

$$PA_{14}=PA_{(WL1)} - PA_{(WL2)}, \quad (13)$$

$$PA_{15}=PA_{(WL3)} - PA_{(WL4)}. \quad (14)$$

This concentration calculation was based on the fact that PA signals have an approximately 90^o phase difference between these two absorption maxima. This means that the subtractions in equations 13 and 14 increases (almost double) these signals. This phase difference property was a result of the applied WM which significantly increased the system's sensitivity while concurrently decreasing the cross-sensitivities. Therefore, for any interfering component generating roughly equal PA signals at the chosen wavelengths with the same phase, this subtraction diminished its influence. For $^{14}NH_3$ concentrations calculation difference between the PA signals measured at WL_1 and WL_2 was used while for $^{15}NH_3$ concentrations calculation difference between the PA signals measured at WL_3 and WL_4 was used. Concentration calculation started with the isotope characterised by a bigger generated signal. Next, the cross effect of this isotope was determined and subtracted from the PA signal of the other isotope. After that, the concentration of the other isotope was determined as well.

5.2 Calibration results of the preliminary PA Cell without back-reflecting mirror

Figure 20 gives the results of the preliminary NIR-PA system calibrations by mass flow controllers and chemical reaction-based gas generation method respectively.

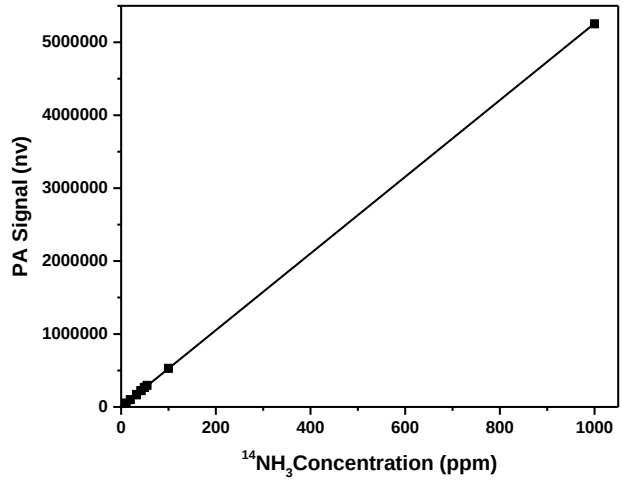

(a)

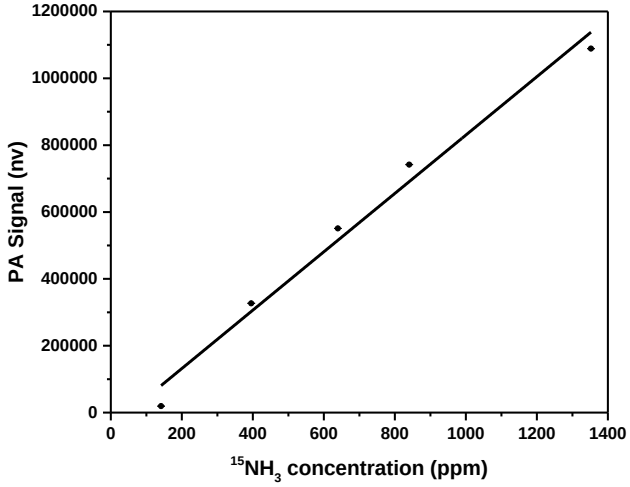

(b)

Figure 20: Results of the calibration measurements of the preliminary NIR-PA system whose PA cell had no back reflecting mirror for (a) $^{14}NH_3$ and (b) $^{15}NH_3$ using different concentrations.

From Figure 20, the minimum detectable concentration for each ammonia isotope was calculated as follows;

- Minimum detectable concentration (MDC) for $^{14}NH_3$ = (3 × Standard deviation of background signal) / Slope, therefore;

  MDC = (3 × 483.3 × 10^9 nV) / 5257.8 × 10^9 nV/ppm = **0.28 ppm.** (15)

- Minimum detectable concentration (MDC) for $^{15}NH_3$ = (3 × Standard deviation of background signal) / Slope, therefore;

  MDC = (3 × 483.3 × 10^9 nV) / 873.1 × 10^9 nV/ppm = **1.7 ppm.** (16)

The detection limit from the two calibration curves for $^{14}NH_3$ and $^{15}NH_3$ was 0.28 ppm and 1.7 ppm (3б) respectively.

5.2.1 Minimum quantifiable concentration (MQC)

MQC is defined as the concentration of the ammonia isotope in the calibration measurements at which the measurement process gives results with a specified relative standard deviation (usually 10%) [114]. The MQC is important in that it gives the smallest concentration of a target analyte in a test sample that can be determined with acceptable repeatability and accuracy. From Figure 20, the minimum quantifiable concentration for each ammonia isotope was calculated as follows;

- MQC = $(10 \times 483.3 \times 10^9$ nV) / 5257.8×10^9 nV/ppm = **0.92 ppm.** (17)
- MQC = $(10 \times 483.3 \times 10^9$ nV) / 873.1×10^9 nV/ppm = **5.5 ppm.** (18)

The quantifiable limit from the two calibration curves for $^{14}NH_3$ and $^{15}NH_3$ was 0.92 ppm and 5.5 ppm (3б) respectively.

5.3 Response time results

The importance of response time measurements for my system was to enable me to determine how efficiently the assembled system could detect and keep track of the changing target gas concentration. Normally, a PA signal would reflect this change more slowly, mostly depending on the flow rate of the gas, a factor that determines the adsorption process on the gas tubes and PA chamber wall. The volume of the cell also dictates how fast the changes reflect. For my case, I tried to use very short gas connection tubes (200 cm), a flow rate of 0.4 Litre/minute to prevent noise due to turbulence and a small PA cell volume. The response time curve was measured and plotted as shown in Figure 21. The response time was calculated to be 24.4 seconds.

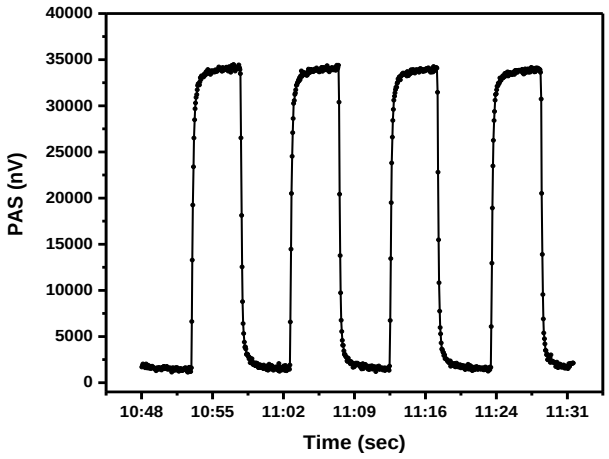

Figure 21: (a) The response of the system to sudden concentration variation. Circles represent the measurement points (a line is drawn to guide the eye).

5.4 Evaluation and improvement of the NIR-PA system

5.4.1 Comparison of the temperature vs. current tuning methods during WM

For improvement of the system, a new and upgraded integrated electronic driver (manufactured by VIDEOTON Holding Plc., Hungary) was fitted into the previously developed and calibrated NIR-PA system. A diffuser was also fitted into the PA cell inlet to reduce the response time as it has been documented that a reduction of at least 35% can be achieved [115]. The system was then wavelength modulated, using the DFB diode lasers, in that the value of $I_{DC} \gg I_{AC}$, i.e. I_{DC} value was only slightly below I_{max}. Unlike in the previous parameter WM explained in section 5.1.2, where temperature values were changing together with both I_{DC} and I_{AC} values such that:

$$I_{DC} + I_{AC} \approx I_{max} , \tag{19}$$

the temperature was kept constant during current tuning. This was because I noted that the modulation process and measurement were a bit slow and wished to improve the systems' performance in terms of speed by switching from temperature to current tuning. The DFB diode laser was, therefore, able to tune the laser wavelength on the sub-second timescale by varying its driving current rather than using the much slower temperature tuning. This was done by keeping both the temperature and I_{AC} values constant while varying only the I_{DC} values. Due to the narrow width of the chosen wavelength range, current tuning from the previously used temperature tuning was deemed successful. The following experimental set-up was then constructed to enable the subsequent measurements.

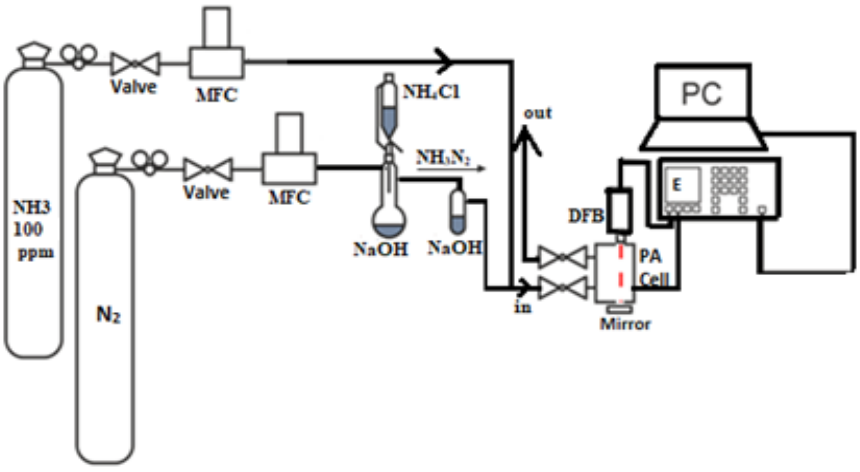

Figure 22: Schematics used for the evaluation of the fabricated NIR-PA system.

Several measurements were then carried out, including;

1. Determination of the resonance frequency using $^{14}NH_3$ gas from the 100 ppm cylinder

The frequency was observed to have slightly shifted from the preliminary NIR-PA system resonance value of 4900 Hz.

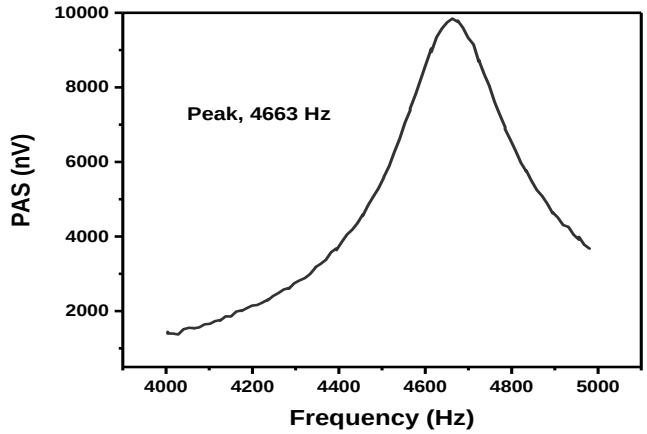

Figure 23: Measured resonance frequency of $^{14}NH_3$ gas.

2. Determination of the NH_3 isotope absorption lines using WM (temperature change)

This was done to identify the optimum temperatures to be used in the current tuning modulations. The I_{AC} / I_{DC} values were set as 14 mA / 230 mA respectively, while the spectra were recorded in temperature steps of 0.05 and a frequency of 4663 Hz.

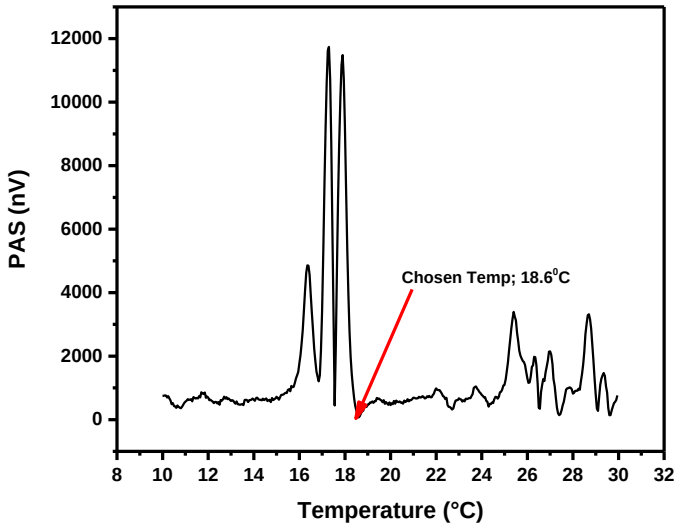

(a)

Figure 24 (a): Measured spectra of the $^{14}NH_3$ absorption lines, recorded by laser 1 using temperature tuning modulation.

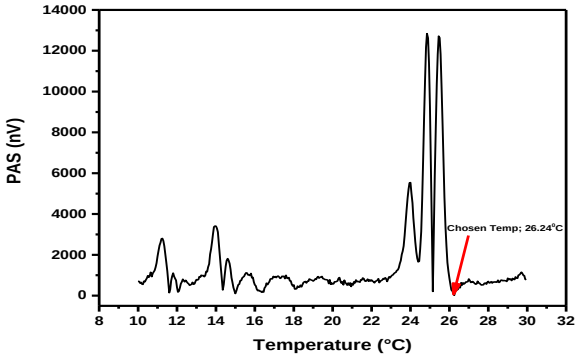

(b)

Figure 25 (b): Measured spectra of the $^{14}NH_3$ absorption lines, recorded by laser 2, using temperature tuning modulation.

3. Determination of the NH_3 absorption lines using current tuning modulations

For this measurement, the temperature values were chosen as shown in Figure 24. The values were then set into the DC spectra Python script and the NH_3 spectra figures below were recorded.

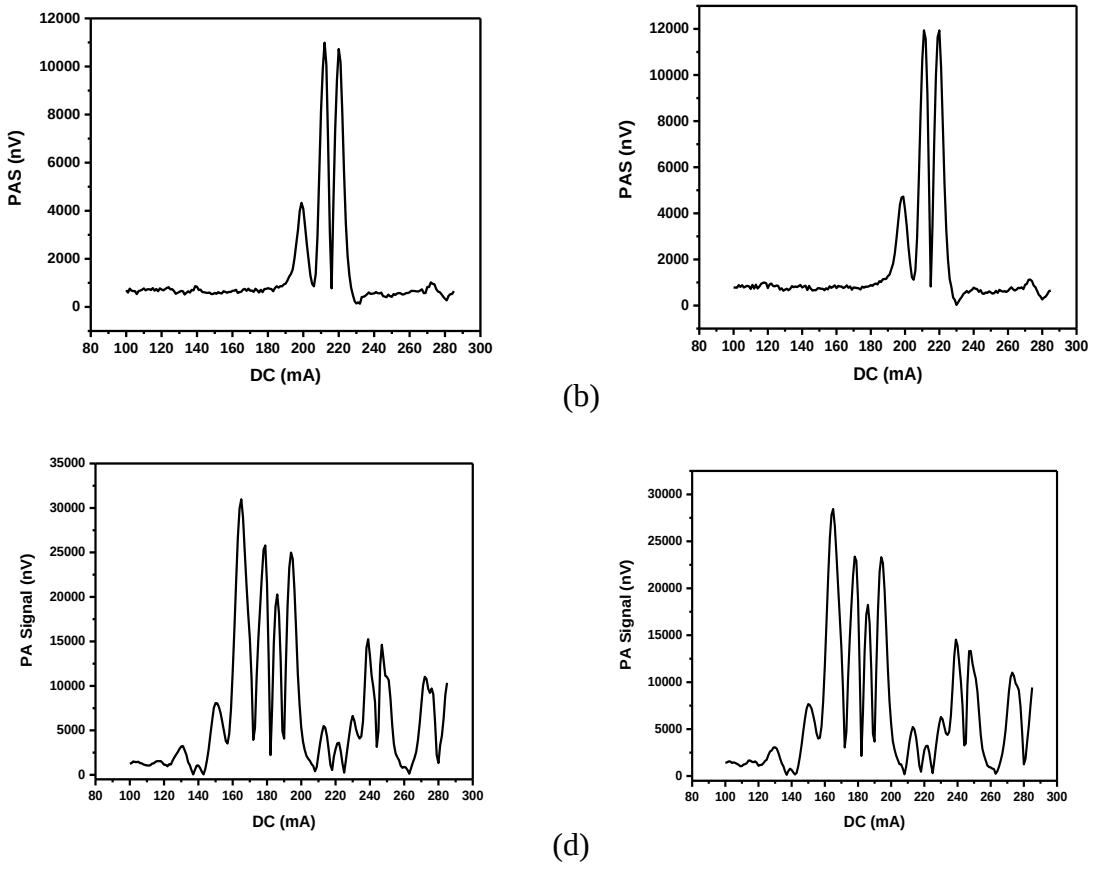

(a) (b)

(c) (d)

Figure 26: Spectra of the $^{14}NH_3$ (a and b) and $^{15}NH_3$ (c & d) absorption lines using current tuning modulation. Spectra (a) and (c) were recorded by laser 1, at a temperature of 18.60 °C while Spectra (b) and (d) were recorded by laser 2, at a temperature of 26.24 °C. The frequency used was 4663 Hz.

4. Spectral interference measurements

i. Determination of the H_2O absorption lines using current tuning modulations and the new integrated electronics. The temperature values were chosen as shown in Figure 24. The I_{AC} was set at 14 mA and frequency at 4663 Hz.

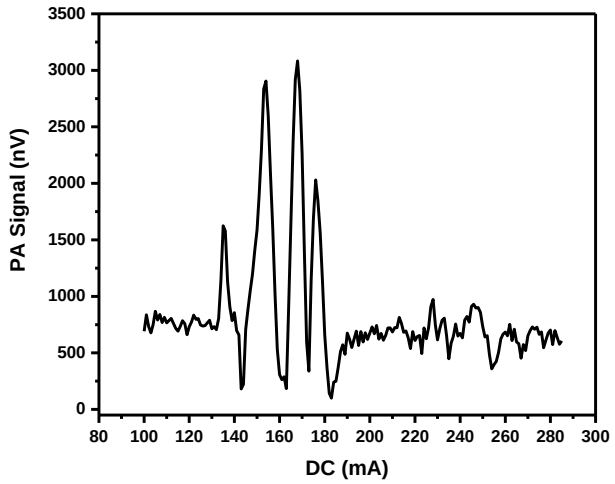

(a)

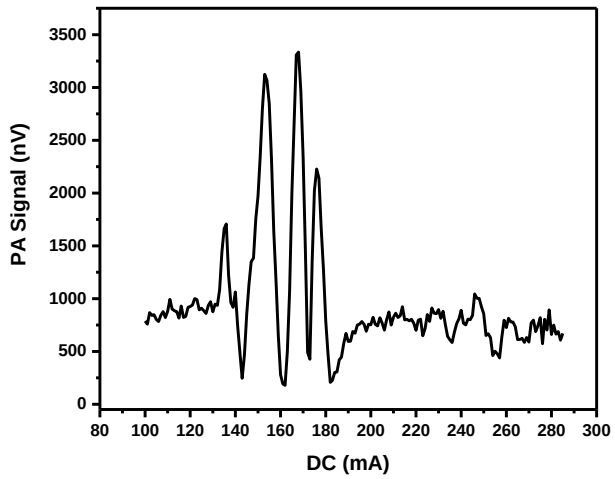

(b)

Figure 27: Spectra of the H_2O absorption lines using current tuning modulations. Spectra (a) and (b), was recorded by laser 1 and laser 2 respectively.

ii. Comparison spectra of the H_2O and NH_3 absorption lines using current tuning modulations. The temperature was set as 18.60 °C and 26.24 °C for laser 1 and laser 2 respectively, while the frequency was set at 4663 Hz.

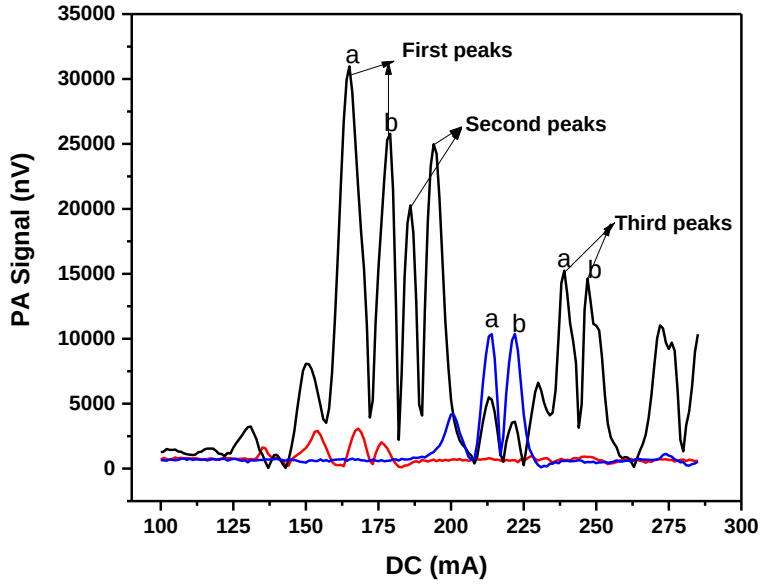

(i).

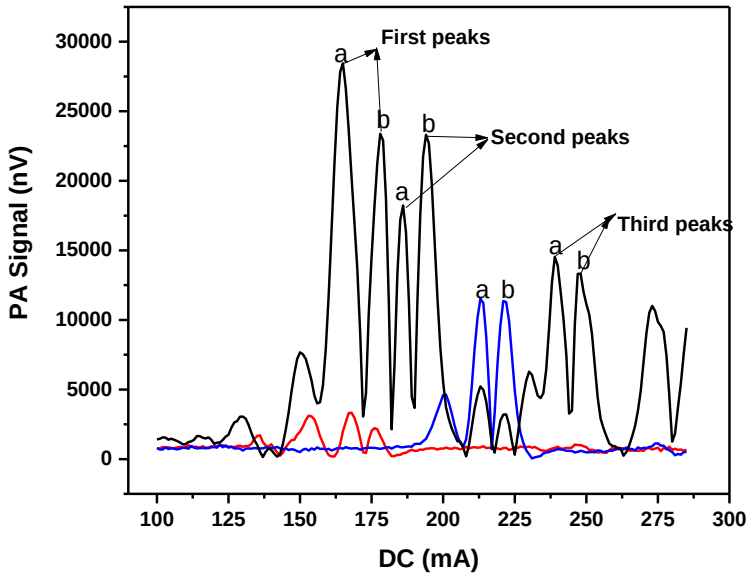

(ii).

Figure 28: Comparison spectra of the H_2O (red), $^{14}NH_3$ (blue) and $^{15}NH_3$ (black) absorption lines using current tuning modulations. Spectra (i) were recorded by laser 1 while spectra (ii) by laser 2.

5. Determination of the optimum DC values for the current tuning modulation

From the above measurements and taking into consideration the H_2O spectral interference, the three $^{15}NH_3$ peaks in Figure 27, marked as the first, second and third peaks, were chosen for further analysis as depicted in Table 8;

Table 8: DC values selected for the current tuning modulation.

LASER	First Peaks (mA)		Second Peaks (mA)		Third Peaks (mA)	
	a	**b**	**a**	**b**	**a**	**b**
1	^{14}N ; 214	^{14}N; 222	^{14}N; 214	^{14}N; 222	^{14}N; 214	^{14}N; 222
	^{15}N ; 165	^{15}N; 179	^{15}N; 186	^{15}N; 194	^{15}N; 239	^{15}N; 247
2	^{14}N ; 213	^{14}N; 221	^{14}N; 213	^{14}N; 221	^{14}N; 214	^{14}N; 222
	^{15}N ; 165	^{15}N; 178	^{15}N; 186	^{15}N; 194	^{15}N; 240	^{15}N; 248

Based on Table 8, laser DC values to temperature conversion were done and four wavelengths were chosen for selective determination of the $^{14}NH_3$ and $^{15}NH_3$ isotope concentrations, namely, 1531.66 nm, 1531.73 nm 1531.374 nm and 1531.45 nm, marked as WL_1, WL_2, WL_3, and WL_4, in Figure 28, respectively. Figure 28 therefore, gives the four wavelengths representing the peak absorption chosen for the $^{14}NH_3$ and $^{15}NH_3$ calibration measurements as defined in Table 9.

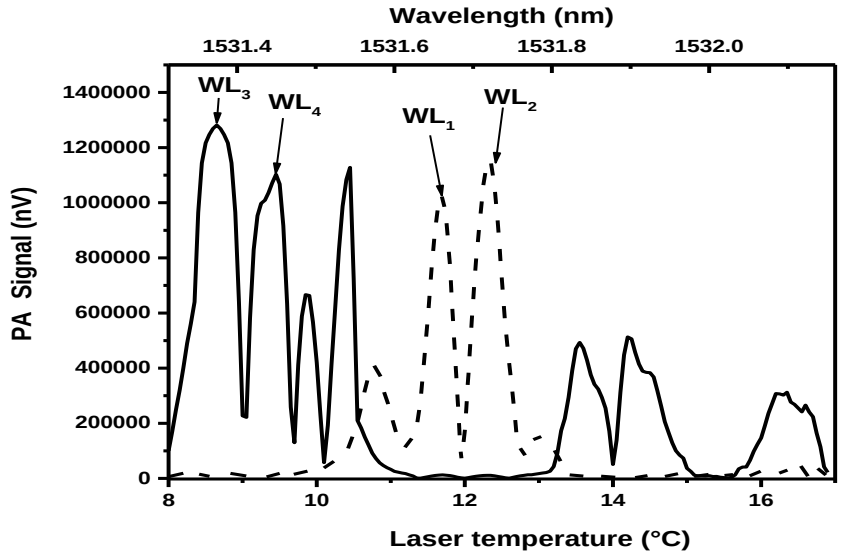

Figure 29: PA spectra of the ammonia isotopes as recorded by DFB diode laser current tuning. Solid and dashed lines are the recorded spectrum of $^{15}NH_3$, and $^{14}NH_3$, respectively. The two-wavelength pairs used for selective determination of the $^{14}NH_3$ and $^{15}NH_3$ isotope concentrations are indicated as WL_1, WL_2 and WL_3, WL_4 respectively.

From Figure 28, the lower x-axis corresponds to the temperature of one of the lasers, while the upper x-axis i.e., laser emission wavelength was approximated by comparing the PA spectrum of $^{14}NH_3$ with data from the spectral database of PNNL [116,117].

Table 9: Selection of temperatures used for the $^{14}NH_3$ and $^{15}NH_3$ calibrations, (see section 5.4.2).

LASER 1	LASER 2
WL1 → 18.10 °C ; $^{14}NH_3$	**WL1** → 20.95 °C ; $^{14}NH_3$
WL2 → 18.69 °C ; $^{14}NH_3$	**WL2** → 21.56 °C ; $^{14}NH_3$
WL3 → 8.65 °C ; $^{15}NH_3$	**WL3** → 11.77 °C ; $^{15}NH_3$
WL4 → 9.45 °C ; $^{15}NH_3$	**WL4** → 12.36 °C ; $^{15}NH_3$

Due to the narrow width of the chosen wavelength range, WM (current tuning) was successful. The laser DC values were optimised to achieve maximum system sensitivity. In this optimised operation mode, the integrated electronics software repeatedly set the unmodulated part of the laser to 176.3 mA, 185 mA, 137.2 mA and 147.4 mA varying the measurement wavelengths between WL_1, WL_2, WL_3, and WL_4, respectively.

5.4.2 Calibration of the improved NIR-PA cell

Figures 29 (a and b) give the results of the calibrations of the NIR-PA system by mass flow controllers and chemical reaction-based gas generation method respectively.

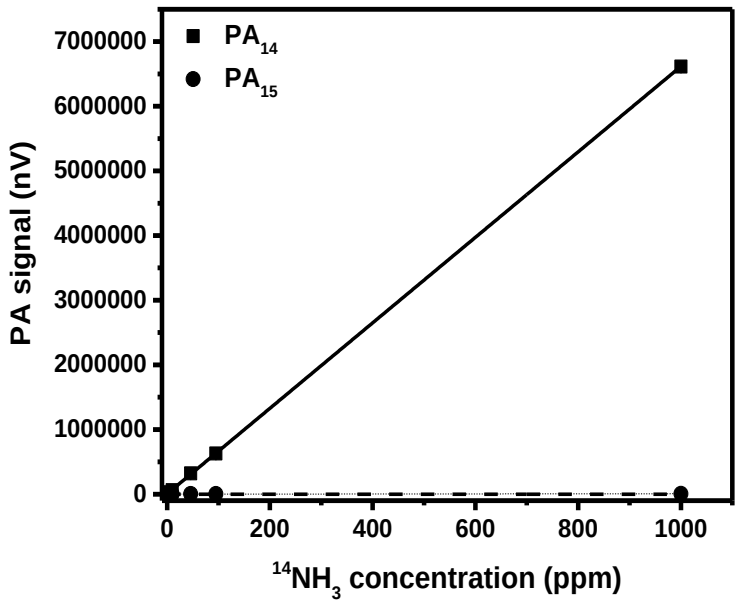

(a).

Figure 30 (a): Results of the calibration and cross-sensitivity measurements of the NIR-PA system performed by the gas generation system operated in the mass flow controller mixing mode. PA_{14} and PA_{15} are the modified photoacoustic signals used to determine the concentration of $^{14}NH_3$ and $^{15}NH_3$, respectively

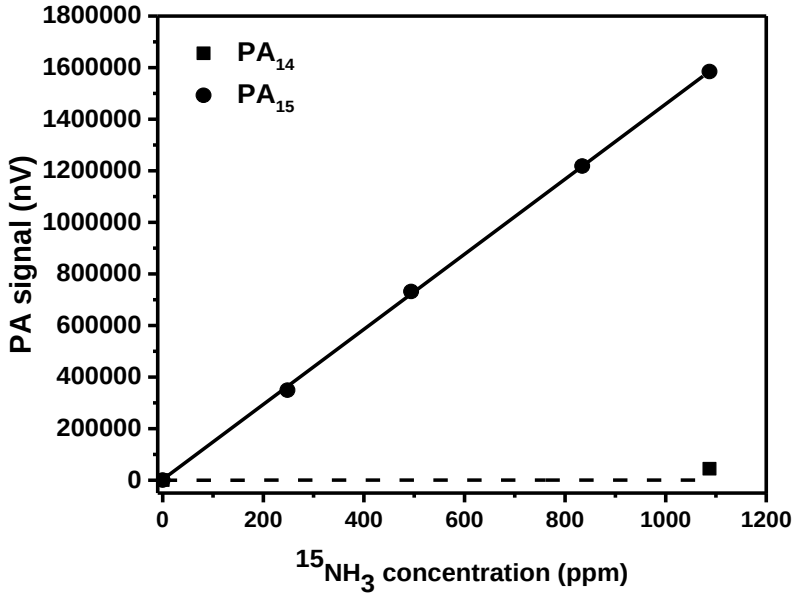

(b).

Figure 31 (b): Results of the calibration and cross-sensitivity measurements of the NIR-PA system performed by the gas generation system operated in the chemical reaction-based mode. PA_{14} and PA_{15} are the modified photoacoustic signals used to determine the concentration of $^{14}NH_3$ and $^{15}NH_3$, respectively.

Rectangles used in Figure 29 (a and b), represent data points of PA_{14} vs. $^{14}NH_3$ concentration and PA_{15} vs. $^{15}NH_3$ concentration respectively, with the corresponding fitted calibration lines represented by solid lines. Meanwhile, the circles in Figure 29 (a and b), represent the results of $^{14}NH_3$ and $^{15}NH_3$ cross-sensitivity determination (represented by dashed lines).

- **For $^{14}NH_3$ concentration determination:**
  - Calibration data (Figure 29a) are deduced from gas cylinder-based PA measurements by calculating the difference between the PA signals measured at wavelengths **WL_1** and **WL_2.**
  - The solid line (calibration) showed a linear regression with an R-squared value of 0.99979 and a slope of 6610 nV/ppm which gives the NIR-PA system sensitivity for $^{14}NH_3$ concentration.
  - Minimum detectable concentration (MDC) = (3 × Standard deviation of background signal) / Slope $_{\text{(solid line)}}$

    therefore, MDC = (3 × 316.3 nV) / 6610 nV/ppm = **0.14 ppm.** (20)

- Calibration slope (dashed line) = 2.52 nV/ppm. Used to determine the cross-sensitivity calculation for $^{14}NH_3$ due to the presence of $^{15}NH_3$:

$$\frac{\text{Slope}_{(\text{dashed line})}}{\text{Slope}_{(\text{solid line})}} = \frac{2.521\ \text{nV/ppm}}{6610\ \text{nV/ppm}} = 3.8\times10^{-4}\ \text{ppm/ppm} \quad (21)$$

- **For $^{15}NH_3$ concentration determination:**
  - Calibration data (Figure 29b) are chemical reaction-based PA measurements by calculating the difference between the PA signals measured at wavelengths **WL_3** and **WL_4.**
  - The solid line (calibration) showed a linear regression with an R-squared value of 0.99977 and a slope of 1300 nV/ppm which gives the NIR-PA system sensitivity for $^{15}NH_3$ concentration.
  - Minimum detectable concentration (MDC) = (3 × Standard deviation of background signal) / Slope $_{(\text{solid line})}$

    therefore, MDC = (3 × 316.3 nV) / 1300 nV/ppm = **0.73 ppm.** (22)
  - Calibration slope (dashed line) = 9.62 nV/ppm. Used to determine the cross-sensitivity calculation for $^{15}NH_3$ due to the presence of $^{14}NH_3$:

$$\frac{\text{Slope}_{(\text{dashed line})}}{\text{Slope}_{(\text{solid line})}} = \frac{9.62\ \text{nV/ppm}}{1300\ \text{nV/ppm}} = 7.4\text{x}10^{-3}\ \text{ppm/ppm} \quad (23)$$

In summary, the detection limit from the two calibration curves for $^{14}NH_3$ and $^{15}NH_3$ was therefore 0.14 ppm and 0.73 ppm (3б) respectively.

5.4.2.1 Minimum quantifiable concentration

From Figure 29, the minimum quantifiable concentration measured by the improved NIR-PA system for each ammonia isotope was calculated as follows;

- MQC = (10 × 316.3 nV) / 6610 nV/ppm = **0.48 ppm.** (24)
- MQC = (10 × 316.3 nV) / 1300 nV/ppm = **2.43 ppm.** (25)

Therefore, the minimum quantifiable limit from the two calibration curves for $^{14}NH_3$ and $^{15}NH_3$ was 0.48 ppm and 2.43 ppm (3б).

5.4.3 Response time results of the improved NIR-PA cell

The schematics shown in Figure 11 and measurement parameters as detailed in section 5.3 were used with the addition of a diffuser into the PA cell. The response time was calculated to be 3.5 sec.

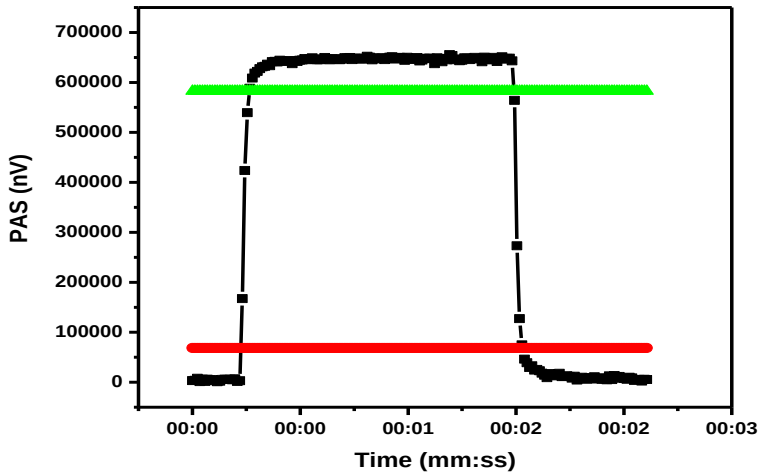

Figure 32: The response of the improved NIR-PA system to sudden concentration variation. The 10% (red) and 90% (green) concentration variations are indicated by horizontal dashed lines.

Two unique properties of my developed NIR-PA system that contributed to the measured low response time were the use of a small volume PA cell (≈10 cm^3) equipped with a diffuser and the current tuning of the measurement wavelengths. The former was responsible for quick complete flushing of the gas through the PA cell even at moderate gas flow rates while the latter was made possible due to the proximity of the selected wavelengths, an attribute that enabled the measuring of the four selected wavelengths to be executed in less than a second.

In summary, the MDC and response time values achieved by the developed NIR-PA system are comparable to other documented ammonia-detecting systems for different applications more specifically Huszár [3] and Pogány [74] who achieved MDC of 50 ppb and 0.5 ppb with a response time of 2 minutes and 30 minutes respectively for their ambient ammonia concentration measurements as discussed in section 2.3.

5.4.4. NIR-PA system evaluation experiment using dynamic measurements.

From the set-up in Figure 22, four wavelength spectra of the $^{14}NH_3$ and the three $^{15}NH_3$ absorption lines (depicted in Figure 27) using Current tuning modulations were carried out. The aim was to study the detection and interaction traits of the isotopes by the developed system

during a rapidly varied measurement. $^{14}NH_3$ gas from the 100 ppm cylinder and N_2 gas passing over granular 0.1g of NaOH placed inside a side-tubed Erlenmeyer flask were measured simultaneously for several minutes until stabilization was observed. 0.14 g of $^{15}NH_4Cl$ was then dissolved in 10 ml of distilled water and added to the flask via a dropping funnel from above. The developed $^{15}NH_3$ - N_2 gas mixture was then passed over granular NaOH for drying and measured simultaneously with the $^{14}NH_3$ gas. The result is recorded in Figure 31.

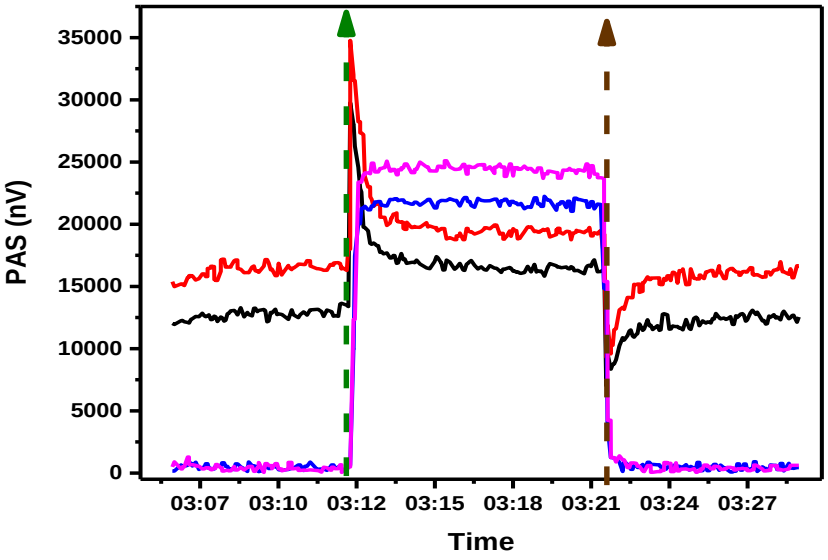

Figure 33: Dynamic measurements of the 4-wavelength spectra for the $^{14}NH_3$ and the $^{15}NH_3$ absorption lines using Current tuning modulation. $^{14}NH_3$ is denoted by black and red lines while $^{15}NH_3$ is denoted by blue and purple lines.

After careful analysis, the dynamic measurements were carried out on the third $^{15}NH_3$ peaks using DC values given in table 9 because only the third $^{15}NH_3$ peaks showed the least H_2O interference as depicted in figure 27.

From the graph in Figure 31, it was observed that the system could detect and distinguish between the two ammonia isotopes. Another observation was the overshooting and undershooting of $^{14}NH_3$ after gas switching at the points marked with green (introduction of $^{15}NH_3$ gas) and brown (switching off $^{15}NH_3$ gas) arrows.

One possible explanation for this is the adsorption-desorption process of NH_3 gas. When $^{15}NH_3$ gas is switched on, it first pushes down $^{14}NH_3$ from the walls of the PA cell causing a peak in $^{14}NH_3$ absorption. It, therefore, takes about 8 seconds after the rise of the $^{14}NH_3$ signal for the $^{15}NH_3$ signal to increase. As for the undershooting the converse would be considered

true, in that when $^{15}NH_3$ gas is switched off, more $^{14}NH_3$ molecules are adsorbed on the PA walls, hence registering a decrease in measured concentration which stabilizes after saturation. Another proposed explanation was that the overshooting and undershooting of $^{14}NH_3$ occurred due to sudden pressure variation on switching $^{15}NH_3$ gas on or off. This theory was tested by repeating the above dynamic measurements with N_2 gas instead of $^{15}NH_3$ gas. The result obtained is shown in Figure 32.

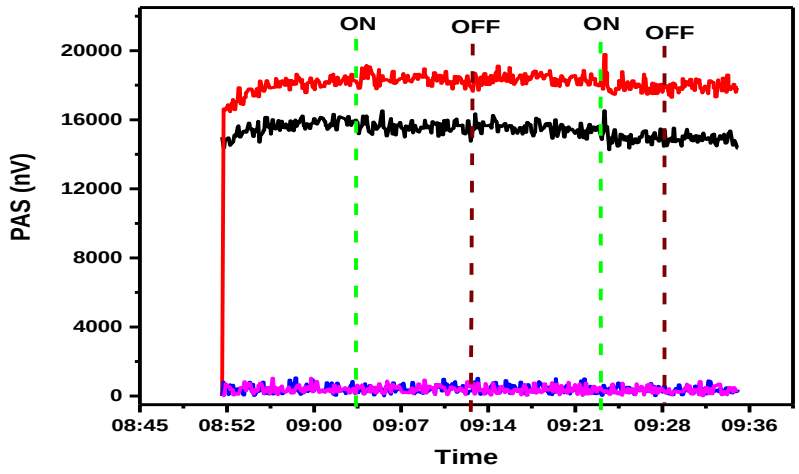

Figure 34: Dynamic measurements of the $^{14}NH_3$ and the $^{15}NH_3$ absorption lines to check for the effect of pressure variation. The points marked with arrows denote the switching on (green line) or switching off (brown line) of the N_2 gas.

Figure 32 shows that on switching on the N_2 gas, at the point marked with a green line, no discernible change occurred on the $^{14}NH_3$ PA signal. Similarly, no variations occurred at the N_2 gas switching-off points. This rules out the theory of sudden pressure variation caused by the doubling of gas flow rates from 100 ml/min to 200 ml/min at the switching-on points and vice versa at the switching-off points. Therefore, only the adsorption-desorption phenomenon of the NH_3 gas effect was accepted.

The amplitude graph of the dynamic measurement (Figure 31) was plotted using the combined $^{14}NH_3$ and $^{15}NH_3$ (third peak) values and the result is shown in Figure 33.

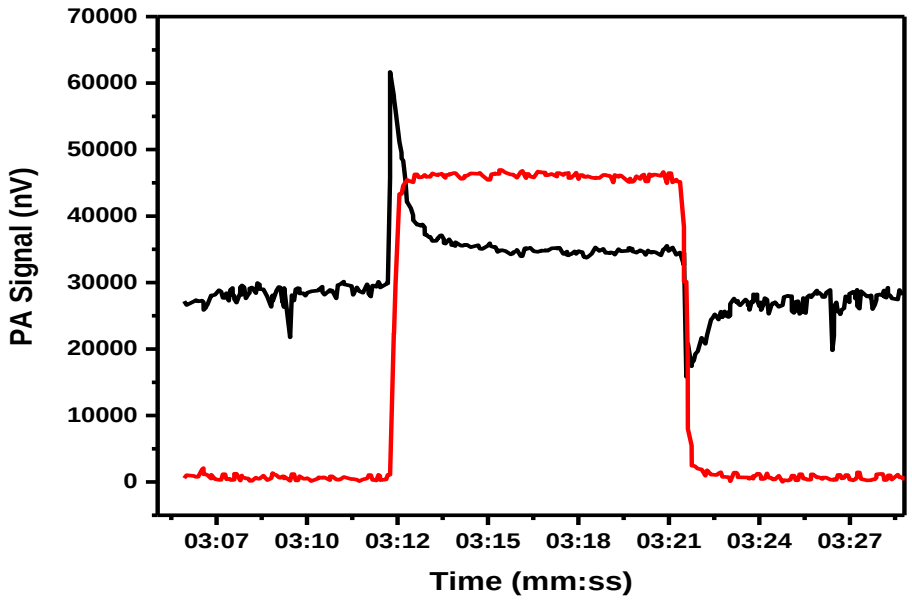

Figure 35: Amplitude graph (black line; $^{14}NH_3$ and red line; $^{15}NH_3$) of the four-wavelength dynamic measurement for $^{14}NH_3$ and $^{15}NH_3$ isotopes.

The purpose of the graph was to analyse the reason for the increase in the $^{14}NH_3$ signal during the peak measurement of the $^{15}NH_3$ gas. At first, cross-sensitivity between the two isotopes was assumed but on plotting the phase graph the $^{14}NH_3$ phase was constant throughout the measurement meaning that there was no discernible spectral cross-interference between the two isotopes. On calculating the percentage increase of the $^{14}NH_3$ signal during the $^{15}NH_3$ measurement, it was found to be ≈ 1 ppm.

It was, therefore, concluded that the rise in the $^{14}NH_3$ signal was due to the impurity of < 2% ^{14}N in the ammonium-^{15}N chloride (Sigma Aldrich), used during the chemical generation of $^{15}NH_3$ gas. The $^{14}NH_3$ concentration (1 ppm) generated by the impurity of ammonium-^{15}N chloride agrees well with the increase of the $^{14}NH_3$ signal. This contamination was considered during the calibration process.

6.0 Conclusions and new scientific results

The main aim of the work presented herein was to develop a near-infrared photoacoustic system that could detect ammonia gas and distinguish between its isotopes ($^{14}NH_3$ and $^{15}NH_3$) i.e. selective measurement of $^{15}NH_3$ ammonia isotope by photoacoustic spectroscopy. A further objective was to provide a robust, easy-to-use, and automated system. This has been achieved and new scientific results are summarised below;

I. Selection of the wavelength and optimisation of the laser modulation parameters

1. Wavelength parameters.
   - I recorded the spectra measurements of $^{14}NH_3$ and $^{15}NH_3$ at wavelength 1470-1590 nm with an ECDL, and based on the data results, **I selected 1520-1523 nm and 1530.5 - 533.5 nm wavelength ranges** for further optimisation.

   - **I have also performed wavelength modulation on the designed NIR-PA system using DFB diode lasers** and chose the **1530.5 - 1533.5 nm** wavelength range as the optimum measuring range since suitable cross interference-free absorption lines were found unlike in the 1520-1523 nm wavelength range.

   - I have optimised both the Modulated (I_{AC}) and unmodulated (I_{DC}) currents of the laser together with the laser temperature to produce a maximum PA signal. **These optimum values were $I_{AC} \approx 9.1$ mA and $I_{DC} \approx 290.1$ mA.**

II. Calibration of the newly developed NIR-PA system.

I have prepared NH_3 gas mixtures using different percentages of ammonium chloride containing ^{14}N and ^{15}N marked isotopes intended to span a wide range of generated gas isotopes.

   - **I have calibrated both the $^{14}NH_3$ and $^{15}NH_3$ gas isotopes. A minimum detectable concentration of up to 0.28 ppm (3б) and 1.7 ppm (3б) for $^{14}NH_3$ and $^{15}NH_3$ respectively was measured.**

III. Design and construction of a NIR-PA system capable of selectively measuring and differentiating between ammonia gas isotopes ($^{14}NH_3$ & $^{15}NH_3$).

I have built a highly selective NIR-PA system, a feature that enables it to not only distinguish between the $^{14}NH_3$ and $^{15}NH_3$ isotopes but also detect and keep interference from other molecular species (cross-sensitivity effects) at a minimum level; especially water vapour. The stability of the system ensures long-term and continuous measurements (2-3 months) after the initial calibration.

IV. Improvement of the newly developed NIR-PA system.

- I have improved the response time of the system by the addition of a diffuser into the PA cell and the application of current tuning instead of the previously used temperature tuning during WM. **The improved response time of the system was calculated as 3.5 seconds as compared to 24.4 seconds found by the preliminary NIR-PA system [118].**

- **I have improved the MDC from 0.28 ppm and 1.7 ppm (3б) for $^{14}NH_3$ and $^{15}NH_3$ respectively in the preliminary NIR-PA system without a back-reflecting mirror, to 0.14 ppm and 0.73 ppm (3б) for $^{14}NH_3$ and $^{15}NH_3$ in the new NIR-PA system with a back-reflecting mirror installation [118,119].**

- **I have improved the MQC values from 0.92 ppm and 5.5 ppm (3б) for $^{14}NH_3$ and $^{15}NH_3$ respectively in the preliminary NIR-PA system without a back-reflecting mirror, to 0.48 ppm and 2.43 ppm (3б) for $^{14}NH_3$ and $^{15}NH_3$ respectively after modifications and improvement to the NIR-PA system.**

- **I have calculated the cross-sensitivities of the isotopes as $-1.3x10^{-4}$ ppm/ppm for the value of $^{14}NH_3$ due to the presence of $^{15}NH_3$, and $7.4x10^{-3}$ ppm/ppm, for the value of $^{15}NH_3$ due to the presence of $^{14}NH_3$, respectively [118].**

7.0 Summary

Globally, the need for green energy to combat or drastically reduce greenhouse gas emissions has in this century intensified in the hopes of tackling the climate change problem. One such gas is carbon dioxide (CO_2) which is a major by-product in the industrial ammonia (NH_3) production, Haber-Bosch process, with an annual output of 300 million metric tons. Although ammonia is an important compound with applications ranging from the chemical, food and beverage, automotive and agricultural industries, its production process has been documented to be highly energy-intensive. The Haber-Bosch process also makes use of high temperatures (~ 450 ^oC) and pressures (~ 20-40 MPa) while consuming a big percentage of the earth's fossil fuel (natural gas 50% or coal 19%) as feedstock thus making it unsustainable and less environmentally friendly.

To tackle this concern, scientists and researchers have developed an alternative method for NH_3 production, namely through electrochemical synthesis. This method although still in the research and developmental stage, has shown great potential and is deemed less polluting and environmentally sustainable. This is because it has a provision for the direct conversion of renewable energy into chemical energy (in form of NH_3) with minimal or zero CO_2 emission. While the process has produced promising results, several problems have been identified of main concern being its low efficiency (0.1 - 8%) and inaccuracy in the assessment of NH_3 levels produced. The latter problem is mostly due to the inability of the current NH_3 detecting equipment and analytical methods to reliably measure the low NH_3 gas produced (sub-ppm levels) without interference from common contaminants. NH_3 being the most abundant alkaline gas in the atmosphere means that it exists almost everywhere and distinguishing between the NH_3 generated by the electrochemical synthesis and general sources e.g., air, human breath, N_2 gas sources used in the synthesis process etc., requires very selective and sensitive analytical methods/equipment. So far, the employed analytical methods especially in spectroscopy are either all very expensive, need large sensing volumes (nuclear magnetic resonance), have uncertainties at very low NH_3 concentrations (molecular spectroscopy), or are limited by the availability of the tunable laser light at the appropriate wavelength (CRDS), or simply have a problem in the control of its background signal (CIMS).

In practice, accurate determination of the generated NH_3 from the electrochemical synthesis process has been a challenge which my studies seek to address and contribute a solution to. Through documented literature, photoacoustic spectroscopy (PAS) has shown a great ability to detect NH_3 at very low sub-ppm concentrations. For the last two decades, the

Photoacoustic Research Group at the University of Szeged of which I am now a member, have dedicated itself to researching, developing and providing applications for their various PA systems. Considering this, my thesis study has focused on the development of the near-infrared (NIR) PA detection method in the making of a detection system capable of selectively and sensitively differentiating between the NH_3 gas isotopes at relatively low concentrations.

To this end, I aimed to design and build an NH_3 gas concentration measurement device for the photo-electrochemistry research group, at the University of Szeged, based on the PAS concept, which could be able to selectively measure and differentiate between NH_3 gas isotopes. To achieve this goal, there was a need for methodological development, construction of the measuring instruments and finally, the development of gas sampling procedures to be used. The following subtasks were therefore performed:

- **Designing a NIR-PA system.**

I considered several factors during this process e.g.:

- The choice of the wavelength ranges to be used.

This was decided between the long wavelength end of the near-infrared (≈ 2000 nm) and the telecommunication window wavelength range (1260 nm-1625 nm), with the latter being chosen as explained in section 4.1.

- The choice of integrated electronics.

This was assembled and settled depending on its expected primary function i.e., temperature control of the laser and PA cell, amplification and filtration of the microphone signal and the modulation of the diode laser driving current. Its operation was controlled by measurement software built from a set of subroutines using the Python programming language.

- The choice of light sources to be used.

I settled on the use of two laser light sources, a tunable external cavity diode laser (ECDL) and the distributed feedback (DFB) diode laser. ECDL laser was used to identify the first optimal measurement wavelengths under AM. DFB diode laser under WM was then used to further optimise the identified wavelength range and find cross-interference-free wavelengths of both NH_3 isotopes to be used in the NIR-PA measurements.

- The choice of the gas handling unit materials.

This encompassed the whole NIR-PA experimental system. The choice of gas tubing materials (PTFE), length size, PA cell material (stainless steel) and gas flow rates were all done with the

main goal of minimising the adsorption-desorption processes brought about by the highly polar NH_3 molecules and the corresponding effect to the systems' response time.

- **Optimisation of the measurement and modulation parameters i.e.,**
    - Wavelength parameters.

This was done by performing an AM using an ECDL in the telecommunication wavelength range. Strong absorption lines of both isotopes ($^{14}NH_3$ and $^{15}NH_3$) overlapping with absorption lines of water vapour were identified by searching for less than 1 nm wide wavelength range. These wavelength ranges were; below 1500 nm which were excluded due to the presence of strong water vapour absorption lines, 1520-1523 nm and the 1530.5-1533.5 nm wavelength ranges which were optimised further.

Next, a WM on the designed NIR-PA system using DFB diode lasers was done. Since the optimum measurement wavelengths of both NH_3 isotopes lay sufficiently close to each other, the application of temperature tuning during WM was made possible. Here, the 1530.5-1533.5 nm wavelength range was chosen as the optimum range since suitable cross interference-free absorption lines were found unlike in the 1520-1523 nm wavelength range. Later, during the evaluation and improvement of the system, the DFB diode laser was used to tune the laser wavelength on the sub-second timescale by varying its driving current rather than using the much slower temperature tuning.

- PA cell temperature.

The PA cell was heated to reduce the measured gas temperature variations and hold it constant. This is because gas temperature tended to change the sound speed and hence the resonance frequency of the cell which in turn dictated the cell constant and the sensitivity of the system.

- Laser operating temperature and current (I_{AC} and I_{DC}) values.

In determining the optimum parameters to be used by the lasers, the values of laser modulation current i.e., both modulated (I_{AC}) and unmodulated (I_{DC}), together with the laser temperature producing a maximum PA signal were varied and noted. For the DFB diode lasers, the I_{AC} values varied between 2.3-22.9 mA such that at any given time, the total sum of $I_{AC} + I_{DC}$ was always 300 mA (maximum applicable current). After measuring the magnitude of the PA signal value at the maximum determined NH_3 absorption line, from each of the different sets of $I_{AC} + I_{DC}$ variations, a maximum peak signal of each laser was identified. These optimum values were $I_{AC} \approx 9.1$ mV and $I_{DC} \approx 290.1$ mV.

- **Calibration of the newly developed NIR-PA system.**

Calibration by both mass flow controllers (for $^{14}NH_3$) and chemical reaction-based gas generation method (for $^{15}NH_3$) was achieved. A minimum detectable concentration of up to 0.14 ppm (3б) and 0.73 ppm (3б) for $^{14}NH_3$ and $^{15}NH_3$ respectively was measured. The cross-sensitivities were recorded as 3.8×10^{-4} ppm/ppm for the value of $^{14}NH_3$ due to the presence of $^{15}NH_3$, and 7.4×10^{-3} ppm/ppm, for the value of $^{15}NH_3$ due to the presence of $^{14}NH_3$, respectively.

- **Improvement of the newly developed NIR-PA system.**

This was achieved by the application of current tuning instead of the previously used temperature tuning, to the DFB diode lasers during the modulation of wavelength parameters. This made it possible to program the operational software of the NIR-PA system in a way as to complete a single concentration measurement cycle on the four selected wavelengths in less than a second. This improved the sensitivity and general response time of the system.

The sensitivity of the system was also improved almost by an order of magnitude by fibre coupling two lasers together, applying a back-reflecting mirror to the PA window cell and subtracting PA signals with opposite phases. MDC values in the preliminary NIR-PA system without a back-reflecting mirror were 0.28 ppm and 1.7 ppm (3б) for $^{14}NH_3$ and $^{15}NH_3$ respectively, while after the back-reflecting mirror installation, at the exit window, the values improved to 0.14 ppm and 0.73 ppm (3б) for $^{14}NH_3$ and $^{15}NH_3$ respectively.

The response time of the system was also improved to 3.5 seconds as compared to the 24.4 seconds measured by the preliminary NIR-PA system.

- **Evaluation of the newly developed NIR-PA system.**

This was done by testing the ensemble NIR-PA system and recording its dynamic response during simultaneous measurements of the ammonia isotopes. One isotope was initially measured, and then by introducing the other isotope midway, the system's response time, sensitivity and selectivity during the detection of the newly introduced isotope were analysed.

In conclusion, due to the newly developed NIR-PA system's robustness, high sensitivity, low cross-sensitivity, and short response time the presented system is expected to find a practical application in the detection and measurement of isotopically labelled NH_3 gas which has been discharged from an electrochemical synthesis process. This will enable it to provide more definitive proof that the ammonia gas produced is from the N_2 electroreduction process rather than the general probable contaminants.

8.0 Összefoglalás

Az éghajlatváltozás problémájának megoldása reményében ebben az évszázadban világszerte egyre nagyobb szükség van a zöld energiára az üvegházhatású gázok kibocsátásának leküzdése vagy drasztikus csökkentése érdekében. Az egyik ilyen gáz a szén-dioxid (CO_2), amely az ipari ammónia (NH_3) előállításának, a Haber-Bosch-folyamatnak az egyik fő melléktermék, amelynek éves kibocsátása 300 millió tonna. Bár az ammónia fontos vegyület, amelynek alkalmazásai a vegyiparban, az élelmiszer- és italgyártásban, az autóiparban és a mezőgazdaságban találhatók, előállítási folyamata rendkívül energiaigényes. A Haber-Bosch-eljárás magas hőmérsékletet (~450°C) és nyomást (~20 40 MPa) igényel, valamint nagy mértékben használja fel alapanyagként a Föld fosszilis tüzelőanyagait (földgáz 50% vagy szén 19%), így nem fenntartható és kevésbé környezetbarát.

Az NH_3 előállítására ezért alternatív módszert dolgoztak ki. Ez a módszer az elektrokémiai szintézis, amely bár még mindig a kutatási és fejlesztési szakaszban van, nagy lehetőségeket rejt magában, és kevésbé szennyezőnek és környezetileg fenntarthatónak tekinthető. Ennek oka, hogy a megújuló energia közvetlen átalakítását teszi lehetővé kémiai energiává (NH_3 formájában), minimális vagy nulla CO_2 kibocsátás mellett. Bár az eljárás ígéretes eredményeket hozott, több problémát is azonosítottak, amelyek közül a fő probléma az alacsony hatékonyság (0,1-8%) és a termelt NH_3 mennyiség meghatározásának pontatlansága. A jelenlegi NH_3 detektáló berendezések és analitikai módszerek nem képesek megbízhatóan mérni a keletkező alacsony NH_3 gázmennyiséget (sub-ppm szintek) anélkül, hogy a folyamat során keletkező egyéb anyagok kereszteffektust okoznának. Az NH_3 a légkör legnagyobb mennyiségben előforduló bázikus gáza, szinte mindenhol megtalálható. Az elektrokémiai szintézis során keletkező NH_3 és az általános források (pl. a levegő, a humán kilégzett levegő, a szintézis során használt N_2 gázforrások stb.) megkülönböztetése nagyon szelektív és érzékeny analitikai módszereket/berendezéseket igényel. A jelenleg alkalmazott analitikai módszerek vagy költségesek, vagy nagy érzékelési térfogatot igényelnek (NMR), kis NH_3 koncentráció esetén bizonytalanok (MS), vagy a megfelelő hullámhosszúságú hangolható lézerfény rendelkezésre állása korlátozza őket (CRDS), vagy egyszerűen problémát jelent a háttérjel ellenőrzése (CIMS).

A gyakorlatban az elektrokémiai szintézis során keletkező NH_3 pontos meghatározása olyan kihívást jelentett, amelyre tanulmányomban megoldást keresek. A dokumentált irodalom révén a fotoakusztikus spektroszkópia (PAS) nagyszerű képességet mutatott az NH_3 kimutatására nagyon alacsony, szub-ppm koncentrációban. A Szegedi Tudományegyetem

Fotoakusztikus kutatócsoportja az elmúlt két évtizedben fotoakusztikus rendszerek kutatásával, fejlesztésével és gyakorlati alkalmazásával foglalkozott. A kutatócsoportban végzett munkám célja egy közeli infravörös lézeren alapuló fotoakusztikus spektroszkópiai elvű (NIR-PA) gáz koncentráció-mérő műszer fejlesztése volt, amely képes szelektíven és érzékenyen mérni az NH_3 gázizotópokat.

A cél eléréséhez szükség volt módszertani fejlesztésre, a mérőműszer megépítésére és végül az alkalmazandó gázmintavételi eljárások kidolgozására. Ezért a következő részfeladatokat végeztem el:

- **NIR-PA rendszer tervezése**
    - Az alkalmazandó hullámhossz-tartományok kiválasztása

Ezt a közeli infravörös tartomány hosszú hullámhosszú vége (≈ 2000 nm) és a távközlési ablak hullámhossz-tartománya (1260 nm-1625 nm) között határoztam meg.

- Az integrált elektronika kiválasztása

A várható elsődleges funkciójának megfelelően állítottam össze és telepítettem, mint például a lézer és a fotoakusztikus kamra hőmérséklet-szabályozása, a mikrofonjel erősítése és szűrése, valamint a diódalézer meghajtó áramának modulálása. Működését a Python programozási nyelvet használó alprogramokból felépülő mérőszoftver vezérelte.

- A használandó fényforrások kiválasztása.

Két fényforrást választottam, egy hangolható külső rezonátoros diódalézert (ECDL) és egy elosztott visszacsatolású (DFB) diódalézert. Elsőként az ECDL lézert használtam az optimális mérési hullámhosszak azonosítására. Ezt követően az azonosított hullámhossz-tartomány további optimalizálására, vagyis a két NH_3 izotóp spektrális átfedéstől mentes abszorpciós vonalainak megtalálásához DFB diódalézert használtam.

- A gázkezelő egység anyagainak kiválasztása

Ez a teljes NIR-PA kísérleti rendszert felölelte. A csövek anyagát (PTFE),hosszát, a PA kamra anyagát (rozsdamentes acél) és a gázáramlási sebességet úgy választottam, hogy minimalizáljam az erősen poláros NH_3 molekulákra jellemző adszorpciós-deszorpciós folyamatokat és a rendszer válaszidejét.

- **A mérési és modulációs paraméterek optimalizálása,**
    - Hullámhossz paraméterek

Ehhez amplitúdó-modulált ECDL segítségével spektrális méréseket végeztem 1470-1590 nm hullámhossz tartományban. A két izotóp ($^{14}NH_3$ és $^{15}NH_3$) erős abszorpciós vonalait, amelyek átfedésben vannak a vízgőz abszorpciós vonalaival, 1 nm-nél kisebb hullámhossz tartományban

keresve azonosítottam. Ezek a hullámhossz-tartományok a következők voltak: 1500 nm alatti hullámhossz, amelyet az erős vízgőz-elnyelési vonalak jelenléte miatt kizártam, valamint az 1520-1523 nm és az 1530,5-1533,5 nm hullámhossz-tartományok, amelyeket tovább optimalizáltam.

Ezt követően hullámhossz-modulált DFB diódalézerekkel vettem fel spektrumokat. Mivel mindkét NH_3 izotóp optimális mérési hullámhossza elég közel van egymáshoz, lehetővé vált a hőmérséklet-hangolás alkalmazása a hullámhossz-moduláció során. Itt az 1530,5-1533,5 nm-es hullámhossztartományt választottam optimális tartománynak, mivel az 1520-1523 nm-es hullámhossz-tartománytól eltérően keresztérzékenység nélküli abszorpciós vonalakat találtam. A későbbiekben a rendszer tesztelése és továbbfejlesztése során a DFB diódalézer vezérlőáramának változtatásával végeztem el a lézer hullámhosszának szub-szekundumos időskálán történő hangolását, a sokkal időigényesebb hőmérséklet-hangolás helyett.

- PA kamra hőmérséklete

A PA kamra 50°C-ra hőmérsékletstabilizált volt, mivel a gáz hőmérsékletének változása a rezonanciafrekvencia változást okoz a kamrában, amely befolyásolja a kamra érzékenységét.

- A lézer hőmérséklet és áram (I_{AC} & I_{DC}) értékeinek optimalizálása

A lézerek által használandó optimális paraméterek meghatározásához a lézermodulációs áram, azaz a modulált (I_{AC}) és a modulálatlan (I_{DC}) lézeráram értékeit, valamint a maximális PA jelet adó lézerhőmérsékletet változtattam és optimalizáltam. A DFB diódalézerek esetében az I_{AC} értékeket 2,3-22,9 mA között változtattam úgy, hogy az I_{AC} + I_{DC} teljes összege mindig 300 mA legyen (maximálisan alkalmazható áram). Az optimális értékek a következők voltak*:* $I_{AC} \approx$ 9,1 mV, és $I_{DC} \approx$ 290,1 mV.

- **Az újonnan fejlesztett NIR-PA rendszer kalibrálása**

A mérőrendszer kalibrálása $^{14}NH_3$ esetében tömegáram-szabályozókkal, valamint $^{15}NH_3$ esetében kémiai reakción alapuló gáztermelő módszerrel történt. A legkisebb kimutatható koncentráció 0,14 ppm (3Ϭ) volt $^{14}NH_3$ esetén és 0,73 ppm (3Ϭ) volt a $^{15}NH_3$ esetében. A keresztérzékenységek $3{,}8 \times 10^{-4}$ ppm/ppm volt $^{14}NH_3$-ra a $^{15}NH_3$ jelenlétében, illetve $7{,}4 \times 10^{-3}$ ppm/ppm volt a $^{15}NH_3$-ra értékére a $^{14}NH_3$ jelenlétében.

- **Az újonnan kifejlesztett NIR-PA rendszer fejlesztése**

A korábban használt hőmérséklet-hangolás helyett áramhangolást alkalmaztam a DFB diódalézereknél a hullámhossz paraméterek modulációja során. Ez lehetővé tette, hogy a NIR-PA rendszer működési szoftverét úgy programozzam, hogy a négy kiválasztott hullámhosszon egyetlen koncentráció mérési ciklus kevesebb, mint egy másodperc alatt befejeződjön. Ez javította a rendszer válaszidejét.

A rendszer érzékenységét több lépéssel közel egy nagyságrenddel javítottam. Két DFB lézer szálcsatolásával kétszereztem a fényteljesítményt, a PA kamra kilépő optikai ablakának helyére tükröt tettem, amellyel kétszereztem a fényutat, valamint az ellentétes fázisú PA jelek differenciális kiértékelésével is érzékenység növekedést értem el. Az előzetes NIR-PA rendszer MDC értékei a tükör nélkül 0,27 ppm és 1,66 ppm (3б) voltak a $^{14}NH_3$ és a $^{15}NH_3$ esetében, míg a tükör felszerelése után az értékek 0,14 ppm-re és 0,73 ppm-re (3б) javultak a $^{14}NH_3$ és a $^{15}NH_3$ esetében.

- **Az újonnan kifejlesztett NIR-PA rendszer vizsgálata**

Ez az ammóniaizotópok egyidejű mérése során történt. Kezdetben az egyik izotópot mértem, majd a másik izotóp bejuttatása után elemeztem a rendszer válaszidejét, érzékenységét és szelektivitását. Az eredmények megerősítették, hogy a $^{14}NH_3$ és a $^{15}NH_3$ mérése szelektíven történik és a válaszidő 3,5 s.

Összefoglalva, az újonnan fejlesztett NIR-PA rendszer alkalmazható az elektrokémiai szintézis folyamatából származó, izotóposan jelölt NH_3 gáz kimutatására és mérésére. Ezt a rendszer robusztussága, nagy érzékenysége, alacsony keresztérzékenysége és rövid válaszideje teszi lehetővé. Segítségével megállapítható, hogy a keletkező ammóniagáz az N_2 elektroredukciós folyamatából származik, nem pedig az általános valószínűsíthető szennyeződésekből.

9.0 Acknowledgement

First and foremost, I give thanks to Almighty God for giving me the gift of life and health that enabled me to carry out this Ph.D. research. I am also thankful to the Tempus Public Foundation and the Ministry of Foreign Affairs and Trade of Hungary for providing financial support for my studies through the Stipendium Hungaricum Scholarship.

I would also like to express my gratitude to my supervisor, Prof. Dr. Zoltan Bozóki, for helping me on my research journey throughout the years and for his optimistic outlook on life which always motivated me to do my best. Heartfelt thanks also go to Dr. Helga Huszár for her patience and guidance, and together with Dr. Csaba Janáky and Prof. László Horváth for thoroughly revising and helping in the publication of my journal articles. A big thank you is also extended to Dr, Anna Szabo for her helpful suggestions and for painstakingly revising my thesis draft together with Nóra Füle-Ducsay for revising and correcting my Hungarian thesis summary.

I would also like to thank my family, especially my Mom, Caroline Ouma and Dad, Thomas Ouma who have been and are always my pillar of strength together with my son Phelyx Ouma who although not quite understanding, has endured separation and loneliness for the last four years. For without their support I would not have stayed strong to finish my study.

Many thanks also go to my employer, Laikipia University, Kenya for granting me study leave and enabling me to pursue my Ph.D. studies in Hungary. The investment in my career progression will not only make me a better employee but also an astute researcher for the betterment of my university, community and country at large.

Last but not least, I would also like to extend my sincere thanks to Rev. Fr. John Kipruto and Rev. Fr. Phillip Kabiru for their prayers and guidance. The same goes for all my colleagues and friends at the University of Szeged without whom four years Ph.D. journey would be too boring.

10.0 References

[1] International Energy Agency, Global Energy Review : CO_2 Emissions in 2021, Global emissions rebound sharply to highest ever level, 2022.

[2] G. Qing, R. Ghazfar, S.T. Jackowski, F. Habibzadeh, M.M. Ashtiani, C.P. Chen, M.R. Smith, T.W. Hamann, Recent Advances and Challenges of Electrocatalytic N_2 Reduction to Ammonia, Chem. Rev. 120 (2020) 5437–5516. https://doi.org/10.1021/acs.chemrev.9b00659.

[3] H. Huszár, A. Pogány, Z. Bozóki, Á. Mohácsi, L. Horváth, G. Szabó, Ammonia monitoring at ppb level using photoacoustic spectroscopy for environmental application, Sensors Actuators, B Chem. 134 (2008) 1027–1033. https://doi.org/10.1016/j.snb.2008.05.013.

[4] S. Giddey, S.P.S. Badwal, A. Kulkarni, Review of electrochemical ammonia production technologies and materials, Int. J. Hydrogen Energy. 38 (2013) 14576–14594. https://doi.org/10.1016/j.ijhydene.2013.09.054.

[5] S. Wang, J. Nan, C. Shi, Q. Fu, S. Gao, D. Wang, H. Cui, A. Saiz-Lopez, B. Zhou, Atmospheric ammonia and its impacts on regional air quality over the megacity of Shanghai, China, Sci. Rep. 5 (2015) 1–14. https://doi.org/10.1038/srep15842.

[6] J. David Felix, E.M. Elliott, T.J. Gish, L.L. McConnell, S.L. Shaw, Characterizing the isotopic composition of atmospheric ammonia emission sources using passive samplers and a combined oxidation-bacterial denitrifier approach, Rapid Commun. Mass Spectrom. 27 (2013) 2239–2246. https://doi.org/10.1002/rcm.6679.

[7] M.J. Roadman, J.R. Scudlark, J.J. Meisinger, W.J. Ullman, Validation of Ogawa passive samplers for the determination of gaseous ammonia concentrations in agricultural settings, Atmos. Environ. 37 (2003) 2317–2325. https://doi.org/10.1016/S1352-2310(03)00163-8.

[8] R. Lan, J.T.S. Irvine, S. Tao, Ammonia and related chemicals as potential indirect hydrogen storage materials, Int. J. Hydrogen Energy. 37 (2012) 1482–1494. https://doi.org/10.1016/j.ijhydene.2011.10.004.

[9] S. Licht, B. Cui, B. Wang, F.F. Li, J. Lau, S. Liu, Ammonia synthesis by N_2 and steam electrolysis in molten hydroxide suspensions of nanoscale Fe_2O_3, Science (80). 345 (2014) 637–640. https://doi.org/10.1126/science.1254234.

[10] Schiller M, Industrial uses of ammonia, (n.d.). http://www.easychem.com.au/monitoring-and-management/maximising-

production/industrial-uses-of-ammonia (accessed October 27, 2021).

[11] G. Busca, L. Lietti, G. Ramis, F. Berti, Chemical and mechanistic aspects of the selective catalytic reduction of NO(x) by ammonia over oxide catalysts: A review, Appl. Catal. B Environ. 18 (1998) 1–36. https://doi.org/10.1016/S0926-3373(98)00040-X.

[12] N.P. Cheremisinoff, P.E. Rosenfeld, Chapter 1; Industry and Products, in: Nicholas P Cheremisinoff, P.E. Rosenfeld (Eds.), Handb. Pollut. Prev. Clean. Prod. Best Pract. Agrochem. Ind., First, Elsevier: Amsterdam, The Netherlands, 2011: pp. 1–24. https://doi.org///doi.org/10.1016/B978-1-4377-7825-0.00001-7.

[13] D. Viveiros, J. Ribeiro, J.P. Carvalho, J. Ferreira, A.M.R. Pinto, R.A. Perez-Herrera, S. Diaz, A. Lopez-Gil, A. Dominguez-Lopez, O. Esteban, H.F. Martins, S. Martin-Lopez, H. Baierl, J.-L. Auguste, R. Jamier, S. Rougier, J.L. Santos, D. Flores, P. Roy, M. González-Herráez, M. López-Amo, J.M. Baptista, Fiber optic sensing system for monitoring of coal waste piles in combustion, in 23rd Int. Conf. Opt. Fibre Sensors, 2014: p. 91573O. https://doi.org/10.1117/12.2059640.

[14] S. Schilt, L. Thévenaz, M. Niklès, L. Emmenegger, C. Hüglin, Ammonia monitoring at trace level using photoacoustic spectroscopy in industrial and environmental applications, Spectrochim. Acta - Part A Mol. Biomol. Spectrosc. 60 (2004) 3259–3268. https://doi.org/10.1016/j.saa.2003.11.032.

[15] D.J. Kearney, T. Hubbard, D. Putnam, Breath ammonia measurement in Helicobacter pylori infection, Dig. Dis. Sci. 47 (2002) 2523–2530. https://doi.org/10.1023/A:1020568227868.

[16] W. Ament, J.R. Huizenga, E. Kort, T.W. Van Der Mark, R.G. Grevink, G.J. Verkerke, Respiratory ammonia output and blood ammonia concentration during incremental exercise, Int. J. Sports Med. 20 (1999) 71–77. https://doi.org/10.1055/s-2007-971096.

[17] L.R. Narasimhan, W. Goodman, C.K.N. Patel, Correlation of breath ammonia with blood urea nitrogen and creatinine during hemodialysis, Proc. Natl. Acad. Sci. U. S. A. 98 (2001) 4617–4621. https://doi.org/10.1073/pnas.071057598.

[18] T.D. Durbin, R.D. Wilson, J.M. Norbeck, J.W. Miller, T. Huai, S.H. Rhee, Estimates of the emission rates of ammonia from light-duty vehicles using standard chassis dynamometer test cycles, Atmos. Environ. 36 (2002) 1475–1482. https://doi.org/10.1016/S1352-2310(01)00583-0.

[19] R. Moos, R. Müller, C. Plog, A. Knezevic, H. Leye, E. Irion, T. Braun, K.J. Marquardt, K. Binder, Selective ammonia exhaust gas sensor for automotive applications, Sensors Actuators, B Chem. 83 (2002) 181–189. https://doi.org/10.1016/S0925-4005(01)01038-

3.

[20] C. Pijolat, C. Pupier, M. Sauvan, G. Tournier, R. Lalauze, Gas detection for automotive pollution control, Sensors Actuators, B Chem. 59 (1999) 195–202. https://doi.org/10.1016/S0925-4005(99)00220-8.

[21] X. Xuan, C. Yue, S. Li, Q. Yao, Selective catalytic reduction of NO by ammonia with fly ash catalyst, Fuel. 82 (2003) 575–579. https://doi.org/10.1016/S0016-2361(02)00321-6.

[22] M. Wallin, C.J. Karlsson, M. Skoglundh, A. Palmqvist, Selective catalytic reduction of NOx with NH_3 over zeolite H-ZSM-5: Influence of transient ammonia supply, J. Catal. 218 (2003) 354–364. https://doi.org/10.1016/S0021-9517(03)00148-9.

[23] B. Timmer, W. Olthuis, A. Van Den Berg, Ammonia sensors and their applications - A review, Sensors Actuators, B Chem. 107 (2005) 666–677. https://doi.org/10.1016/j.snb.2004.11.054.

[24] R.E. De La Hoz, D.P. Schlueter, W.N. Rom, Chronic lung disease secondary to ammonia inhalation injury: A report on three cases, Am. J. Ind. Med. 29 (1996) 209–214. https://doi.org/10.1002/(SICI)1097-0274(199602)29:2<209::AID-AJIM12>3.0.CO;2-7.

[25] G.H. Mount, B. Rumburg, J. Havig, B. Lamb, H. Westberg, D. Yonge, K. Johnson, R. Kincaid, Measurement of atmospheric ammonia at a dairy using differential optical absorption spectroscopy in the mid-ultraviolet, Atmos. Environ. 36 (2002) 1799–1810. https://doi.org/10.1016/S1352-2310(02)00158-9.

[26] J.W. Erisman, R. Otjes, A. Hensen, P. Jongejan, P. Van Den Bulk, A. Khlystov, H. Möls, S. Slanina, Instrument development and application in studies and monitoring of ambient ammonia, Atmos. Environ. 35 (2001) 1913–1922. https://doi.org/10.1016/S1352-2310(00)00544-6.

[27] S. Kelly, K. Heaton, J. Hoogewerff, Tracing the geographical origin of food: The application of multi-element and multi-isotope analysis, Trends Food Sci. Technol. 16 (2005) 555–567. https://doi.org/10.1016/j.tifs.2005.08.008.

[28] G. Duxbury, D. Wilson, K. Hay, N. Langford, Study of the Q branch structure of the 14N and 15N isotopologues of the ν4 band of ammonia using frequency chirped quantum cascade lasers, J. Phys. Chem. A. 117 (2013) 9738–9745. https://doi.org/10.1021/jp3123665.

[29] M.B. Esler, D.W.T. Griffith, S.R. Wilson, L.P. Steele, Precision trace gas analysis by FT-IR spectroscopy. 2. The $^{13}C/^{12}C$ isotope ratio of CO_2, Anal. Chem. 72 (2000) 216–

221. https://doi.org/10.1021/ac990563x.

[30] P. Högberg, Tansley review no. 95 natural abundance in soil-plant systems, New Phytol. 137 (1997) 179–203. https://doi.org/10.1046/j.1469-8137.1997.00808.x.

[31] Y. Pan, M. Gu, L. Song, S. Tian, D. Wu, W.W. Walters, X. Yu, X. Lü, X. Ni, Y. Wang, J. Cao, X. Liu, Y. Fang, Y. Wang, Systematic low bias of passive samplers in characterizing nitrogen isotopic composition of atmospheric ammonia, Atmos. Res. 243 (2020) 105018. https://doi.org/10.1016/j.atmosres.2020.105018.

[32] W.W. Walters, L. Song, J. Chai, Y. Fang, N. Colombi, Characterizing the spatiotemporal nitrogen stable isotopic composition of ammonia in vehicle plumes, Atmos. Chem. Phys. 20 (2020) 11551–11567.

[33] J.D. Felix, E.M. Elliott, D.A. Gay, Spatial and temporal patterns of nitrogen isotopic composition of ammonia at U . S . ammonia monitoring network sites, Atmos. Environ. 150 (2017) 434–442. https://doi.org/10.1016/j.atmosenv.2016.11.039.

[34] Y. Chang, X. Liu, C. Deng, A.J. Dore, G. Zhuang, Source apportionment of atmospheric ammonia before, during, and after the 2014 APEC summit in Beijing using stable nitrogen isotope signatures, Atmos. Chem. Phys. 16 (2016) 11635–11647. https://doi.org/10.5194/acp-2016-432.

[35] N. Bhattarai, S. Wang, Q. Xu, Z. Dong, X. Chang, Science of the Total Environment Sources of gaseous NH3 in urban Beijing from parallel sampling of NH3 and NH4 +, their nitrogen isotope measurement and modeling, Sci. Total Environ. 747 (2020) 141361. https://doi.org/10.1016/j.scitotenv.2020.141361.

[36] Y. Pan, S. Tian, D. Liu, Y. Fang, X. Zhu, Q. Zhang, B. Zheng, G. Michalski, Y. Wang, Fossil Fuel Combustion-Related Emissions Dominate Atmospheric Ammonia Sources during Severe Haze Episodes : Evidence from 15N - Stable Isotope in Size-Resolved Aerosol Ammonium, Environ. Sci. Technol. 50 (2016) 8049–8056. https://doi.org/10.1021/acs.est.6b00634.

[37] A.H. Berner, J.D. Felix, Science of the Total Environment Investigating ammonia emissions in a coastal urban airshed using stable isotope techniques, Sci. Total Environ. 707 (2020) 134952. https://doi.org/10.1016/j.scitotenv.2019.134952.

[38] C. Lee, A.N. Hristov, T. Cassidy, K. Heyler, Nitrogen Isotope Fractionation and Origin of Ammonia Nitrogen Volatilized from Cattle Manure in Simulated Storage, Atmosphere (Basel). 2 (2011) 256–270. https://doi.org/10.3390/atmos2030256.

[39] T.H.E. Heaton, $^{15}N/^{14}N$ ratios of nitrate and ammonium in rain at Pretoria, South Africa, Atmos. Environ. 21 (1987) 843–852. https://doi.org/10.1016/0004-6981(87)90080-1.

[40] S.D. Kelly, A.S. Bateman, Fertilizer nitrogen isotope signatures, Isotopes Environ. Health Stud. 43 (2007) 237–247. https://doi.org/10.1080/10256010701550732.

[41] C. Ti, S. Ma, L. Peng, L. Tao, X. Wang, W. Dong, Changes of δ15 N values during the volatilization process after applying Urea on soil., Environ. Pollut. 270 (2021) 116204. https://doi.org/10.1016/j.envpol.2020.116204.

[42] E.M. Elliott, Z. Yu, A.S. Cole, J.G. Coughlin, Science of the Total Environment Isotopic advances in understanding reactive nitrogen deposition and atmospheric processing, Sci. Total Environ. 662 (2019) 393–403. https://doi.org/10.1016/j.scitotenv.2018.12.177.

[43] L. Wang, M. Xia, H. Wang, K. Huang, C. Qian, C.T. Maravelias, G.A. Ozin, Greening Ammonia toward the Solar Ammonia Refinery, Joule. 2 (2018) 1055–1074. https://doi.org/10.1016/j.joule.2018.04.017.

[44] U.S Geological Survey, U.S Department of the Interior, Mineral commodity summaries 2019, U.S. Government Publishing Office, Washington DC, 2019. https://doi.org///doi.org/10.3133/70202434.

[45] C.Y. Yoo, J.H. Joo, S.Y. Jang, J.H. Yu, H.N. Jeong, C.H. Hyeong, H.C. Yoon, J.N. Kim., Electrochemical ammonia synthesis from water and nitrogen using solid-state ion conductors, in: NH3 Fuel Conf., 2013.

[46] Y. Song, D. Johnson, R. Peng, D.K. Hensley, P. V. Bonnesen, L. Liang, J. Huang, F. Yang, F. Zhang, R. Qiao, A.P. Baddorf, T.J. Tschaplinski, N.L. Engle, M.C. Hatzell, Z. Wu, D.A. Cullen, H.M. Meyer, B.G. Sumpter, A.J. Rondinone, A physical catalyst for the electrolysis of nitrogen to ammonia, Sci. Adv. 4 (2018) 1–9. https://doi.org/10.1126/sciadv.1700336.

[47] A.J. Medford, M.C. Hatzell, Photon-Driven Nitrogen Fixation: Current Progress, Thermodynamic Considerations, and Future Outlook, ACS Catal. 7 (2017) 2624–2643. https://doi.org/10.1021/acscatal.7b00439.

[48] Y. Lu, Y. Yang, T. Zhang, Z. Ge, H. Chang, P. Xiao, Y. Xie, L. Hua, Q. Li, H. Li, B. Ma, N. Guan, Y. Ma, Y. Chen, Photoprompted Hot Electrons from Bulk Cross-Linked Graphene Materials and Their Efficient Catalysis for Atmospheric Ammonia Synthesis, ACS Nano. 10 (2016) 10507–10515. https://doi.org/10.1021/acsnano.6b06472.

[49] T. Oshikiri, K. Ueno, H. Misawa, Selective Dinitrogen Conversion to Ammonia Using Water and Visible Light through Plasmon-induced Charge Separation, Angew. Chemie - Int. Ed. 55 (2016) 3942–3946. https://doi.org/10.1002/anie.201511189.

[50] Z.W. Seh, J. Kibsgaard, C.F. Dickens, I. Chorkendorff, J.K. Nørskov, T.F. Jaramillo, Combining theory and experiment in electrocatalysis: Insights into materials design,

Science (80-.). 355 (2017) 1–33. https://doi.org/10.1126/science.aad4998.

[51] Y. Yao, J. Wang, U. Bin Shahid, M. Gu, H. Wang, H. Li, M. Shao, Electrochemical Synthesis of Ammonia from Nitrogen Under Mild Conditions: Current Status and Challenges, Springer Singapore, 2020. https://doi.org/10.1007/s41918-019-00061-3.

[52] A. Tsuneto, A. Kudo, T. Sakata, Lithium-mediated electrochemical reduction of high pressure N_2 to NH_3, J. Electroanal. Chem. 367 (1994) 183–188. https://doi.org/10.1016/0022-0728(93)03025-K.

[53] T.M. Pappenfus, K. Lee, L.M. Thoma, C.R. Dukart, Wind to Ammonia: Electrochemical Processes in Room Temperature Ionic Liquids, ECS Trans. 16 (2019) 89–93. https://doi.org/10.1149/1.3159311.

[54] T. Murakami, T. Nishikiori, T. Nohira, Y. Ito, Electrolytic synthesis of ammonia in molten salts under atmospheric pressure, J. Am. Chem. Soc. 125 (2003) 334–335. https://doi.org/10.1021/ja028891t.

[55] S. Giddey, S.P.S. Badwal, A. Kulkarni, Review of electrochemical ammonia production technologies and materials, Int. J. Hydrogen Energy. 38 (2013) 14576–14594. https://doi.org/10.1016/j.ijhydene.2013.09.054.

[56] F. Köleli, D.B. Kayan, Low overpotential reduction of dinitrogen to ammonia in aqueous media, J. Electroanal. Chem. 638 (2010) 119–122. https://doi.org/10.1016/j.jelechem.2009.10.010.

[57] R. Lan, J.T.S. Irvine, S. Tao, Synthesis of ammonia directly from air and water at ambient temperature and pressure, Sci. Rep. 3 (2013) 1–7. https://doi.org/10.1038/srep01145.

[58] L. Pospíšil, J. Bulíčková, M. Hromadová, M. Gál, S. Civiš, J. Cihelka, J. Tarábek, Electrochemical conversion of dinitrogen to ammonia mediated by a complex of fullerene C60 and γ-cyclodextrin, Chem. Commun. (2007).

[59] G. Qing, R. Ghazfar, S.T. Jackowski, F. Habibzadeh, M.M. Ashtiani, C.P. Chen, M.R. Smith, T.W. Hamann, Recent Advances and Challenges of Electrocatalytic N2Reduction to Ammonia, Chem. Rev. 120 (2020) 5437–5516. https://doi.org/10.1021/acs.chemrev.9b00659.

[60] L.F. Greenlee, J.N. Renner, S.L. Foster, The Use of Controls for Consistent and Accurate Measurements of Electrocatalytic Ammonia Synthesis from Dinitrogen, ACS Catal. 8 (2018) 7820–7827. https://doi.org/10.1021/acscatal.8b02120.

[61] L.A. Harper, Ammonia : Measurement Issues, in: J.L. Hatfield, J.M. Baker (Eds.), Agron. Monogr., 2005: pp. 345–379.

https://doi.org/https://doi.org/10.2134/agronmonogr47.c15.

[62] N. Bhattarai, S. Wang, Y. Pan, Q. Xu, Y. Zhang, δ^{15}N-stable isotope analysis of NHx : An overview on analytical measurements, source sampling and its source apportionment, Front. Environ. Sci. Eng. 15 (2021). https://doi.org/doi.org/10.1007/s11783-021-1414-6.

[63] J. Alexander, O. Saraz, R.S. Gates, M.O.D.E. Paula, L.B. Mendes, Evaluation of different methods for determining Ammonia emissions in poultry buildings and their applicability to open facilities, DYNA. Mag. Fac. Mines, Natl. Univ. Colomb. (2012) 51–60.

[64] J.J. Schwab, Y. Li, M.S. Bae, K.L. Demerjian, J. Hou, X. Zhou, B. Jensen, S.C. Pryor, A laboratory intercomparison of real-time gaseous ammonia measurement methods, Environ. Sci. Technol. 41 (2007) 8412–8419. https://doi.org/10.1021/es070354r.

[65] B. Galle, L. Klemedtsson, B. Bergqvist, M. Ferm, K. Törnqvist, D.W.T. Griffith, N.O. Jensen, F. Hansen, Measurements of ammonia emissions from spreading of manure using gradient FTIR techniques, Atmos. Environ. 34 (2000) 4907–4915. https://doi.org/10.1016/S1352-2310(00)00220-X.

[66] J.B. Nowak, J.A. Neuman, K. Kozai, L.G. Huey, D.J. Tanner, J.S. Holloway, T.B. Ryerson, G.J. Frost, S.A. McKeen, F.C. Fehsenfeld, A chemical ionization mass spectrometry technique for airborne measurements of ammonia, J. Geophys. Res. Atmos. 112 (2007) 1–12. https://doi.org/10.1029/2006JD007589.

[67] H. Borsdorf, G.A. Eiceman, Ion mobility spectrometry: Principles and applications, Appl. Spectrosc. Rev. 41 (2006) 323–375. https://doi.org/10.1080/05704920600663469.

[68] J.E. Sickles, L.L. Hodson, W.A. McClenny, R.J. Paur, T.G. Ellestad, J.D. Mulik, K.G. Anlauf, H.A. Wiebe, G.I. Mackay, H.I. Schiff, D.K. Bubacz, Field comparison of methods for the measurement of gaseous and particulate contributors to acidic dry deposition, Atmos. Environ. Part A, Gen. Top. 24 (1990) 155–165. https://doi.org/10.1016/0960-1686(90)90451-R.

[69] B.A. Paldus, B.G. Fidric, S.S. Sanders, S.M. Tan, H. Pham, A.A. Kachanov, E.H. Wahl, E.R. Crosson, High-sensitivity detectors based on cavity ring-down spectroscopy, Opt. Based Biol. Chem. Sens. Def. 5617 (2004) 312. https://doi.org/10.1117/12.578374.

[70] A. O'Keefe, D.A.G. Deacon, Cavity ring-down optical spectrometer for absorption measurements using pulsed laser sources, Rev. Sci. Instrum. 2544 (1988). https://doi.org/https://doi.org/10.1063/1.1139895.

[71] J.D. Whitehead, M. Twigg, D. Famulari, E. Nemitz, M.A. Sutton, M.W. Gallagher, D.

Fowler, Evaluation of laser absorption spectroscopic techniques for eddy covariance flux measurements of ammonia, Environ. Sci. Technol. 42 (2008) 2041–2046. https://doi.org/10.1021/es071596u.

[72] K. Von Bobrutzki, C.F. Braban, D. Famulari, S.K. Jones, T. Blackall, T.E.L. Smith, M. Blom, H. Coe, M. Gallagher, M. Ghalaieny, M.R. McGillen, C.J. Percival, J.D. Whitehead, R. Ellis, J. Murphy, A. Mohacsi, A. Pogany, H. Junninen, S. Rantanen, M.A. Sutton, E. Nemitz, Field inter-comparison of eleven atmospheric ammonia measurement techniques, Atmos. Meas. Tech. 3 (2010) 91–112. https://doi.org/10.5194/amt-3-91-2010.

[73] A. Schmohl, A. Miklós, P. Hess, Detection of ammonia by photoacoustic spectroscopy with semiconductor lasers, Appl. Opt. 41 (2002) 1815. https://doi.org/10.1364/ao.41.001815.

[74] A. Pogány, A. Mohácsi, A. Varga, Z. Bozóki, Z. Galbács, L. Horváth, G. Szabó, A compact ammonia detector with sub-ppb accuracy using near-infrared photoacoustic spectroscopy and preconcentration sampling, Environ. Sci. Technol. 43 (2009) 826–830. https://doi.org/10.1021/es802638z.

[75] Z. Bozóki, Á. Mohácsi, G. Szabó, Z. Bor, M. Erdélyi, W. Chen, F.K. Tittel, Near-infrared diode laser based spectroscopic detection of ammonia: A comparative study of photoacoustic and direct optical absorption methods, Appl. Spectrosc. 56 (2002) 715–719. https://doi.org/10.1366/000370202760077658.

[76] D.J. Miller, K. Sun, L. Tao, M.A. Khan, M.A. Zondlo, Open-path, quantum cascade-laser-based sensor for high-resolution atmospheric ammonia measurements, Atmos. Meas. Tech. 7 (2014) 81–93. https://doi.org/10.5194/amt-7-81-2014.

[77] Z. Wang, W. Zhiying, Y. Qingxu, Photoacoustic Spectroscopy for fast and sensitive ammonia detection, Chinese Opt. Lett. 5 (2007) 677–699.

[78] J. Wang, W. Zhang, L. Li, Q. Yu, Breath ammonia detection based on tunable fibre laser photoacoustic spectroscopy, Appl. Phys. B Lasers Opt. 103 (2011) 263–269. https://doi.org/10.1007/s00340-011-4550-z.

[79] J.P. Besson, S. Schilt, L. Thevenaz, Sup-ppb ammonia detection based on photoacoustic spectroscopy, in 17th Int. Conf. Opt. Fibre Sensors, 2005: p. 415. https://doi.org/10.1117/12.623666.

[80] O.E. Bonilla-Manrique, J.E. Posada-Roman, J.A. Garcia-Souto, M. Ruiz-Llata, Sub-ppm-level ammonia detection using photoacoustic spectroscopy with an optical microphone based on a phase interferometer, Sensors (Switzerland). 19 (2019).

https://doi.org/10.3390/s19132890.

[81] M. Guo, K. Chen, Z. Gong, Q. Yu, Trace Ammonia Detection Based on Near-Infrared Fiber-Optic Cantilever-Enhanced Photoacoustic Spectroscopy, Photonic Sensors. 9 (2019) 293–301. https://doi.org/10.1007/s13320-019-0545-x.

[82] C.E. Bower, T. Holm-Hansen, A Salicylate–Hypochlorite Method for Determining Ammonia in Seawater, Can. J. Fish. Aquat. Sci. 37 (1980) 794–798. https://doi.org/10.1139/f80-106.

[83] R. Michalski1, I. Kurzyca, Determination of nitrogen species (Nitrate, Nitrite and Ammonia Ions) in environmental samples by ion chromatography, Polish J. Environ. Stud. 15 (2006) 5–18. http://www.pjoes.com/pdf/15.1/5-18.pdf.

[84] C. Liu, K.K. Sakimoto, B.C. Colón, P.A. Silver, D.G. Nocera, Ambient nitrogen reduction cycle using a hybrid inorganic-biological system, Proc. Natl. Acad. Sci. U. S. A. 114 (2017) 6450–6455. https://doi.org/10.1073/pnas.1706371114.

[85] R.Y. Hodgetts, A.S. Kiryutin, P. Nichols, H.L. Du, J.M. Bakker, D.R. MacFarlane, A.N. Simonov, Refining Universal Procedures for Ammonium Quantification via Rapid 1H NMR Analysis for Dinitrogen Reduction Studies, ACS Energy Lett. 5 (2020) 736–741. https://doi.org/10.1021/acsenergylett.9b02812.

[86] W. Yu, N.S. Lewis, H.B. Gray, N.F. Dalleska, Isotopically Selective Quantification by UPLC-MS of Aqueous Ammonia at Submicromolar Concentrations Using Dansyl Chloride Derivatization, ACS Energy Lett. 5 (2020) 1532–1536. https://doi.org/10.1021/acsenergylett.0c00496.

[87] L. Anh, S. Rejean, Testing of an ammonia ion selective electrode for ammonia nitrogen measurement in the methanogenic sludge, J. Chem. Inf. Model. 53 (2013) 1689–1699. https://doi.org/https://doi.org/10.1007/BF00132830.

[88] M.C. Phillips, B.E. Brumfield, S.S. Harilal, Real-time standoff detection of nitrogen isotopes in ammonia plumes using a swept external cavity quantum cascade laser, Opt. Lett. 43 (2018) 4065. https://doi.org/10.1364/ol.43.004065.

[89] S.Z. Andersen, V. Čolić, S. Yang, J.A. Schwalbe, A.C. Nielander, J.M. McEnaney, K. Enemark-Rasmussen, J.G. Baker, A.R. Singh, B.A. Rohr, M.J. Statt, S.J. Blair, S. Mezzavilla, J. Kibsgaard, P.C.K. Vesborg, M. Cargnello, S.F. Bent, T.F. Jaramillo, I.E.L. Stephens, J.K. Nørskov, I. Chorkendorff, A rigorous electrochemical ammonia synthesis protocol with quantitative isotope measurements, Nature. 570 (2019) 504–508. https://doi.org/10.1038/s41586-019-1260-x.

[90] ASTM, Manual of water and environmental technology, D1426-92 standard: test

methods for ammonia nitrogen in water., (2015).

[91] E. Rice, R. Baird, A. Eaton, L. Clesceri, Standard methods for the examination of water and wastewater, 22nd ed., American Public Health Association, American Water Works Association, Water Environment Federation, Washington DC, USA., 2012. http://www.standardmethods.org/.

[92] T. Murakami, T. Nohira, T. Goto, Y.H. Ogata, Y. Ito, Electrolytic ammonia synthesis from water and nitrogen gas in molten salt under atmospheric pressure, Electrochim. Acta. 50 (2005) 5423–5426. https://doi.org/10.1016/j.electacta.2005.03.023.

[93] S. Klinsrisuk, J.T.S. Irvine, Electrocatalytic ammonia synthesis via a proton conducting oxide cell with BaCe0.5Zr0.3Y0.16Zn0.04O3-δ electrolyte membrane, Catal. Today. 286 (2017) 41–50. https://doi.org/10.1016/j.cattod.2016.06.051.

[94] E. Vasileiou, V. Kyriakou, I. Garagounis, A. Vourros, M. Stoukides, Ammonia synthesis at atmospheric pressure in a BaCe0.2Zr0.7Y0.1O2.9 solid electrolyte cell, Solid State Ionics. 275 (2015) 110–116. https://doi.org/10.1016/j.ssi.2015.01.002.

[95] E. Vasileiou, V. Kyriakou, I. Garagounis, A. Vourros, A. Manerbino, W.G. Coors, M. Stoukides, Reaction Rate Enhancement during the Electrocatalytic Synthesis of Ammonia in a BaZr0.7Ce0.2Y0.1O2.9 Solid Electrolyte Cell, Top. Catal. 58 (2015) 1193–1201. https://doi.org/10.1007/s11244-015-0491-9.

[96] D.H. Thomas, M. Rey, P.E. Jackson, Determination of inorganic cations and ammonium in environmental waters by ion chromatography with a high-capacity cation-exchange column, J. Chromatogr. A. 956 (2002) 181–186. https://doi.org/10.1016/s0021-9673(02)00141-3.

[97] L. Zhou, C.E. Boyd, Comparison of Nessler, phenate, salicylate and ion selective electrode procedures for determination of total ammonia nitrogen in aquaculture, Aquaculture. 450 (2016) 187–193. https://doi.org/10.1016/j.aquaculture.2015.07.022.

[98] Y. Liu, T. Asset, Y. Chen, E. Murphy, E.O. Potma, I. Matanovic, D.A. Fishman, P. Atanassov, Facile All-Optical Method for In Situ Detection of Low Amounts of Ammonia, IScience. 23 (2020) 1–11. https://doi.org/10.1016/j.isci.2020.101757.

[99] Z. Bozóki, A. Pogány, G. Szabó, Photoacoustic instruments for practical applications: Present, potentials, and future challenges, Appl. Spectrosc. Rev. 46 (2011) 1–37. https://doi.org/10.1080/05704928.2010.520178.

[100] A. Miklós, P. Hess, Z. Bozóki, Application of acoustic resonators in photoacoustic trace gas analysis and metrology, Rev. Sci. Instrum. 72 (2001) 1937–1955. https://doi.org/10.1063/1.1353198.

[101] S. Schilt, J.P. Besson, L. Thévenaz, Near-infrared laser photoacoustic detection of methane: The impact of molecular relaxation, Appl. Phys. B Lasers Opt. 82 (2006) 319–329. https://doi.org/10.1007/s00340-005-2076-y.

[102] H.S. Kasana, Complex Variables, Theory and Applications, Second, Asoke K. Ghosh, PHI Learning Private Limited, Rimjhim House, 111, Patparganj Industrial Estate, Delhi-110092, 2005. https://doi.org/10.1201/b14924-7.

[103] A. Pogány, T. Weidinger, Z. Bozóki, Á. Mohácsi, J. Bieńkowski, D. Józefczyk, A. Eredics, Á. Bordás, A.Z. Gyöngyösi, L. Horváth, G. Szabó, Application of a novel photoacoustic instrument for Ammonia concentration and flux monitoring above agricultural landscape - results of a field measurement campaign in Choryń, Poland, Idojaras. 116 (2012) 93–107.

[104] D. Tátrai, Z. Bozóki, H. Smit, C. Rolf, N. Spelten, M. Krämer, A. Filges, C. Gerbig, G. Gulyás, G. Szabó, Dual-channel photoacoustic hygrometer for airborne measurements: Background, calibration, laboratory and in-flight intercomparison tests, Atmos. Meas. Tech. 8 (2015) 33–42. https://doi.org/10.5194/amt-8-33-2015.

[105] E. Tuboly, A. Szabó, G. Erös, Á. Mohácsi, G. Szabó, R. Tengölics, G. Rákhely, M. Boros, Determination of endogenous methane formation by photoacoustic spectroscopy, J. Breath Res. 7 (2013). https://doi.org/10.1088/1752-7155/7/4/046004.

[106] A. Szabó, Á. Mohácsi, G. Gulyás, Z. Bozóki, G. Szabó, In situ and wide range quantification of hydrogen sulfide in industrial gases by means of photoacoustic spectroscopy, Meas. Sci. Technol. 24 (2013). https://doi.org/10.1088/0957-0233/24/6/065501.

[107] A. Varga, Z. Bozóki, M. Szakáll, G. Szabó, Photoacoustic system for online process monitoring of hydrogen sulfide (H2S) concentration in natural gas streams, Appl. Phys. B Lasers Opt. 85 (2006) 315–321. https://doi.org/10.1007/s00340-006-2388-6.

[108] A. Miklós, P. Hess, Z. Bozóki, Application of acoustic resonators in photoacoustic trace gas analysis and metrology, Rev. Sci. Instrum. 72 (2001) 1937–1955.

[109] Sacher Lasertechnik Group, Tunable Littman External Cavity Diode Laser, User's Man. (2004) 1–58. http://www.sacher-laser.com.

[110] G. Galzerano, P. Laporta, Modulators, Optical, in: Ref. Modul. Mater. Sci. Mater. Eng., Elsevier Ltd., 2016: pp. 1–20. https://doi.org/10.1016/b978-0-12-803581-8.01086-9.

[111] S. Schilt, L. Thévenaz, P. Robert, Wavelength Modulation Spectroscopy: Combined Frequency and Intensity Laser Modulation, Appl. Opt. 42 (2003) 6728. https://doi.org/10.1364/ao.42.006728.

[112] D. Viveiros, J. Ferreira, S.O. Silva, J. Ribeiro, D. Flores, J.L. Santos, O. Frazão, J.M. Baptista, Ammonia sensing system based on wavelength modulation spectroscopy, Photonic Sensors. 5 (2015) 109–115. https://doi.org/10.1007/s13320-015-0242-3.

[113] B. Lins, F. Pflaum, R. Engelbrecht, B. Schmauss, Absorption line strengths of 15NH3 in the near-infrared spectral region, Appl. Phys. B Lasers Opt. 102 (2011) 293–301. https://doi.org/10.1007/s00340-010-4217-1.

[114] United States Environmental Protection Agency, National Institute of Standards and Technology, Detection and Quantification Capabilities, 2004. https://www.epa.gov/sites/production/files/2015-05/documents/402-b-04-001c-20_final.pdf%0Ahttps://www.epa.gov/radiation/marlap-manual-and-supporting-documents.

[115] D. Kiss, A. Szabó, A. Czirják, G. Szabó, Z. Bozóki, Response Time Optimization of Photoacoustic Gas Analyzers "[Abstract]," in 20th Int. Conf. Photoacoust. Photothermal Phenom., Moscow, Russia, 2019: pp. 369–370.

[116] S.W. Sharpe, T.J. Johnson, R.L. Sams, P.M. Chu, G.C. Rhoderick, P.A. Johnson, Gas-phase databases for quantitative infrared spectroscopy, Appl. Spectrosc. 58 (2004) 1452–1461. https://doi.org/10.1366/0003702042641281.

[117] S.W. Sharpe, R.L. Sams, T.J. Johnson, P.M. Chu, G.C. Rhoderick, F.R. Guenther, Creation of 0.10-cm -1 resolution quantitative infrared spectral libraries for gas samples, Vib. Spectrosc. Sens. Syst. 4577 (2002) 12. https://doi.org/10.1117/12.455730.

[118] E. Awuor, H. Huszár, L. Horváth, G. Szabó, C. Janáky, Z. Bozóki, Development of a Near-Infrared Photoacoustic System for Selective, Fast, and Fully Automatized Detection of Isotopically Labelled Ammonia, Anal. Chem. (2022). https://doi.org/10.1021/acs.analchem.2c01191.

[119] Emily Awuor, Helga Huszár, Z. Bozóki, Measurement of Ammonia Isotopes ($^{14}NH_3$ and $^{15}NH_3$) Using Photoacoustic Method, Évkönyv. (2021) 208–220. https://doi.org/https://doi.org/10.18485/uns_evkonyv.2021.13.

11.0 List of publications

Hungarian Scientific Bibliography (MTMT) **Author ID: 10082771**

Publications and conferences related to the scientific topic of the dissertation:

[1]. ***Emily Awuor,*** *Helga Huszár, Zoltán Bozóki*

Measurement of Ammonia Isotopes ($^{14}NH_3$ and $^{15}NH_3$) using Photoacoustic method, // **évkönyv**. (2021), p. 208 – 220. (ISSN 2217-8198).

https://doi.org/10.18485/uns_evkonyv.2021.13

[2]. ***Emily Awuor****, Helga Huszár, László Horváth, Gábor Szabó, Csaba Janáky and Zoltán Bozóki,*

Development of a Near-Infrared Photoacoustic System for Selective, Fast and Fully Automatized Detection of Isotopically Labelled Ammonia, **Analytical Chemistry** (2022), https://doi.org/10.1021/acs.analchem.2c01191. ***(Q1, IF = 8.008)***

[3]. ***Emily Awuor,*** *Helga Huszár, László Horváth, Gábor Szabó, and Zoltán Bozóki*

Possible environmental applications of a recently developed ammonia isotope monitoring photoacoustic system. **Időjárás** (Quarterly Journal of the Hungarian Meteorological Service), (2022), (ISSN 0324-6329).

Accepted for publication. ***(Q4, IF = 0.896)***

Lecture:

Emily Awuor*, Helga Huszár, Tibor Ajtai, Gábor Szabó, Csaba Janáky and Zoltán Bozóki* "Selective Measurement of Ammonia Isotopes by Using Photoacoustic Spectroscopy", **ICPPP21,** International Conference on Photoacoustic and Photothermal Phenomena, (2022), Bled, Slovenia.

Posters:

Emily Awuor*, Helga Huszár, Csaba Janáky, Tibor Ajtai, Gábor Szabó, Zoltan Bozóki*

"Selective and Highly Sensitive Measurement of $^{15}NH_3$ Using Photoacoustic Spectroscopy for Environmental Applications", **ICAQMM 2021**; 23rd International Conference on Air Quality Management and Monitoring, May 03 – 04, (2021), Rome Italy. (Best Poster Presentation).

***Emily Awuor**, Helga Huszár, Zoltan Bozóki*

"Measurement of Ammonia Isotopes ($^{14}NH_3$ and $^{15}NH_3$) using Photoacoustic method", Organization for Women in Science for the Developing World (**OWSD) 6th General Assembly and International Conference**, November 8 – 19, (2021).

<u>Other Lectures not directly related to Thesis Work.</u>

***Emily Awuor**, Anna Szabo, Zoltan Bozóki*

Measurement of Aerosol from Exhaust Emission of Motor Vehicles using Photoacoustic Spectroscopy, **25th International Symposium on Analytical and Environmental Problems,** (2019), pp. 366 – 368, Szeged, Hungary.

ISBN 978-963-306-702-4.